UNIVERSITY OF NAPLES FEDERICO II

Department of Structures for Engineering and Architecture

PH.D. PROGRAMME IN STRUCTURAL, GEOTECHNICAL AND SEISMIC ENGINEERING

COORDINATOR PROF. LUCIANO ROSATI

XXXI CYCLE

PASQUALE CITO

PH.D. THESIS

Tools, methodologies and discussions about single-site, multi-site and sequence-based probabilistic seismic hazard analysis

ADVISOR: PROF. IUNIO IERVOLINO

CO-ADVISOR: DR. EUGENIO CHIOCCARELLI

YEAR 2019

To my father Carmine and my mother Antonella,

To my sister Annamaria,

To Federica.

ACKNOWLEDGEMENTS

First of all I would like to express my gratitude to my advisor, Prof. Iunio Iervolino, for his guidance and technical support during these three years. He gave me important opportunities and the possibility to face different and interesting challenges.

A special thanks goes to my co-advisor, Dr. Eugenio Chioccarelli for having guided me in these three years. His scientific knowledge gave me a fundamental support in the elaboration of my Ph.D. thesis.

A big thank goes to my friend and colleague Roberto Baraschino. My Ph.D. would have not been the same without your friendship. Thank you for sharing with me your passion for structural and seismic engineering.

Another thank goes to Dr. George Baltzopoulos for his suggestions on the different issues I dealt with during these years.

I wish to acknowledge the H2020-MSCA-RISE-2015 research project EXCHANGE-Risk for having given me the possibility to develop part of my research studies at Vienna Consultant Engineers (Vienna, Austria), which is also sincerely acknowledged.

A great and loving thank goes to Federica for having supported me in these three years. Your love gave me the strength for never stopping and made this work part of a biggest project.

There are not words to express my gratitude to my parents, Carmine and Antonella. Your every-day sacrifices made this goal possible and you will always be a model to me. I am also grateful to my sister, Annamaria. Your dediction to medicine studies is an example to follow.

Another important thank goes to Matteo. Three years ago, for the first time, our roads became different, but our brotherhood is still the same, from 1999.

Finally, I want to say thank you to my old and new friends for the good times of these years.

TABLE OF CONTENTS

LIST OF TABLES

LIST OF FIGURES

Chapter 1 - INTRODUCTION

1.1. Background and motivations

In the framework of performance-based earthquake engineering (Cornell and Krawinkler, 2000), actions the structures must withstand are based on probabilistic seismic hazard analysis (PSHA). Classical formulation of PSHA goes back to the second half of the twentieth century (Cornell, 1968), but its implementation can still be demanding for engineers dealing with practical applications. Moreover, in the last years, a number of developments of PSHA have been introduced; e.g., vector-valued and advanced ground motion intensity measure (IM) hazard, the inclusion of the effect of aftershocks in single-site hazard assessment, and multi-site analysis requiring the characterization of random fields of spatially cross-correlated IMs. Although several software to carry out PSHA have been available since quite some time (see Danciu et al., 2010), generally, they do not feature a user-friendly interface and do not embed most of the recent methodologies relevant from the earthquake engineering perspective. These are the main motivations behind the development of a practice-oriented software, namely REgionAl, Single-SitE and Scenario-based Seismic hazard analysis (REASSESS V2.0). The tool, which has been developed within the activities of the AXA-DiSt 2014-2017 research program of AXA-Matrix Risk Consultants and Dipartimento di Strutture per l'Ingegneria e l'Architettura, is one main results of the thesis and has been used to develop all the other studies introduced in the following.

In the most advanced countries, where PSHA is adopted for the definition of the design seismic actions, the code typically provides them in the form of hazard maps for different pseudo-spectral accelerations and return periods. In other words, for each of the sites the design spectrum is derived from the uniform hazard spectrum in which all the ordinates

have the same return period of exceedance (the return period is usually a function of the design limit-state).

PSHA has also been often questioned (e.g., Castanos and Lomnitz, 2002; Stein et al., 2003; Reiter, 2004; Musson et al., 2005; Wang, 2012). The ongoing debate on the adequacy of PSHA is (often) feed by the actually-observed seismic actions on structures. For example, when an earthquake occurs at a site, researchers typically compare the design spectrum with the recorded counterpart (e.g., Masi and Chiauzzi, 2009). In this sense, several studies show that the cases where the design spectra are exceeded are not rare (see, for example, Crowley et al., 2009).

Another relevant issue is that, in order to describe the occurrence of earthquakes according to the homogeneous Poisson process, PSHA is often implemented neglecting the effect of aftershocks, that can in fact be strong (e.g., Masi et al., 2011); as a consequence, seismic codes at the state-of-the-art worldwide implicitly assume that the effect of aftershocks is negligible and do not consider that failure of structures can be due to an aftershock rather than by a mainshock (i.e., the event of highest magnitude within a sequence).

Finally, in the recent years, PSHA estimates have been confirmed or disproved through hazard validation studies performing formal tests against observed ground motions at multiple sites over the years (e.g., Schorlemmer et al., 2007; Albarello and D'Amico, 2008); the nature and form of these studies implies that results they provide are sensitive to the adopted hypothesis of spatial dependence/independence between ground motions at the sites and, also important, require a careful evaluation of the involved data. For these reasons, the thesis proposes a study which, not questioning PSHA (which is a rational method to quantify the seismic threat for a site), recalls some of the recent advances in the seismic hazard assessment to deepen the above-introduced issues. To do so, the whole discussion is addressed with reference to the case-study of Italy and adopting the same source model used to develop the national seismic hazard. In

particular, PSHA is herein studied under three non-conventional points of view, by means of which:

- it is demonstrated that the exceedance of design spectrum in the epicentral areas of earthquakes of even moderate magnitude is well expected, identifying the seismic scenarios for which such exceedance is more probable, and quantifying the expected amount of the exceedance when such exceedance occurs;
- profiting of sequence-based PSHA (SPSHA) introduced by Iervolino et al. (2014), it is quantitatively shown that the hazard increase due to aftershocks for structural design is not very high, even if it is not negligible. It is also illustrated that the contribution of aftershocks to hazard for a site can strongly vary with return period and that, given the return period, it is different from site to site;
- profiting of multi-site PSHA (MSPSHA; Giorgio and Iervolino, 2016), it is demonstrated that hazard validation studies via observed exceedances at multiple sites over the years should always consider the spatial dependence existing between ground motions at the sites generated by a common earthquake, to avoid erroneous conclusions about the inadequateness of PSHA.

1.2. Outline of the thesis

In **Chapter 2**, the basics of the hazard assessment methodologies are recalled first. In particular, the algorithms and numerical procedures for the implementation of single- and multi-site PSHA are illustrated. Subsequently, the REASSESS V2.0 software, which has been used to develop the studies illustrated in the other chapters, is presented.

In **Chapter 3,** with reference to two spectral ordinates, in terms of pseudo-acceleration with 475 years return period of exceedance, the maps of Italian seismic hazard and disaggregation are recalled first. Subsequently, two results in the form of maps are discussed. The first is the expected value of acceleration to observe given the exceedance of design spectrum. The second is the minimum magnitude of strong earthquakes, that

is, the minimum magnitude of earthquakes for which the exceedance is more likely than not. In particular, they show that the exceedance of the design threshold is not uncommon in the epicentral area of an earthquake of magnitude even far from the maximum deemed possible for the site. This issue is further explored in the chapter by comparing the maximum magnitude which can occur, according the adopted source model, and the minimum magnitude of strong earthquakes. Then the study provides, for two sites exposed to low (Milan, northern Italy) and high hazard (L'Aquila, central Italy), the analysis of each magnitude-distance scenario in terms of probability of exceeding the threshold conditional to the occurrence of that scenario, rate of earthquakes occurrence and rate of earthquakes causing the exceedance of the threshold. Still with reference to Milan and L'Aquila, the effect of return period on the introduced results is also investigated.

In **Chapter 4**, with reference to the spectral ordinates and return period of exceedance considered in Chapter 3, the differences existing between PSHA and SPSHA maps, introduced in Iervolino et al. (2018), are recalled first. Subsequently the SPSHA results are presented in detail for two sites, Frosinone and Messina, located in medium- and high-seismicity areas. The chapter then focuses on the two kinds of SPSHA disaggregation discussed in Chapter 2. In fact, starting from the comparison of aftershock disaggregations for Frosinone and Messina, which provide the probability that an aftershock is causative for the exceedance of the threshold, the influence on results of the source-to-site distance and the hypotheses on spatial distribution of aftershocks is discussed. Subsequently, the study moves to a national scale. In particular, the maps of disaggregation in terms of mainshock average magnitude and distance are compared with the PSHA counterparts illustrated in Chapter 3. The Frosinone and Messina case-studies, along with other examples illustrated in the chapter, reveal a strong variability of the contribution of aftershocks to hazard with return period for a given site. For this reason, the study of the general trend of aftershock disaggregation as a function of return period is explored, with reference to two different ranges: the first

considers return periods between ten and one-hundred-thousand years, while the second assumes a range of interest according to the Italian building code. Finally, the site to site differences in terms of probabilities that an aftershock causes the exceedance of the threshold for fixed return periods are investigated.

In **Chapter 5**, the causes and effects of spatial dependence in MSPSHA are recalled first. To quantitively evaluate these effects, the previous hazard validation study for Italy of Albarello and D'Amico (2008), via observed ground motions at multiple sites over time, is revised. In particular, the chapter discusses the results of a statistical test of the hazard map, carried out in the two cases where spatial dependence is considered and not. The importance of the careful evaluation of data involved in hazard validation is also underlined.

In **Chapter 6**, the general outcomes deriving from the presented PSHA studies are finally summarized. In addition, a short paragraph illustrating the future developments is also provided.

Chapter 2 – SINGLE- AND MULTI-SITE HAZARD ASSESSMENT: THEORY AND IMPLEMENTATION IN REASSESS V2.0

This chapter is derived from the following paper:

Chioccarelli E, Cito P, Iervolino I, Giorgio M (2018) REASSESS V2.0: Software for single- and multi-site seismic hazard analysis. Bull Earthq Eng http://dx.doi.org/10.1007/s10518-018-00531-x.

2.1. Introduction

In most of the countries probabilistic seismic hazard analysis is at the basis of the seismic risk assessment according to the performance-based earthquake engineering paradigm (Cornell and Krawinkler, 2000), and serves for the determination of seismic actions for structural design. The main result of classical PSHA is the rate of earthquakes causing exceedance of a ground motion intensity measure threshold (*im*) at a site of interest (Cornell, 1968). In fact, the collection of the rates computed for different *im* values provides the so-called hazard curve. However, classical PSHA has been significantly extended since its introduction in the late sixties. In fact, several results and applications can be found nowadays, including disaggregation of seismic hazard (Bazzurro and Cornell, 1999), conditional mean spectrum (Baker, 2011) and conditional spectrum (Lin et al., 2013), vector-valued PSHA (Baker and Cornell, 2006b), conditional hazard (Iervolino et al., 2010), PSHA for more efficient IMs (e.g., Cordova et al., 2000; Bianchini et al., 2009; Bojorquez and Iervolino, 2011).

PSHA, as normally implemented, only considers the exceedance of the *im* threshold of interest due to prominent magnitude earthquakes within a cluster of events; i.e., the

typical way earthquakes occur (e.g., Boyd, 2012; Marzocchi and Taroni, 2014). This is to take advantage of the ease of calibration and mathematical manageability of the homogeneous Poisson process (HPP) (e.g., Cornell, 1968; McGuire, 2004). Nevertheless, a generalized hazard integral able to account for the effect of aftershocks, without losing the advantages of HPP, was recently developed and named sequence-based probabilistic seismic hazard analysis (Iervolino et al., 2014). Finally, there are cases, for example risk assessment of building portfolios, or spatially-distributed infrastructures, in which hazard assessment must account for exceedances at multiple sites jointly. In this case, which may be referred to as multi-site probabilistic seismic hazard analysis, the key issue is to account for the existence of stochastic dependence among the processes counting exceedances at each of the considered sites (e.g., Eguchi, 1991; Giorgio and Iervolino, 2016).

In the last forty years several computer programs implementing classical PSHA have been developed. The first available was EQRISK (McGuire, 1976). Other relevant codes are, for example, SEISRISK III (Bender and Perkins, 1987), OpenSHA (Field et al., 2003) and CRISIS (Ordaz et al., 2013); see Danciu et al. (2010). Recently, the global earthquake model (GEM) foundation developed OpenQuake (Pagani et al., 2014) that has been adopted, among others, within the EMME (Giardini et al., 2018) and SHARE (Giardini et al., 2013) hazard assessment projects.

To provide an engineering-oriented tool including the advanced probabilistic seismic hazard analysis, a stand-alone software named REgionAl, Single-Site and Scenario-based Seismic hazard analysis (REASSESS V2.0) with a graphical user interface (GUI) has been developed.

In this framework, this chapter is structured such that the above-mentioned hazard assessment methodologies are recalled first, along with the algorithms and numerical procedures developed for their implementation. Subsequently, the REASSESS V2.0 software is presented with the main input and output options.

2.2. Single-site PSHA

Under the hypothesis of classical PSHA (e.g., Reiter, 1990), the process describing the occurrence of earthquakes on a seismic source follows a homogeneous Poisson process. This means that the stochastic process counting the number of events occurring on the generic seismic source over time is completely defined by the rate of earthquakes, ν. In other words, the probability of observing in the time interval, ΔT, a number of earthquakes, $N(\Delta T)$, exactly equal to n is given by equation (2.1).

$$P\left[N(\Delta T)=n\right]=\frac{(\nu\cdot\Delta T)^n}{n!}\cdot e^{-\nu\cdot\Delta T} \tag{2.1}$$

As stated in the introduction, the objective of PSHA is to compute the rate of seismic events exceeding the *im* threshold at a site of interest, λ_{im}. Such a rate completely defines the HPP describing the occurrence of the events causing exceedance of *im* at the site. Indeed, the probability that, in the time interval ΔT, the number of earthquakes causing exceedance of *im* at the site, $N_{im}(\Delta T)$, being equal to n is given by Equation (2.2).

$$P\left[N_{im}(\Delta T)=n\right]=\frac{\left(\lambda_{im}\cdot\Delta T\right)^n}{n!}\cdot e^{-\lambda_{im}\cdot\Delta T} \tag{2.2}$$

For a site subjected to earthquakes generated at n_s seismic sources, λ_{im} can be computed as illustrated in Equation (2.3), known as the hazard integral.

$$\lambda_{im}=\sum_{i=1}^{n_s}\nu_i\cdot\int_M\int_X\int_Y P\left[IM>im\middle|m,x,y\right]_i\cdot f_{M,i}(m)\cdot f_{X,Y,i}(x,y)\cdot dm\cdot dx\cdot dy \tag{2.3}$$

In the equation the *i* subscript indicates the *i*-th seismic source. ν_i is the rate of earthquakes above a minimum magnitude of interest and below the maximum magnitude deemed possible for the source. $f_{M,i}(m)$ represents the distribution of earthquake magnitude (M); typically, it is modeled as an exponential distribution, in an interval of

interest, of Gutenberg-Richter (G-R) type (Gutenberg and Richter, 1944); however, other models are also considered by literature (e.g., Convertito et al., 2006). The $f_{X,Y,i}(x,y)$ term denotes the distribution of earthquake location $\{X,Y\}$; it often reflects the hypothesis of uniformly-distributed probability on the source. Magnitude and location of the earthquake are often considered stochastically independent, that is $f_{M,i}(m)\cdot f_{X,Y,i}(x,y)=f_{M,X,Y,i}(m,x,y)$. Finally, $P\left[IM>im\middle|m,x,y\right]_i$, is the probability of exceeding the *im* threshold, conditional to magnitude and location; it is typically provided by a ground motion prediction equation (GMPE). It is noted that GMPEs, usually, also account for soil type, rupture mechanism and other parameters that are not explicitly considered in the notation here for the sake of simplicity.

It is also only for simplicity that the location is defined in Equation (2.3) by means of two horizontal coordinates that can represent, for example, the epicenter. This representation is typically used in the case of areal source zones; however, it is frequent that hazard assessments have to account for three-dimensional faults (see Section 2.5.1). Moreover, it also happens that the distance metric of the selected GMPE is not consistent with the way location is defined. In these cases, because the relationship between location and source-to-site distance is not necessarily deterministic, the hazard integral has to account for the probabilistic distribution of the distance metric of the GMPE, conditional to the considered location parameters (see, for example, Scherbaum et al., 2004).

2.2.1. Matrix algebra-based approach

Equation (2.3) can be numerically solved via a matrix formulation approximating the integrals with summations. To this aim, the domain of the possible realizations of the magnitude random variable (RV) is discretized via k magnitude bins represented by the values $\{m_1,m_2,...,m_k\}$, while the seismic source is discretized by means of *s* point-like seismic sources, $\{(x,y)_1,(x,y)_2,...,(x,y)_s\}$. Given these two vectors of size $1\times k$ and

$1\times s$, Equation (2.3) can be approximated by Equation (2.4), where the row vector approximates $f_{X,Y,i}(x,y)$ by a mass probability function (PMF) described by a vector in a way that each element is repeated k times; i.e., the first k elements are the probabilities of $(x,y)_1$, the elements from $k+1$ until $2k$ are for $(x,y)_2$ and so on, until $(x,y)_s$. Thus, the row vector has dimension $1\times(k\cdot s)$. The first column vector of Equation (2.4) is a $(k\cdot s)\times 1$ vector and accounts for the GMPE: each element represents the exceedance probability conditional to event magnitude and location. The second column vector of the equation collects the finite k probabilities of event's magnitude, identically repeated *s*-times, as shown and it is, again, a $(k\cdot s)\times 1$ vector. Finally, in the equation, the pointwise multiplication between matrices of the same dimensions (i.e., the *Hadamard product*, represented by the $\otimes$ symbol) results in a matrix of the dimensions of those multiplied in which each element is the product of the corresponding elements of the original matrices.

$$\lambda_{im}=\sum_{i=1}^{n_s}\nu_i\cdot\left\{P\left[(x,y)_1\right]\;\; P\left[(x,y)_1\right]\;\;\cdots\;\; P\left[(x,y)_1\right]\;\;\cdots\;\; P\left[(x,y)_s\right]\;\; P\left[(x,y)_s\right]\;\;\cdots\;\; P\left[(x,y)_s\right]\right\}_i\cdot \left(\begin{Bmatrix} P\left[IM>im\,|\,m_1,(x,y)_1\right]\\ P\left[IM>im\,|\,m_2,(x,y)_1\right]\\ \vdots\\ P\left[IM>im\,|\,m_k,(x,y)_1\right]\\ \vdots\\ P\left[IM>im\,|\,m_1,(x,y)_s\right]\\ P\left[IM>im\,|\,m_2,(x,y)_s\right]\\ \vdots\\ P\left[IM>im\,|\,m_k,(x,y)_s\right]\end{Bmatrix}_i \otimes \begin{Bmatrix} P[m_1]\\ P[m_2]\\ \vdots\\ P[m_k]\\ \vdots\\ P[m_1]\\ P[m_2]\\ \vdots\\ P[m_k]\end{Bmatrix}_i\right)$$

(2.4)

Equation (2.4), as already discussed with respect to Equation (2.3), is written in the case location can be defined by means of two coordinates and the distance metric of the

GMPE is a deterministic function of the location. Otherwise, it is necessary to account for the non-deterministic transformation of the location in source-to-site distance, which can be done in the same framework presented herein.

To compute the hazard curve, that is the function providing λ_{im} as a function of *im*, the hazard integral has to be computed for a number of values of *im*, say *q* in number, discretizing the domain of IM, that is $\{im_1, im_2, ..., im_q\}$. The corresponding rates $\{\lambda_{im_1}, \lambda_{im_2}, ..., \lambda_{im_q}\}$ can be obtained via a single matrix operation conceptually equivalent to Equation (2.4); see Iervolino et al. (2016a).

2.2.2. Disaggregation

Given a spectral ordinate and return period of interest, disaggregation of seismic hazard (e.g., Bazzurro and Cornell, 1999) allows to identify the earthquakes having the largest contribution to hazard. From the engineering perspective, disaggregation can be helpful for the definition of design scenarios and, consequently, for hazard-consistent record selection for nonlinear dynamic analysis (e.g., Lin et al., 2013), for example. In particular, disaggregation allows the identification of the hazard contribution of one or more random variables involved in the hazard integral: e.g., magnitude and source-to-site distance, R, which is a deterministic function of the event location. Another random variable typically considered in hazard disaggregation is ε (*epsilon*). It is the number of standard deviations that *im* is away from the median of the GMPE considered in hazard assessment. In fact, GMPEs provide the probabilistic distribution of IM given magnitude, distance and other parameters and, under the hypothesis of lognormality of IM, they are typically of the type in Equation (2.5).

$$\log(im) = \mu(m,r) + \theta + \sigma \cdot \varepsilon \tag{2.5}$$

In the equation, the $\mu(m,r)$ term depends on magnitude and distance; θ represents one or more coefficients accounting, for example, for soil site class. Under the above-

mentioned hypothesis of lognormality of IM, $\mu(m,r)+\theta$ is the mean, and the median, of the logarithms of IM given $\{m,r,\theta\}$. The $\sigma\cdot\varepsilon$ term is a zero-mean Gaussian random variable with standard deviation σ; often it is split in inter- and intra- components, denoted as inter- and intra-event residuals, in a way that $\sigma=\sqrt{\sigma_{\text{inter}}{}^2+\sigma_{\text{intra}}{}^2}$, where σ_{inter} and σ_{intra} represent the standard deviation of the inter- and intra-event residual, respectively (see Section 5.2 for details). Note that, although the majority of the GMPEs is of the type in Equation 2.5, see Stewart et al. (2015), most of the recent models have soil factors that also change with magnitude and distance; this representation is considered herein to discuss some shortcuts implemented in REASSESS and that apply only in this case; see Sections 2.2.3 and 2.4.3.

Given the exceedance of an IM threshold, disaggregation provides the joint probability density function (pdf) of $\{m,r,\varepsilon\}$, $f_{M,R,\varepsilon|IM>im}(m,r,\varepsilon)$, as per Equation (2.6).

$$f_{M,\mathrm{R},\varepsilon|IM>im}(m,\mathrm{r},\varepsilon)=\frac{\sum_{i=1}^{n_s}\nu_i\cdot I\left[IM>im\,|\,m,r,\varepsilon\right]\cdot f_{M,R,\varepsilon,i}(m,r,\varepsilon)}{\lambda_{im}} \tag{2.6}$$

In the equation, I is an indicator function that equals one if IM is larger than *im* for a given magnitude, distance and ε while $f_{\mathrm{M,R},\varepsilon,i}(m,\mathrm{r},\varepsilon)$ is the marginal joint pdf obtained from the product $f_{M,R,i}(m,r)\cdot f_{\varepsilon}(\varepsilon)$.

Finally, it is worthwhile to note that disaggregation can also be easily obtained for the occurrence of *im*, that is $f_{M,R,\varepsilon|IM=im}(m,r,\varepsilon)$; i.e., McGuire (1995). For a discussion on whether exceedance or occurrence disaggregation is needed in earthquake engineering, see, for example, Fox et al. (2016).

2.2.3. Logic tree and shortcuts for GMPEs with additive soil factors

Logic tree allows to account for model uncertainty (see, for example, McGuire, 2004; Kramer, 1996). Modeling the uncertainty through a logic tree is a common practice in

PSHA. In fact, it allows to adopt alternative models in terms of seismic sources or GMPEs, for example. Each model is weighted by a factor that is interpreted as the probability of that model being the true one. In the case of logic tree, the rate of exceedance of the threshold of interest for each of the n_b modeled branches, $\lambda_{im,j}$, is computed according to Equation (2.3). Subsequently, λ_{im}, is computed through Equation (2.7) in which p_j is the weight of each branch of the logic tree.

$$\lambda_{im} = \sum_{j=1}^{n_b} \lambda_{im,j} \cdot p_j \tag{2.7}$$

In the case of GMPEs of the type in Equation (2.5), the θ coefficient only affects the mean of $\log(IM)$. As a consequence of this structure of the GMPE, it can be easily demonstrated that, if PSHA is performed without logic tree: (i) hazard curves for the condition represented by θ (e.g., a specific site soil class) can be obtained shifting, in the log space, those for a reference condition when $\theta = 0$; and (ii) disaggregation distribution does not depend on θ (i.e., disaggregation does not change with the soil site class). On the other hand, if a logic tree featuring different GMPEs is adopted in PSHA, the discussed translation of hazard curves can be applied to the result of each branch, then re-applying Equation (2.7) provides the hazard in the changed conditions (Iervolino, 2016). These considerations may have a relevant impact on PSHA from the computational demand point of view. For example, if hazard map on rock soil condition for all sites has been carried out, the corresponding on site-dependent soil conditions can be obtained instantly, without repeating the analysis (see also Section 3.4.3).

2.2.4. Conditional men spectrum and conditional spectrum

Nonlinear dynamic analysis of structures always requires the selection of the seismic input, which should be derived from the seismic hazard at the sites in which the structures are located (see, for example, Katsanos et al., 2010). Typically, ground motions are selected so that they match a target uniform hazard spectrum (UHS), that is,

a spectrum with ordinates that have the same probability of exceedance in a given time interval. However, such spectrum does not account for the correlation existing between spectral ordinates (e.g., Baker and Jayaram, 2008). In fact, it is not representative of any real ground motion, as it is an envelope of the spectral amplitude from different magnitude-distance scenarios (e.g., Reiter, 1990). In particular, Baker (2011) discusses on the unsuitability of the UHS and introduces the conditional mean spectrum (CMS) for ground motion selection purposes. Given the occurrence of a spectral ordinate in terms of pseudo-spectral acceleration (Sa) at a period of interest (T_1), $Sa(T_1)$, the CMS accounts for the statistical correlation of residuals between the different pseudo-spectral accelerations of the same GMPE. Under the hypothesis that, given magnitude and distance, Sa is lognormally distributed, Equation (2.8) provides the expected value of the logarithm of the generic *t*-th spectral ordinate, $\log Sa(T_t)$, conditional to $\log Sa(T_1)$.

$$E[\log Sa(T_t) \mid \log Sa(T_1)] = E[\log Sa(T_t) \mid m^*, r^*, \theta] + \sigma_{\log Sa(T_t)} \cdot \rho(T_t, T_1) \cdot \varepsilon(T_1) \qquad (2.8)$$

In the equation, m^*, r^* and $\varepsilon(T_1)$ are often chosen to be representative of the whole disaggregation distribution (e.g., modal values) of $Sa(T_1)$; $\sigma_{\log Sa(T_t)}$ is the standard deviation of the residual of $\log Sa(T_t)$; $\rho(T_t, T_1)$ is the correlation coefficient between the residuals of $\log Sa(T_1)$ and $\log Sa(T_t)$ (e.g., Inoue and Cornell, 1990; Baker and Jayaram, 2008). The CMS is then obtained by applying Equation (2.8) for different periods, that is by varying the *t* subscript.

Nevertheless, in the not rare situations of non-unimodal disaggregation (see Iervolino et al., 2011), Equation (2.8) is not capable to provide a fully hazard-consistent CMS. In such cases, one of the alternatives is to account for all the possible earthquake scenarios conditional to the occurrence of $Sa(T_1)$ as per Equation (2.9), in which $f_{M,R,\varepsilon|Sa(T_1)}(m, r, \varepsilon)$ represents the disaggregation for the occurrence of $Sa(T_1)$.

$$E\left[\log Sa(T_t)\middle|\log Sa(T_1)\right]=\int_M\int_R\int_\varepsilon\left\{E\left[\log Sa(T_t)\middle|m,r,\theta\right]+\sigma_{\log Sa(T_t)}\cdot\rho(T_t,T_1)\cdot\varepsilon\right\}\cdot \\ \cdot f_{M,R,\varepsilon|Sa(T_1)}(m,r,\varepsilon)\cdot dm\cdot dr\cdot d\varepsilon \tag{2.9}$$

According to the equation, the expected value of the logarithm of $Sa(T_t)$ conditional to $Sa(T_1)$ is computed for each earthquake scenario first; then, all the obtained values are summed with the corresponding weights, which derive from disaggregation.

In the case a logic tree is considered, which may involve different GMPEs in PSHA, the expected value of $\log Sa(T_t)$ can be computed via the Equation (2.10).

$$E\left[\log Sa(T_t)\middle|\log Sa(T_1)\right]=\sum_{j=1}^{n_b}p_j\cdot E\left[\log Sa(T_t)\middle|\log Sa(T_1)\right]_j \tag{2.10}$$

The CMS only provides the conditional mean of the logarithms of pseudo-spectral accelerations. As an extension of CMS, the conditional spectrum (CS) introduced by Lin et al. (2013) is a target spectrum which also includes the conditional variability of the log of $Sa(T_t)$. In fact, still referring to the *t*-th spectral ordinate, the CS provides the compete lognormal distribution of $Sa(T_t)$ conditional to the occurrence of $Sa(T_1)$ by combining the conditional mean (Equation 2.8 or 2.9) with the conditional standard deviation (Equation 2.11).

$$\sigma_{\log Sa(T_t)|\log Sa(T_1)}=\sigma_{\log Sa(T_t)}\sqrt{1-\rho^2(T_t,T_1)} \tag{2.11}$$

2.2.5. Conditional hazard

Conditional hazard is a procedure which allows to integrate the hazard characterization of the site in terms of other IMs beyond that for which hazard was originally computed. In fact, it provides the distribution of a secondary intensity measure (IM_2), conditional to the occurrence of a threshold of the primary one (IM_1). Under the hypothesis of bivariate lognormality of the two IMs, and in the generic case that are not both in terms

of Sa, the distribution of the logarithm of IM_2 conditional to the occurrence of IM_1, $f_{\log IM_2|IM_1}$, is given by Equation (2.12).

$$f_{\log IM_2|IM_1}\left(\log im_2\right)=\int_M\int_R\int_\varepsilon f_{\log IM_2|IM_1,M,R,\varepsilon}\left(\log im_2\left|im_1,m,r,\varepsilon\right.\right)\cdot f_{M,R,\varepsilon|IM_1}\left(m,r,\varepsilon\right)\cdot dm\cdot dr\cdot d\varepsilon \tag{2.12}$$

In the equation, $f_{M,R,\varepsilon|IM_1}\left(m,r,\varepsilon\right)$ is from the occurrence disaggregation of IM_1. $f_{\log IM_2|IM_1,M,R,\varepsilon}$, whose parameters are given in Equation (2.13), represents the lognormal distribution of IM_2 given IM_1, magnitude, distance and epsilon.

$$\begin{cases}\mu_{\log IM_2|IM_1,M,R,\varepsilon}=\mu_{\log IM_2|M,R}+\sigma_{\log IM_2}\cdot\rho(IM_2,IM_1)\cdot\varepsilon\\ \sigma_{\log IM_2|IM_1}=\sigma_{\log IM_2}\cdot\sqrt{1-\rho^2(IM_2,IM_1)}\end{cases} \tag{2.13}$$

The $\mu_{\log IM_2|IM_1,M,R,\varepsilon}$ and $\sigma_{\log IM_2|IM_1}$ terms provide the conditional mean and standard deviation of $f_{\log IM_2|IM_1,M,R,\varepsilon}$, respectively. In particular, $\mu_{\log IM_2|M,R}$ and $\sigma_{\log IM_2}$ are the mean and standard deviation of $\log IM_2$ according to the selected GMPE; as shown in the previous section, $\rho(IM_2,IM_1)$ is the correlation coefficient between residuals of $\log IM_2$ and $\log IM_1$ (e.g., Baker and Jayaram, 2008; Bradley, 2012).

The formulation of Equation (2.12) allows to compute vector-valued probabilistic seismic hazard analysis (VPSHA), originally introduced by Bazzurro and Cornell (2002), which provides the rate of earthquakes causing joint exceedance of the thresholds of two (or possibly more) IMs at the site. In fact, $f_{\log IM_2|IM_1}$ multiplied by the absolute value of the derivative of the hazard curve from Equation (2.3), allows to obtain the joint annual rate of $\{IM_1,IM_2\}$ for any pair of arbitrarily-selected realizations of the two IMs, λ_{im_1,im_2}, as per Equation (2.14).

$$\lambda_{im_1,im_2}=\left|d\lambda_{im_1}\right|\cdot f_{log\,IM_2|IM_1}\left(log\,im_2\right) \tag{2.14}$$

From the structural engineering point of view, VPSHA could improve the accuracy in the prediction of structural damage (e.g., Baker, 2007), for example.

2.3. Sequence-based PSHA

The rate of earthquakes occurrence on a seismic source, ν, for the evaluation of the annual average number of earthquakes causing the exceedance of a threshold of interest (i.e., Equation 2.3) does not include foreshocks and aftershocks. In other words, ν derives from a declustered catalog, which only refers to mainshocks. In fact, according to Gardner and Knopoff (1974), such a catalog is needed to profit of the HPP (see Section 2.2).

Recently, Iervolino et al. (2014) demonstrated the possibility to include the effect of aftershocks in PSHA still working with HPP and declustered catalogs. In particular, PSHA was combined with the aftershock probabilistic seismic hazard analysis (APSHA) of Yeo and Cornell (2009). Thus, profiting of the fact that, according to Boyd (2012), mainshock-aftershock sequences occur on the seismic source with the same rate of the mainshocks, the hazard integral accounting for the aftershocks' effect was formulated. As a result, SPSHA provides, for any given *im*-value, the annual rate of mainshock-aftershock sequences that cause exceedance of *im* at the site, λ_{im}, which can be computed via Equation (2.15). In particular, λ_{im} is still the rate of the HPP of the kind in Equation (2.2), which now regulates the occurrence of sequences causing exceedance of *im*.

$$\lambda_{im} = \sum_{i=1}^{n_s} \nu_i \cdot \left\{ 1 - \int_M \int_X \int_Y P\left[IM \le im \,|\, m,x,y\right]_i \cdot e^{-E\left[N_{A,im|m}(0,\Delta T_A)\right]} \cdot f_{M,X,Y,i}(m,x,y) \cdot dm \cdot dx \cdot dy \right\} \tag{2.15}$$

In the equation, the terms: ν_i, $P\left[IM \le im \,|\, m,x,y\right]_i = 1 - P\left[IM > im \,|\, m,x,y\right]_i$ and $f_{M,X,Y,i}(m,x,y)$ are the same defined in Equation (2.3). The exponent

$E\left[N_{A,im|m}(0,\Delta T_A)\right]$ refers to aftershocks, as indicated by the A subscript: it represents the average number of aftershocks that cause exceedance of *im* in a sequence conditional to the mainshock of magnitude and location $\{m,x,y\}$, as per Equation (2.16).

$$E\left[N_{A,im|m}(0,\Delta T_A)\right] = \\ = E\left[N_{A|m}(0,\Delta T_A)\right]\cdot \int_{M_A}\int_{X_A}\int_{Y_A} P\left[IM_A > im \mid m_A,x_A,y_A\right]_i \cdot f_{M_A,X_A,Y_A,i|M,X,Y}(m_A,x_A,y_A)\cdot \\ \cdot dm_A \cdot dx_A \cdot dy_A \tag{2.16}$$

In the equation, $E\left[N_{A|m}(0,\Delta T_A)\right]$ is the expected number of aftershocks to the mainshock of magnitude m in the ΔT_A time interval. The $P\left[IM_A > im \mid m_A,x_A,y_A\right]_i$ term is the probability that *im* is exceeded given an aftershock of magnitude and location identified by the vector $\{m_A,x_A,y_A\}$; it derives from a GMPE for aftershocks, which, in several applications, is assumed to be the same for mainshock. The term $f_{M_A,X_A,Y_A,i|M,X,Y}$ is the distribution of magnitude and location of aftershocks, which is conditional on the magnitude and location of the mainshock. This distribution can be written as $f_{M_A,X_A,Y_A,i|M,X,Y} = f_{M_A,i|M}\cdot f_{X_A,Y_A,i|M,X,Y}$, where $f_{M_A,i|M}$ is the pdf of aftershock magnitude of G-R type, and $f_{X_A,Y_A,i|M,X,Y}$ is the distribution of the location of the aftershocks and depends on the magnitude and location of the mainshock (e.g., Utsu, 1970).

According to Yeo and Cornell (2009), $E\left[N_{A|m}(0,\Delta T_A)\right]$ can be computed via Equation (2.17) in which $m_{A,min}$ is the minimum magnitude of aftershocks, $\{c,p\}$ are parameters of the *modified Omori Law* and $\{a,b\}$ are the parameters of the G-R for aftershocks.

$$E\left[N_{A|m}(0,\Delta T_A)\right] = \frac{10^{a+b\cdot(m-m_{A,\min})}-10^{a}}{p-1}\cdot\left[c^{1-p}-\left(\Delta T_A+c\right)^{1-p}\right] \tag{2.17}$$

The matrix formulation presented in Equation (2.4) for the numerical computation of PSHA can be extended to the SPSHA case as reported in Equation (2.18). In the latter, vectors are arranged as discussed referring to Equation (2.4) but a new column vector is introduced: it has the same $(k \cdot s) \times 1$ dimension and each element of it accounts for the probability that none of the aftershocks conditional to the mainshock of given magnitude and location cause the exceedance of *im*.

$$\lambda_{im} = \sum_{i=1}^{n_{source}} \nu_i \cdot \left[1 - \left\{ P\left[(x,y)_1\right] \;\; P\left[(x,y)_1\right] \;\; \cdots \;\; P\left[(x,y)_1\right] \;\; \cdots \;\; P\left[(x,y)_s\right] \;\; P\left[(x,y)_s\right] \;\; \cdots \;\; P\left[(x,y)_s\right] \right\}_i \cdot \right.$$
$$\left. \cdot \left(\begin{Bmatrix} P\left[IM \le im \mid m_1, (x,y)_1\right] \\ P\left[IM \le im \mid m_2, (x,y)_1\right] \\ \vdots \\ P\left[IM \le im \mid m_k, (x,y)_1\right] \\ \vdots \\ P\left[IM \le im \mid m_1, (x,y)_s\right] \\ P\left[IM \le im \mid m_2, (x,y)_s\right] \\ \vdots \\ P\left[IM \le im \mid m_k, (x,y)_s\right] \end{Bmatrix}_i \otimes \begin{Bmatrix} e^{-E\left[N_{A\mid m_1}(0,\Delta T_A)\right] \cdot P\left[IM_A > im \mid m_1, (x,y)_1\right]} \\ e^{-E\left[N_{A\mid m_2}(0,\Delta T_A)\right] \cdot P\left[IM_A > im \mid m_2, (x,y)_1\right]} \\ \vdots \\ e^{-E\left[N_{A\mid m_k}(0,\Delta T_A)\right] \cdot P\left[IM_A > im \mid m_k, (x,y)_1\right]} \\ \vdots \\ e^{-E\left[N_{A\mid m_1}(0,\Delta T_A)\right] \cdot P\left[IM_A > im \mid m_1, (x,y)_s\right]} \\ e^{-E\left[N_{A\mid m_2}(0,\Delta T_A)\right] \cdot P\left[IM_A > im \mid m_2, (x,y)_s\right]} \\ \vdots \\ e^{-E\left[N_{A\mid m_k}(0,\Delta T_A)\right] \cdot P\left[IM_A > im \mid m_k, (x,y)_s\right]} \end{Bmatrix}_i \otimes \begin{Bmatrix} P\left[m_1\right] \\ P\left[m_2\right] \\ \vdots \\ P\left[m_k\right] \\ \vdots \\ P\left[m_1\right] \\ P\left[m_2\right] \\ \vdots \\ P\left[m_k\right] \end{Bmatrix}_i \right)$$

(2.18)

2.3.1. SPSHA disaggregation

Similarly to PSHA, the joint distribution of mainshock and magnitude distance, given that the ground motion intensity of the mainshock, IM, or the maximum ground motion intensity of the following aftershock sequence $\left(IM_{\cup A}\right)$ is larger than the *im* threshold, can be computed as per Equation (2.19).

$$f_{M,R|IM>im\cup IM_{\cup A}>im}(m,r)=\frac{\sum_{i=1}^{n_s}\nu_i}{\lambda_{im}}\cdot \cdot\left\{1-P\left[IM\le im\,|\,m,r\right]_i\cdot e^{-E\left[N_{A|m}(0,\Delta T_A)\right]\cdot\int_{M_A}\int_{R_A}P\left[IM_A>im|m_A,r_A\right]_i\cdot f_{M_A,R_A,i|M,R}(m_A,r_A)\cdot dm_A\cdot dr_A}\right\}\cdot f_{M,R,i}(m,r) \tag{2.19}$$

In the equation, similarly to what discussed in Section 2.2.2, $\{X,Y\}$ and $\{X_A,Y_A\}$ vectors random variables are substituted by R and R_A, respectively.

Moreover, in the case of SPSHA it can be worthwhile to compute the contribution of aftershocks to hazard given that exceedance of *im* has been observed during the mainshock-aftershock sequence, $\left(IM>im\cup IM_{\cup A}>im\right)$, while the mainshock was below the threshold: i.e., $\left(IM\le im\cap IM_{\cup A}>im\right)$. In other words, the computation of the aftershocks' contribution, herein after referred to as aftershock disaggregation, results in the evaluation of the probability that, given the *im* exceedance, such exceedance is caused by an aftershock rather than by a mainshock, $P\left[IM\le im\cap IM_{\cup A}>im\middle|IM>im\cup IM_{\cup A}>im\right]$, as per Equation (2.20).

$$P\left[IM\le im\cap IM_{\cup A}>im\middle|IM>im\cup IM_{\cup A}>im\right]=\sum_{i=1}^{n_s}\frac{\nu_i}{\lambda_{im}}\cdot\iint_{M,R}P\left[IM\le im\,|\,m,r\right]_i\cdot \cdot\left(1-e^{-E\left[N_{A|m}(0,\Delta T_A)\right]\cdot\int_{M_A}\int_{R_A}P\left[IM_A>im|m_A,r_A\right]_i\cdot f_{M_A,R_A,i|M,R}(m_A,r_A)\cdot dm_A\cdot dr_A}\right)\cdot f_{M,R,i}(m,r)\cdot dm\cdot dr \tag{2.20}$$

All the terms of the equation have been already defined discussing Equation (2.15); see Iervolino et al. (2018) for derivation of the equation.

2.4. Multi-site hazard

2.4.1. Framework

MSPSHA allows to account for the stochastic dependence existing between the site-specific processes, each counting the number of exceedances of a threshold of interest over time. In fact, even if the process counting exceedances at each of the sites is a HPP, that is Equation (2.2), these HPPs are (in general) not independent. Then, the process that counts the total number of exceedances observed at the ensemble of the sites over time is not a HPP (see Giorgio and Iervolino, 2016). In other words, the IMs generated at different sites by the same event are somehow correlated; the sources of dependence among IMs are explored in more detail in Section 5.2.

Considering a set of spatially-distributed sites, say n_{sts} in number, one can define the vector collecting the thresholds of the IM of interest, one for each site, $\left\{im_{thr,1}, im_{thr,2}, ..., im_{thr,n_{sts}}\right\}$. Given the vector of thresholds, MSPSHA allows to obtain different results when multiple sites are of concern. For example, two possible outcomes can be the probabilistic distribution of the number of sites experiencing at least one exceedance of the vector of thresholds in the ΔT time interval, or the distribution of the total number of exceedances collectively observed at the sites in ΔT.

In general, thresholds at the sites can be in terms of different IMs. In this case, the same reasoning discussed for one IM can be applied. For example, if one considers, as IMs, two pseudo accelerations at two spectral periods, $IM_1 = Sa(T_1)$ and $IM_2 = Sa(T_2)$, it is generally assumed that, given an earthquake of m and $\{x, y\}$ characteristics, the logarithms of IMs at the sites form a Gaussian random field (GRF), a realization of which is a $1 \times (n_{sts} \cdot 2)$ vector of the type $\left\{im_{1,1}, im_{1,2}, ..., im_{1,n_{sts}}, im_{2,1}, im_{2,2}, ..., im_{2,n_{sts}}\right\}$. This means that the logarithms of IMs have a multivariate normal distribution where the components of the mean vector are given by the $E(\log IM_1 | m, r_j, \theta)$ and

$E\left(\log IM_2 | m, r_j, \theta\right)$ terms, being r_j the distance between the site j and the location of the seismic event, and the covariance matrix, Σ, is in Equation (2.21). In the equation, $\sigma_{\text{inter},1}$ and $\sigma_{\text{inter},2}$ are the standard deviations of the inter-event residuals of the GMPE of the two IMs, while $\sigma_{\text{intra},1}$ and $\sigma_{\text{intra},2}$ are the standard deviation of intra-event residuals of $Sa\left(T_1\right)$ and $Sa\left(T_2\right)$, respectively; $\rho_{\text{inter}}\left(T_1, T_2\right)$ is the correlation coefficient between inter-event residuals at the two spectral periods in the same earthquake, while $\rho_{\text{intra}}\left(T_1, T_2, h_{i,j}\right)$ is the correlation coefficient between intra-event residuals of the GMPE of $Sa\left(T_1\right)$ and $Sa\left(T_2\right)$ for sites i and j; $h_{i,j}$ is the inter-site distance. In this case, Σ is the sum of two square matrices, each of $\left(n_{sts} \cdot 2\right) \times \left(n_{sts} \cdot 2\right)$ size. The first matrix accounts for the cross-correlation (i.e., spectral correlation) of inter-event residuals which is, by definition, independent on the inter-site distance; the second matrix accounts for the intra-event residuals spatial cross-correlation and is dependent on both inter-site distance and selected spectral periods. Assigning the mean vector and the covariance matrix completely defines the GRF in one earthquake (e.g., Baker and Jayaram, 2008; Esposito and Iervolino, 2012; Loth and Baker, 2013; Markhvida et al., 2018).

$$\Sigma = \begin{bmatrix} \sigma^2_{\text{inter},1} & \cdots & \sigma^2_{\text{inter},1} & \rho_{\text{inter}}(T_1,T_2)\cdot\sigma_{\text{inter},1}\cdot\sigma_{\text{inter},2} & \cdots & \rho_{\text{inter}}(T_1,T_2)\cdot\sigma_{\text{inter},1}\cdot\sigma_{\text{inter},2} \\ & \ddots & \vdots & \vdots & \ddots & \vdots \\ & & \sigma^2_{\text{inter},1} & \rho_{\text{inter}}(T_1,T_2)\cdot\sigma_{\text{inter},1}\cdot\sigma_{\text{inter},2} & \cdots & \rho_{\text{inter}}(T_1,T_2)\cdot\sigma_{\text{inter},1}\cdot\sigma_{\text{inter},2} \\ & & & \sigma^2_{\text{inter},2} & \cdots & \sigma^2_{\text{inter},2} \\ & & \textit{sym} & & \ddots & \vdots \\ & & & & & \sigma^2_{\text{inter},2} \end{bmatrix} + \\ + \begin{bmatrix} \sigma^2_{\text{intra},1} & \cdots & \rho_{\text{intra}}(T_1,T_1,h_{1,n_{sts}})\cdot\sigma^2_{\text{intra},1} & \rho_{\text{intra}}(T_1,T_2,h_{1,1})\cdot\sigma_{\text{intra},1}\cdot\sigma_{\text{intra},2} & \cdots & \rho_{\text{intra}}(T_1,T_2,h_{1,n_{sts}})\cdot\sigma_{\text{intra},1}\cdot\sigma_{\text{intra},2} \\ & \ddots & \vdots & \vdots & \ddots & \vdots \\ & & \sigma^2_{\text{intra},1} & \rho_{\text{intra}}(T_1,T_2,h_{n_{sts},1})\cdot\sigma_{\text{intra},1}\cdot\sigma_{\text{intra},2} & \cdots & \rho_{\text{intra}}(T_1,T_2,h_{n_{sts},n_{sts}})\cdot\sigma_{\text{intra},1}\cdot\sigma_{\text{intra},2} \\ & & & \sigma^2_{\text{intra},2} & \cdots & \rho_{\text{intra}}(T_2,T_2,h_{1,n_{sts}})\cdot\sigma^2_{\text{intra},2} \\ & & \textit{sym} & & \ddots & \vdots \\ & & & & & \sigma^2_{\text{intra},2} \end{bmatrix} \quad (2.21)$$

2.4.2. Simulation-based approach

Computing MSPSHA requires collecting realizations of the GRF with the discussed covariance structure at the sites. One of the possible approaches is the Monte Carlo simulation. In this context, this section describes a two-step procedure for simulation of the IM random fields, illustrated in Figure 2.1, which has been implemented in the software presented in Section 2.5. For simplicity, a single seismic source is considered.

In the first step, magnitudes and locations of the earthquakes occurring on the source are sampled according to their distribution. Thus, in accordance with the adopted GMPE and Σ, the realizations of the IMs at the sites are simulated. In other words, this first step collects a dataset of IMs at the sites conditional to the occurrence of a seismic event. With reference to Figure 2.1, n_m, n_{xy} and n_ε are the indices counting the number of simulations for magnitude, event location and GRF residuals at the sites, respectively; the total number of simulations for each variable is indicated with N_m, N_{xy} and N_ε. Thus, at the end of the first step $N_m \cdot N_{xy} \cdot N_\varepsilon$ vectors are obtained. Each vector represents the realizations of IMs at the sites in one generic event, which is time-invariant. For example, if two IMs are considered in the analysis, the generic vector is of the type $\left\{im_{1,1}, im_{1,2}, ..., im_{1,n_{sts}}, im_{2,1}, im_{2,2}, ..., im_{2,n_{sts}}\right\}$.

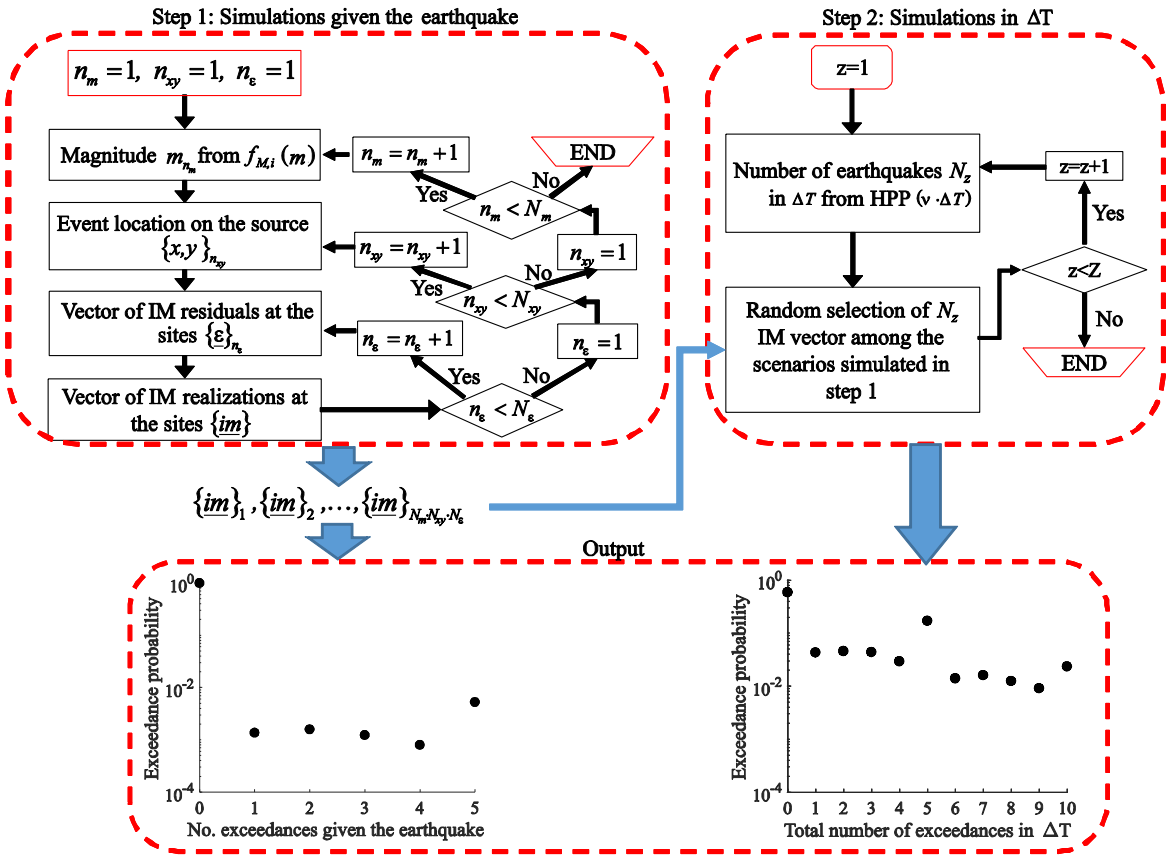

Figure 2.1. Flowchart of the simulation procedure for MSPSHA in the case of single seismic source.

The second step simulates Z seismic histories at the sites in the ΔT of interest. In particular, at the *z*-th run the number of earthquakes on the source is sampled from a HPP with mean $\nu \cdot \Delta T$. Then, a number of IM random fields, equal to the sampled number of events, is randomly selected among those generated in the first step of the procedure. Thus, at the end of this step, each of the Z seismic histories collects a certain number of IM random fields, representing what would occur in ΔT at the sites.

The realizations of the random fields given the occurrence of a generic event and the simulated seismic histories can be used to compute any MSPSHA result (see Section 2.6.2). For example, if three sites are considered in the analysis, one can be interested in computing the joint probability of observing in ΔT two exceedances of the threshold at first site and one exceedance at second and third site. Given the simulated seismic histories, it is sufficient to count in how many two exceedances at first site and one exceedance at second and third site of the $\{im_{thr,1}, im_{thr,2}, im_{thr,3}\}$ vector have been observed, and then divide by the total number of simulated histories.

In the case of n_s seismic sources, the first step of the above-described procedure is simulated n_s times. Thus, at the end of the step, for each source the random fields at the sites are collected. In the second step, at the *z*-th run the number of earthquakes occurring collectively on all the sources in ΔT is sampled from a HPP with mean $\Delta T \cdot \sum_i \nu_i$. Similarly to the case of single source, the sampled number of earthquakes is used to sample the same number of random fields among those generated in the first step. The number of realizations to be selected for each source is proportional to the probability that given that an earthquake occurs it is from source i, that is $\nu_i / \sum_i \nu_i$. At this point the seismic history in ΔT for the sites is obtained in analogy to the case of one source.

2.4.3. MSPSHA shortcuts for GMPEs with additive factors

Similarly to Section 2.2.3, this section is intended to provide some helpful shortcuts that apply (only) in the case of GMPEs of the type in Equation (2.5). In fact, since the

covariance of two or more RVs does not change adding constant terms, the structure of the GMPE of the type in Equation (2.5) implies that the RV representing the logarithms of IM for a site with soil conditions represented by θ, is obtained by adding such a coefficient to the RV representing the logarithms of IM for a reference condition for which $\theta = 0$ (i.e., rock). In other words, the covariance matrix of the GRF is not dependent of the soil class of each site. This means that GRF realizations reflecting the different soil conditions at the sites from those for the reference case can be obtained by adding to the logarithms of the simulated IMs the site-specific coefficients, that is $\left\{\theta_1, \theta_2, \ldots, \theta_{n_{sts}}\right\}$, from the GMPE.

This issue has important practical consequences for multi-site hazard. In fact, one may seek the probability of observing, in a given time interval, a certain number of exceedances of the ground motion intensity measure thresholds vector. Once realizations of GRF are carried out considering rock soil condition for all sites, simulations are not required to be run again if one wants to compute such probability considering different soil conditions for the sites. It is interesting to note that, equivalently, and even simpler, one can account for the different soil conditions by simply subtracting to each element of the thresholds vector the site-specific soil coefficients.

In closing this section, it has to be emphasized that, as mentioned, several recent GMPEs are not of the type in Equation (2.5) for what concerns the soil term, and these shortcuts do not apply. Nevertheless, this same reasoning holds in the case θ of Equation (2.5) represents any other factor affecting the IMs, not only soil site class.

2.5. REASSESS V2.0: functionalities and input of the analyses

REASSESS V2.0 implements the types of hazard assessment discussed in the previous sections. It is coded in MATHWORKS®-Matlab and profits of a graphical user interface. The GUI features one input panel and two output panels, one for PSHA/SPSHA and one for MSPSHA. In fact, the main GUI is complemented by

secondary interfaces that pop up when needed (see Figure 2.2). Note that, in the case of extended analyses (e.g., several seismic sources or sites), input can also be defined via dedicated Microsoft®-Excel spreadsheets, as a shortcut.

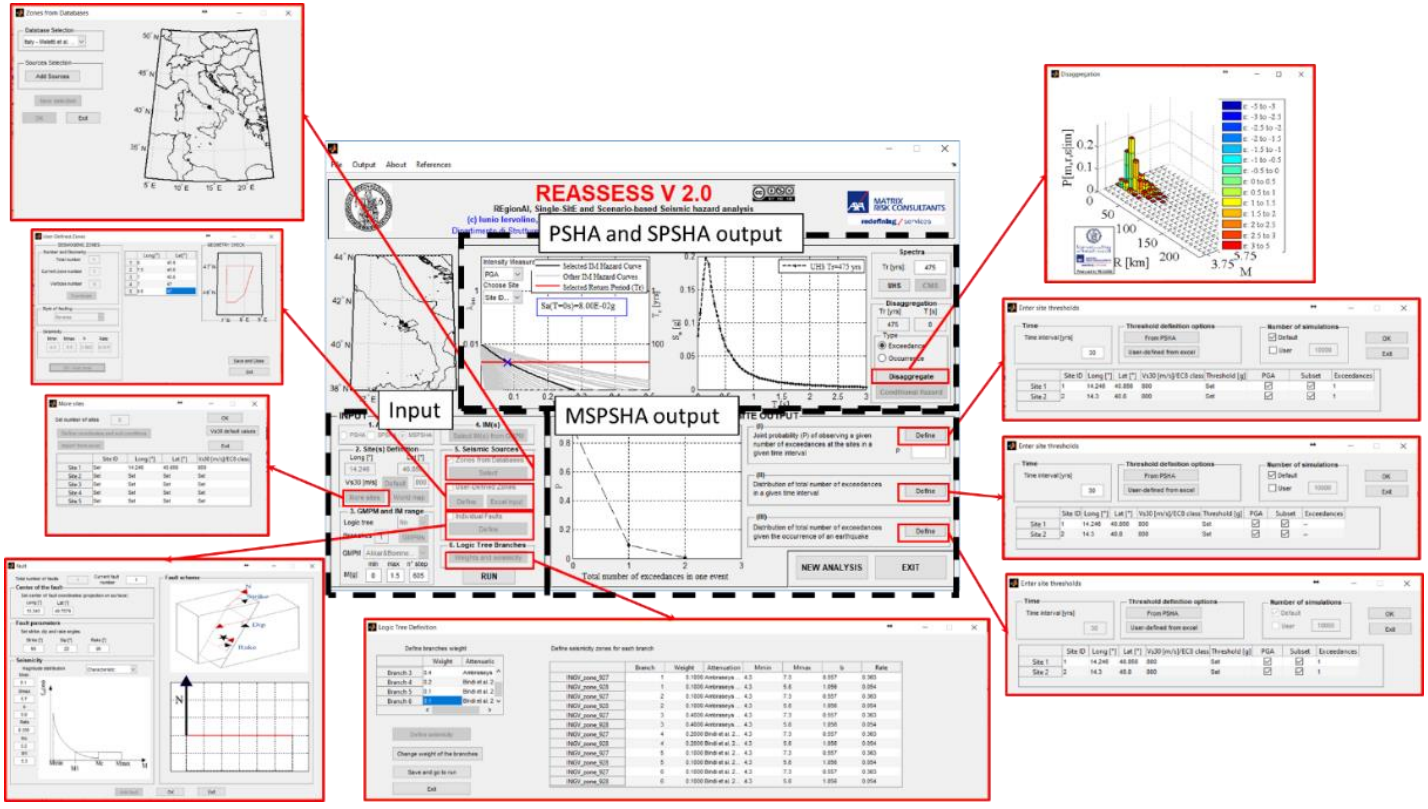

Figure 2.2. Principal and auxiliary GUIs of REASSESS V2.0.

Figure 2.3 provides a schematic flowchart of the way the software operates. It can be observed that the definition of the input of the analysis is divided in five different steps. The first step requires the user to declare the type of analysis to be performed; i.e., PSHA, SPSHA, or MSPSHA. If MSPSHA is selected, more than one site must be defined, and the analyses are performed according to what discussed in Section 2.4.2. When MSPSHA is selected, the corresponding PSHA is also performed for the considered sites, as it is considered a reference case according to Giorgio and Iervolino (2016). However, in the case of PSHA or SPSHA, multiple sites can also be defined. In this case, REASSESS V2.0 will run single-site PSHA or SPSHA separately for each of them according to Section 2.2 or Section 2.3. It is noted that when SPSHA is selected, the software also provides results of the corresponding PSHA.

The definition of the coordinates and soil conditions of the sites is the second step. It can be carried out via the GUI or via an Excel spreadsheet, for which a template is given. The soil conditions can be defined in terms of the soil classes (from A to E) according to the Eurocode 8 classification of sites (CEN, 2004), or also in terms of shear wave velocity of the top 30 meters of subsurface profile $(V_{S,30})$ expressed in meter/second.

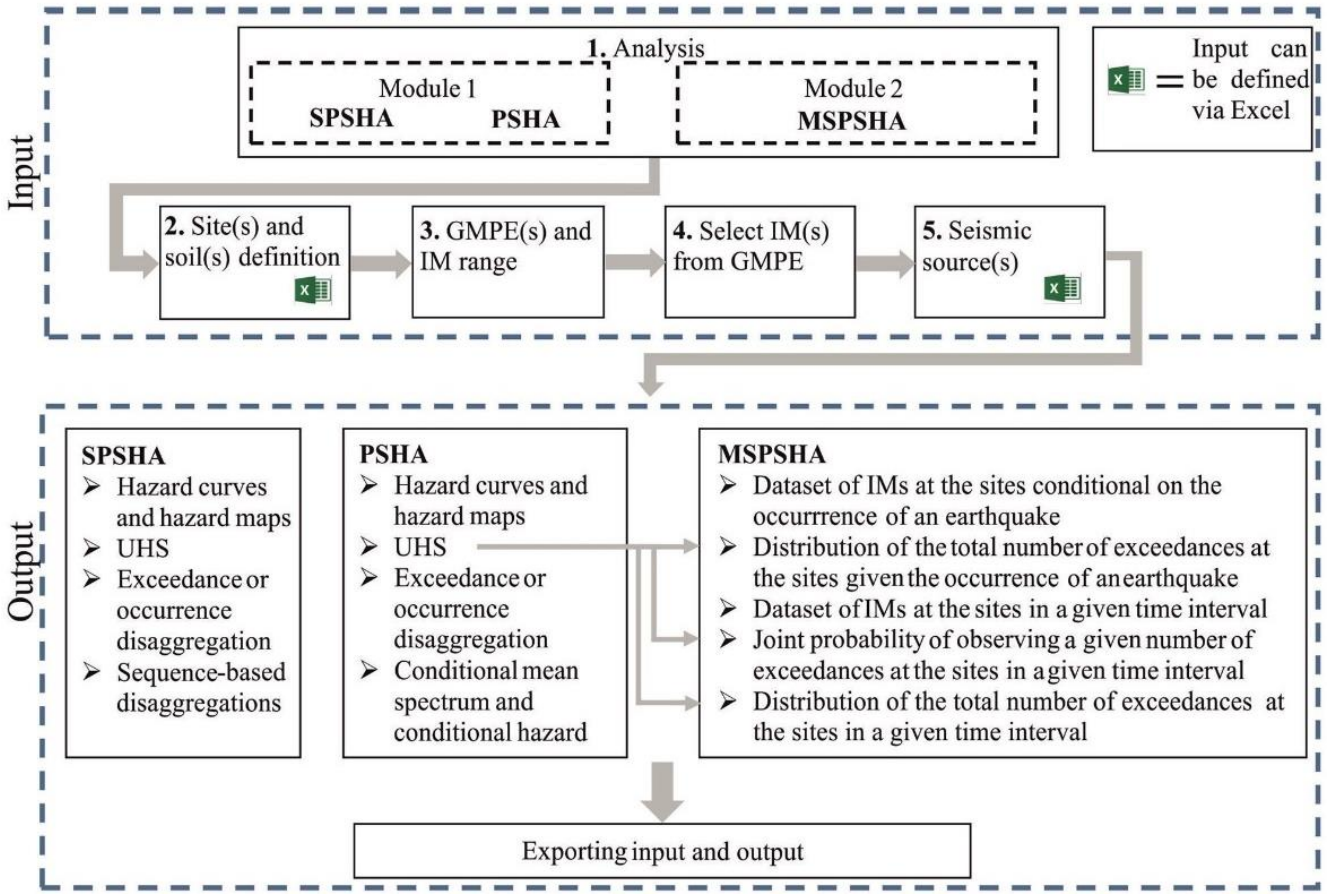

Figure 2.3. REASSESS V2.0 flowchart showing single-site and multi-site modules functionalities.

The third step is dedicated to the selection of the GMPE. A database of alternative GMPEs is included in the current release of REASSESS V2.0: Ambraseys et al. (1996), fitted on a European dataset, Akkar and Bommer (2010), which refers to data from southern Europe, North Africa, and active areas of the Middle East, Bindi et al. (2011), fitted on Italian dataset and Cauzzi et al. (2015), based on a worldwide dataset. It is worthwhile to note that these GMPEs are of the type in Equation (2.5), then the shortcuts discussed in Section 2.2.3 and Section 2.4.3 apply. Also note that although the Ambraseys et al. (1996) GMPE dates more than twenty years ago, it has been implemented because it is the one the current official Italian hazard model is based on (Stucchi et al., 2011). At this step, also the discretization of the domain of the intensity measure for single-site PSHA, which serves to lump the hazard curves, has to be defined in terms of minimum, maximum values and number of intermediate steps (constant in logarithmic scale). In the case of PSHA, the third step also allows the definition of a logic tree (Section 2.2.3) in terms of: (i) parameters of the magnitude distributions, (ii) mean annual frequency of earthquake occurrence on the sources and (iii) GMPEs (among those available).

The current version of the software allows to consider as IMs only spectral pseudo-acceleration for different natural vibration periods (or advanced spectral-shape-based IMs, as shown in the following). However, the choice of the IMs (fourth step) is dependent on the selected GMPE. If a logic tree with different GMPEs for each branch has been defined, the selection is among the IMs of the GMPE belonging to the branch with the highest weight. If different branches have the same weight, the selection is among the IMs of the GMPE selected for the first branch.

When PSHA is of concern, REASSESS also allows to perform analysis for advanced spectral-shape-based intensity measures such as I_{Np} proposed by Bojórquez and Iervolino (2011) and reported in Equation (2.22) in logarithmic. The I_{Np} is a proxy of the pseudo-acceleration response spectral shape in a range of periods $(T_1...T_N)$ and is

dependent on a reference period $(\bar{T})$ belonging to the $(T_1...T_N)$ interval and an α parameter. In its analytical expression $Sa_{avg}(T_1...T_n)$ appears; it is the geometric mean of the spectral acceleration in the $(T_1...T_N)$ range of periods (Baker and Cornell, 2006a). In the software, $(T_1...T_N)$, $\bar{T}$ and α can be selected by the user, as Figure 2.4 shows (the periods can be chosen among those of the selected GMPE). It is easy to see that when the α parameter equals one, I_{Np} corresponds to $Sa_{avg}(T_1...T_n)$.

$$\log(I_{Np}) = \log[Sa(\bar{T})] + \alpha \log\left[\frac{Sa_{avg}(T_1...T_N)}{Sa(\bar{T})}\right] \tag{2.22}$$

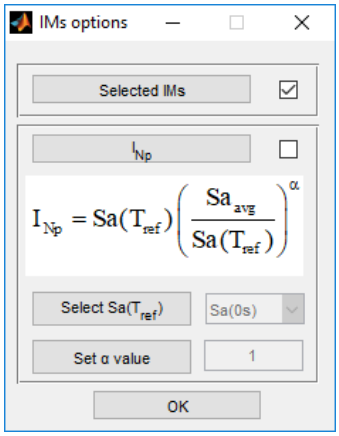

Figure 2.4. GUI for the definition of the parameters for I_{Np} in REASSESS.

In the case of MSPSHA, when a single spectral ordinate is selected as IM, the user is allowed to choose the model of spatial correlation of intra-event residuals of Esposito and Iervolino (2012) or Loth and Baker (2013). On the other hand, when the IMs at the sites are spectral ordinates for several natural vibration periods, simulated spatially cross-correlated scenarios are computed adopting the models of (i) Loth and Baker (2013) for the spatial cross-correlation of intra-event residuals and (ii) Baker and Jayaram (2008) for the cross-correlation of inter-event residuals.

Step 5 is dedicated to the seismic source definition. In REASSESS V2.0, seismic source zones and/or finite three-dimensional faults can both be input of analysis. Source zones can be completely defined by the user or selected from an embedded database. In the first case, the user is required to define the coordinates of the vertices of the zone, the annual rate of occurrence of earthquakes and the event's magnitude distribution, which is assumed to be a truncated exponential distribution; hence, the slope of the G-R relationship, together with minimum and maximum values of magnitude, are required. If known, a rupture faulting style can be associated to the seismic zone. All the required parameters can be alternatively given via GUI (see Figure 2.5) or Excel spreadsheet.

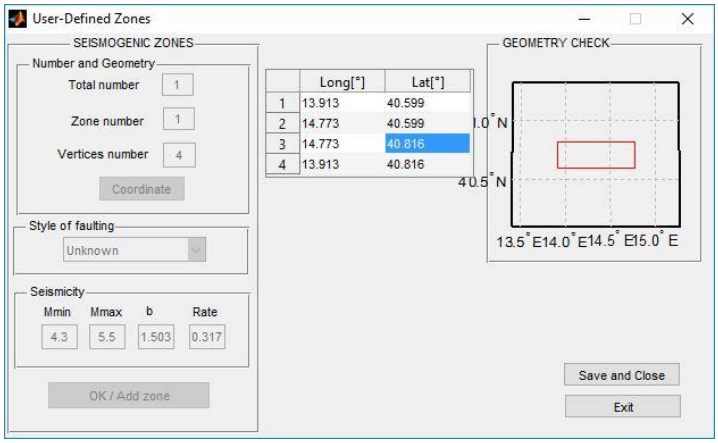

Figure 2.5. GUI for the definition of seismogenic zones in REASSESS.

In the second case, the user can select one or more seismic zones from an existing database. In fact, a number of literature databases of seismic zones is implemented in the current version of REASSESS. Referring to Italy, it is known that the seismic hazard study of Stucchi et al. (2011) lies at the basis of the hazard assessment for the Italian current building code and features a logic tree made of several branches; the branch named 921 is the one producing the results claimed to be the closest to those provided by the full logic tree. This branch considers the seismic source model of thirty-six areal zones of Meletti et al. (2008) and the GMPE by Ambraseys et al. (1996) (see also Section 3.2). It is implemented in REASSESS V2.0 and is named *Meletti et al. (2008)* –

Magnitude rates from DPC-INGV-S1–- Branch 921. It is the sole database selection which implies an automatic selection of GMPE and seismic zones. An alternative source model for Italy is named *Meletti et al. (2008) – Magnitude rates from Barani et al. (2009),* in which the same source model of Meletti et al. (2008) is considered, but the associated seismic characterization is from Barani et al. (2009). Other databases in REASSES are the one from the SHARE project, which covers the Euro-Mediterranean region, the one from the EMME project, which covers middle-east; i.e., Afghanistan, Armenia, Azerbaijan, Cyprus, Georgia, Iran, Jordan, Lebanon, Pakistan, Syria and Turkey. Moreover, included databases are: El-Hussain et al. (2012), Ullah et al. (2015) and Nath and Thingbaijam (2012), referring to the Sultanate of Oman, Kazakhstan, Kyrgyzstan, Tajikistan, Uzbekistan and Turkmenistan, and India, respectively. The area covered by the embedded databases is given in Figure 2.6.

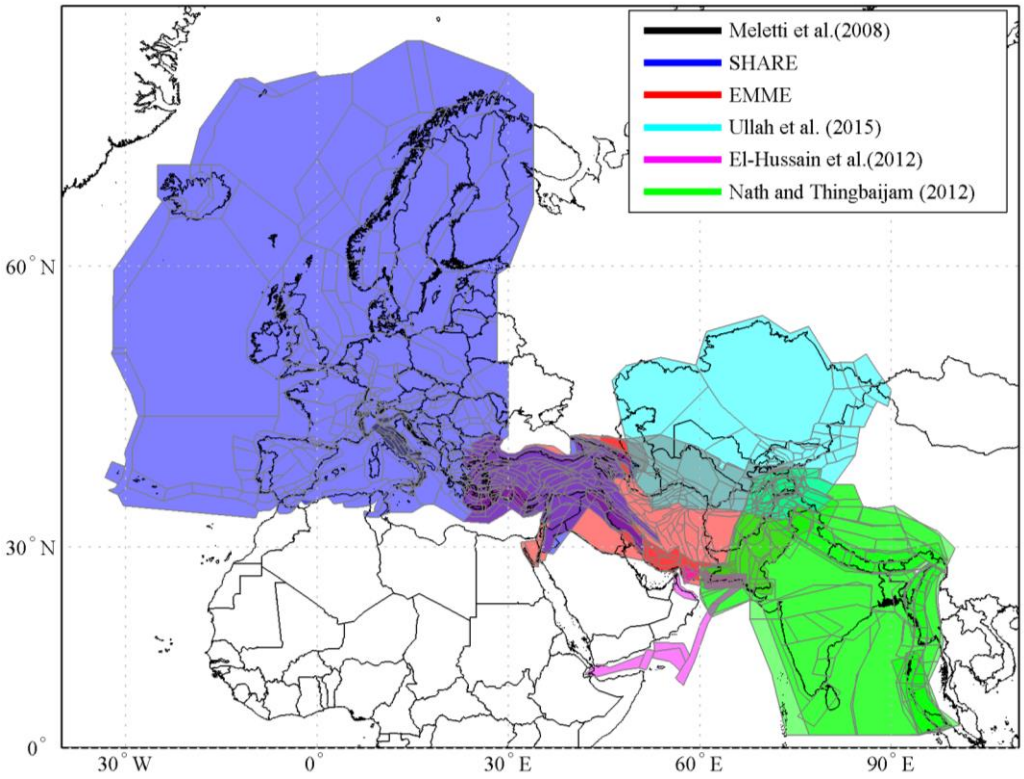

Figure 2.6. Embedded databases of seismogenic sources.

One or more finite faults can also be defined. There are many alternative ways to define the characteristics of a fault and to simulate the possible ruptures on it (Scherbaum et al., 2004). In the current version of REASSESS, the fault characterization can be done following two different approaches. In the first, the surface coordinates of the center of the fault are required. Then, the dip, rake, and strike angles (Aki and Richard, 1980) have to be defined. In the second, the fault can be defined through the trace along with its rake and dip angles, upper and lower seismogenic depth and ruptures' aspect ratio. The definition of seismicity is common to both the models. The magnitude distribution of generated earthquakes can be chosen among the G-R and the characteristic model (e.g., Convertito et al., 2006). The details on hazard computation, in the case one or more faults are considered, are given in Section 2.5.1.

As introduced above, REASSESS allows the user to account for the model uncertainty through the logic tree. The alternative branches of the logic tree can account for different GMPEs, G-R parameters and annual rates of earthquakes occurrence. On the other hand, the number and geometry of the seismic sources cannot change in each branch. A weight has to be assigned to each branch (all the weights must sum to one).

When SPSHA is performed, the model describing the aftershock occurrence has to be specified, that is the parameters of Equation (2.17). The available models are those of Reasenberg and Jones (1989 and 1994), Lolli and Gasperini (2003) and Eberhart-Phillips (1998) which refer to generic California, Italian and New Zealand aftershock sequence, respectively. Such models, can be selected through a dedicated window (Figure 2.7), automatically opened by REASSESS before running the SPSHA. In the current version of the software, the GMPE selected for PSHA is also applied to account for the evaluation of aftershock's IM.

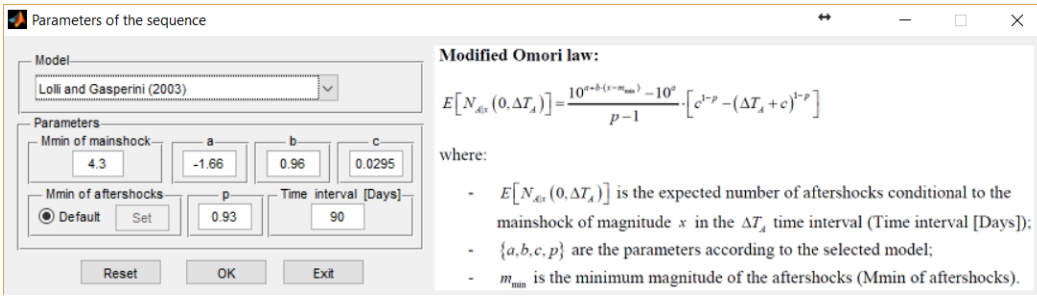

Figure 2.7. Graphical interface window for calibration of the aftershock occurrence models.

2.5.1. Analysis with finite faults

REASESS also allows to compute hazard analysis (both PSHA and MSPSHA) in the case the seismic sources are represented by means of one or more finite faults. As introduced in the previous section, in the current version of REASSESS there are two alternative ways to define the characteristics of a fault. In the first, a fault can be defined by means of a point representing its center and the dip, rake, and strike angles. In this case, PSHA is carried out according to Equation (2.23), which is an adaptation of Equation (2.3) and is written, for simplicity, in the case a single fault is considered.

$$\lambda_{im} = \nu \cdot \int_X \int_Y \int_M \int_A \int_S P\left[IM > im \mid m,x,y\right] \cdot f_{S|A}(s) \cdot f_{A|M}(a) \cdot f_M(m) \cdot \cdot f_{X,Y}(x,y) \cdot ds \cdot da \cdot dm \cdot dx \cdot dy \tag{2.23}$$

In the equation, ν is the rate; $\{X,Y\}$ is the position of the center of the rupture with respect to the center of the fault and its distribution, $f_{X,Y}(x,y)$, is taken according to Mai et al. (2005); $f_M(m)$ is the magnitude distribution that can be defined as G-R or characteristic; $f_{A|M}(a)$ is the distribution of the rupture size conditional to the magnitude, which is modelled according to Wells and Coppersmith (1994); finally, $f_{S|A}(s)$ is the aspect ratio (length-to-width ratio) of the rupture and is probabilistically modelled lognormally according to Iervolino et al. (2016b). The depth of the top of the rupture is assumed to be equal to five kilometres for all events of magnitude less than

6.5 and one kilometre for events of larger magnitude, following the practice of the U.S. Geological Survey[1].

Alternatively, a fault can be defined by means of its trace, rake and dip angles, upper and lower depth. Thus, differently from the previous case, the user completely defines the geometry of the fault. In the hazard computation, the area and aspect ratio of the ruptures are not considered as RVs, and Equation (2.24) applies.

$$\lambda_{im} = \nu \cdot \int_X \int_Y \int_M P\left[IM > im \mid m,x,y\right] \cdot f_M(m) \cdot f_{X,Y}(x,y) \cdot dm \cdot dx \cdot dy \tag{2.24}$$

In particular, given the magnitude, the rupture's area is the median area from the area-magnitude scaling relationship of Wells and Coppersmith (1994), while the aspect ratio is an input of the analysis. Similarly to Equation (2.23), $f_M(m)$ is the magnitude distribution and $\{X,Y\}$ denotes the position of the rupture on the fault, which is assumed to be uniformly distributed.

2.6. Output of REASSESS V2.0

At the end of the analysis, all the results can be consulted via the GUI in the format of figure or text file. The user is allowed to save all the input and output (figures and text files) in a compressed folder; in addition, it is also possible to save and load the whole work-session. In Section 2.6.1 and Section 2.6.2 the available outputs from single- and multi-site PSHA are described, respectively.

2.6.1. Single-site PSHA analysis

When the analysis is finished, the hazard curves for the selected IMs are plotted in the single-site output panel (see Figure 2.2). A dropdown menu allows the user to select a specific IM and the corresponding hazard curve is automatically highlighted. The UHS

[1] However, this constraint is not strictly needed and could be relaxed in updated versions of REASSESS.

can be computed for any return period available due to the range of IMs defined at the beginning. It is displayed in the right plot of the single-site output panel. If the analysis is performed for multiple sites, the hazard curves and UHS for each of the sites can be displayed (via a dropdown menu).

REASSSES V2.0 is able to provide exceedance or occurrence disaggregation (see Sections 2.2.2) for a return period and IM of interest. The return period is the one chosen for the UHS, while the IM corresponds to the selected hazard curve. When the disaggregation for the exceedance is computed, the software also provides the value of the expected exceedance over the threshold being disaggregated (see Section 3.4). Moreover, given the return period and IM for which disaggregation has been computed, the software is able to provide CS (Section 2.2.4) and conditional hazard (Section2.2.5). In particular, the CS is computed by REASSESS V2.0 profiting of the model of Baker and Jayaram (2008), which provides the correlation among spectral acceleration values at different spectral periods; it is noted that the CS is displayed on the same plot for UHS. Conditional hazard can be carried out in the secondary GUI shown in Figure 2.8, in which a dropdown menu allows the user to select the secondary IM. The software performs conditional hazard profiting of the models of Baker and Jayaram (2008) and Bradley (2012); the latter provides correlation between peak ground velocity (PGV) and spectral accelerations. Indeed, the distribution of PGV or pseudo-acceleration response spectra at any vibration period conditional to occurrence of the primary IM is displayed in the dedicated plot (see Figure 2.8).

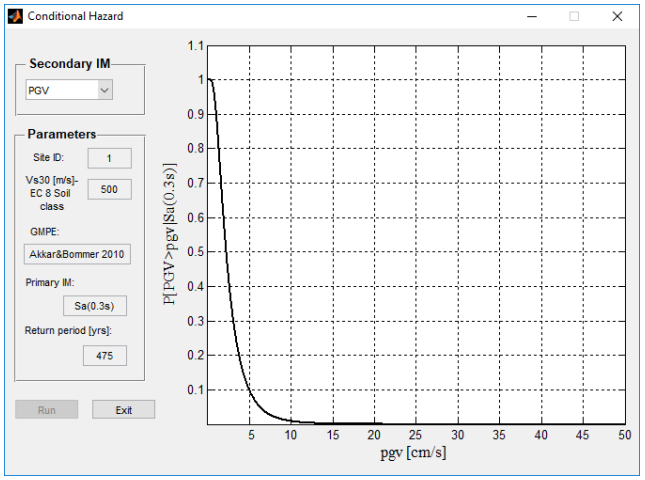

Figure 2.8. GUI for conditional hazard in REASSESS.

Results of SPSHA are similar to those for PSHA; however, disaggregation is of two kinds (see Section 2.3.1). The first is the joint pdf of magnitude and distance of the mainshock conditional to the exceedance, or the occurrence, of a chosen hazard threshold during the corresponding cluster (Equation 2.19). The second disaggregation provided represents the probability that, given that exceedance of *im* has been observed during the mainshock-aftershock sequence, it was in fact an aftershock to cause it (Equation 2.20). Finally, SPSHA/PSHA results can be alternatively displayed on the GUI via a dedicated drop down menu, as Figure 2.9 shows.

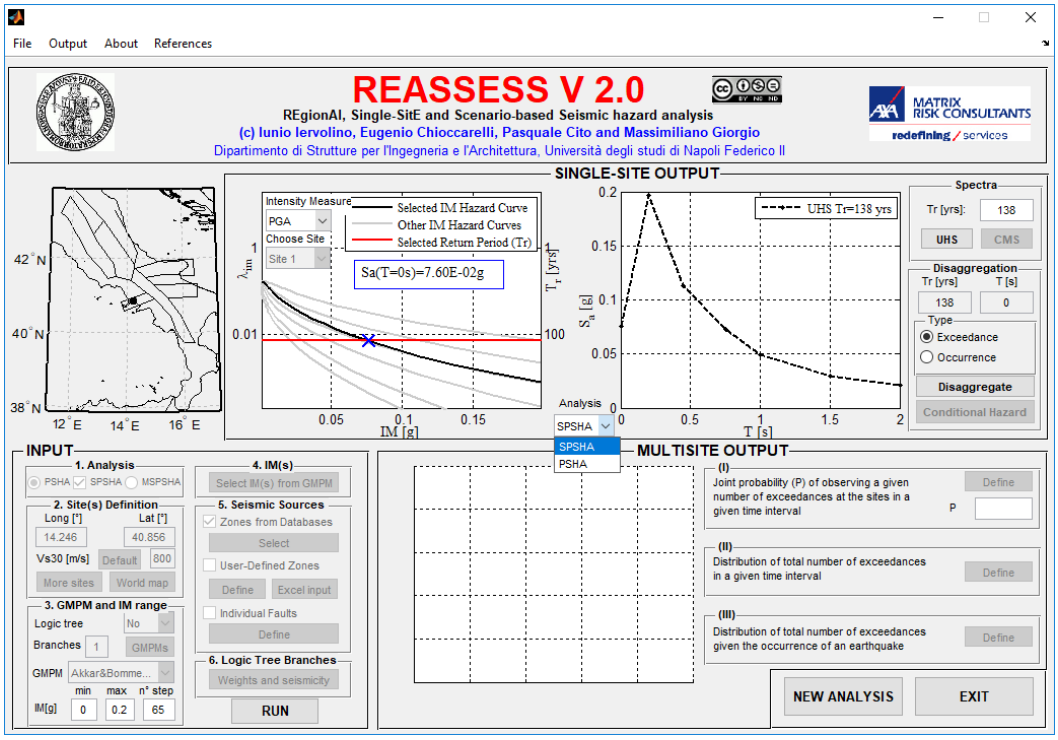

Figure 2.9. Main GUI of REASSESS with single-site PSHA output. The analysis drop down menu for selecting SPSHA/PSHA is also shown.

2.6.2. Multi-site PSHA analysis

As stated in Section 2.4.2, MSPSHA is performed through the described two-step simulation procedure. At the end of the first step, the simulated scenarios of IM realizations at the sites given the occurrence of an earthquake on the source(s) are available. At this point, REASSESS V2.0 is able to provide three different results, which can be carried out considering all or a subset of the sites defined at the beginning of the analysis:

(i) the probability of observing an arbitrarily chosen number of exceedances at the sites in a given time interval;

(ii) the distribution of the total number of exceedances at the sites in a given time interval;

(iii) the distribution of the number of exceedances at the sites given the occurrence of an earthquake (time-invariant).

For each of the listed results some additional information are required. First, the time interval and the vector collecting sites thresholds have to be defined. The latter can be completely defined by the user. Alternatively, REASSESS V2.0 allows to define the element of the thresholds vector according to the results of single-site PSHA. For example, the thresholds can be chosen as the values with the same exceedance return period at each site. Furthermore, thresholds can be defined through an automatically generated Excel file. The IM to be considered for each threshold can be selected trough dedicated checkboxes. Before proceeding, the user is also allowed to modify the soil condition for each site. With reference to results (i) and (ii), the second step of MSPSHA computation is involved to simulate the realizations of GRF in a given time interval. Thus, the number of simulations (by default, the software performs 10000 simulations) and the time interval are also required. This step of analysis can be very time-consuming lasting for several hours. Reducing the number of simulations makes the analysis faster but can drastically affect the accuracy of results. Moreover, in the case of (i), which provides the probability of observing an arbitrarily chosen number of exceedances at the sites in a given time interval, the number of exceedances of the thresholds to be observed at each site has to be defined entering the values in the last column of the table in Figure 2.10.

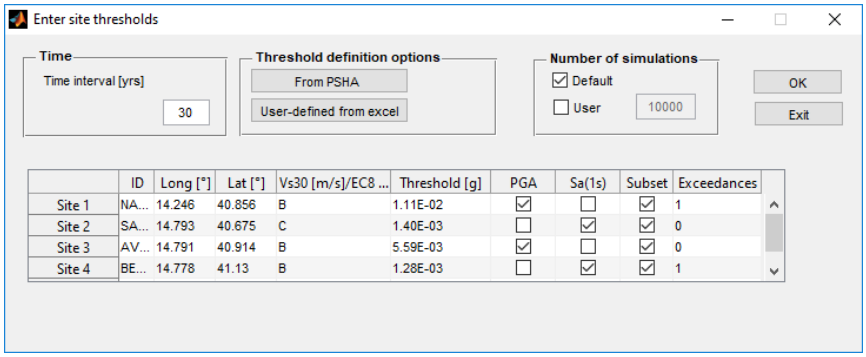

Figure 2.10. GUI for definition of parameters to compute the joint probability of observing a given number of exceedances at the sites in a given time interval in REASSESS.

In the case of result (ii), which provides the PMF of the total number of exceedances observed at the sites in a given time interval, the random variable is the total number of exceedances for the considered subset of sites. Thus, in this second case, the number of exceedances for each site cannot be defined and the corresponding column in the table is neglected (Figure 2.11). If the analysis is performed after having obtained result (i) and if the time interval and number of simulations to be considered are not modified, no more simulations are required and REASSESS only post-processes the simulations taking a reduced computational time.

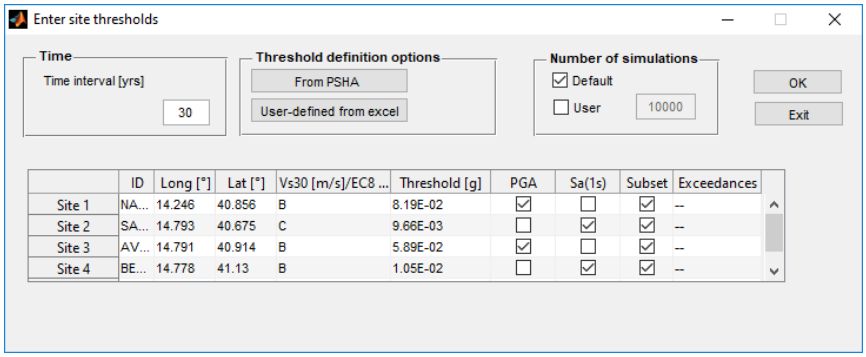

Figure 2.11. GUI for definition of parameters to compute the distribution of total number of exceedances in a given time interval in REASSESS.

Results (i) and (ii) are computed by REASSESS V2.0 for any time interval without repeating the simulations of the first step of analysis thus reducing the required time of

computation. Text files with the GRFs simulated conditional to a generic event and in the selected time interval are also available at the end of the analyses.

Result (iii), which provides the PMF of the total number of exceedances observed at the sites given the occurrence of an earthquake, does not involve any further simulation. In fact, the realizations of GRFs obtained in the first step of MSPSHA are only needed. Thus, the time interval and number of simulations are not required to be defined. Furthermore, since in one earthquake a single exceedance of the threshold at each site can be observed, the last column of the table is neglected and returns "1" for all the sites (Figure 2.12).

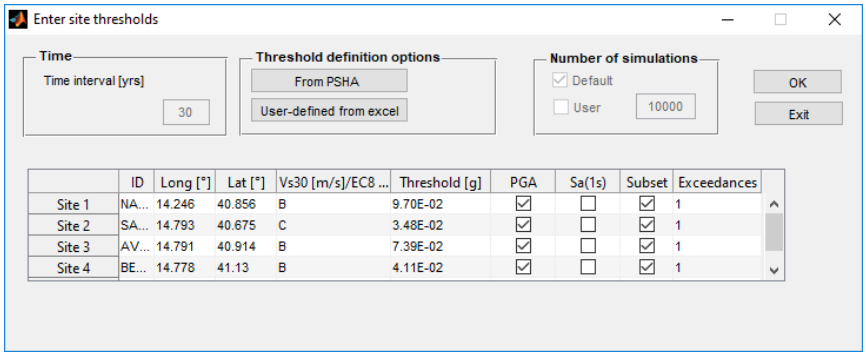

Figure 2.12. GUI for definition of parameters to compute the distribution of total number of exceedances given the occurrence of an earthquake in REASSESS.

Finally, all the described results are displayed on the main GUI of REASSESS. Figure 2.13 shows an example in which the probability mass function of the total number of exceedances observed at the sites in 30 years, from result (ii), is computed.

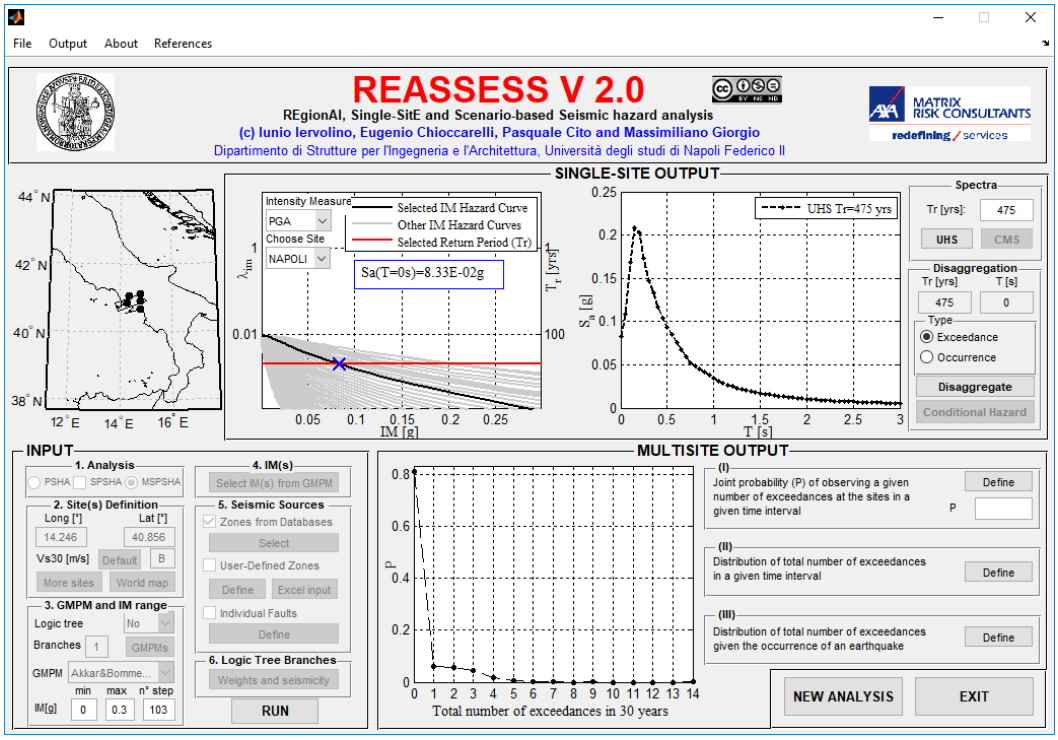

Figure 2.13. Main GUI of REASSESS with single- and multi-site PSHA results.

2.7. Conclusions

In the chapter the basics of classical PSHA were introduced first. Then, two non-conventional hazard methodologies were recalled. In fact, SPSHA allows to account for the effect of aftershocks in the hazard assessment. It was also shown that disaggregation can be performed in the case of SPSHA. In particular, given the exceedance of a threshold of interest during the whole mainshock-aftershock sequence, the mainshock magnitude-distance distribution and the probability that the exceedance is due to an aftershock can be carried out. MSPSHA accounts for the spatial dependence existing between the site-specific processes, each counting the number of exceedances of the threshold over time. Given a vector of thresholds of interest for a portfolio of sites, accounting for the correlation of ground motion IMs is required to investigate different

probabilistic results related to the exceedance possibly observed at the sites. Furthermore, the matrix formulation for the implementation of PSHA and SPSHA were explored; on the other hand, MSPSHA simulates realizations of IM random fields through a two-step procedure which was also illustrated.

In the last forty years several computer programs for PSHA have been developed; in most cases, they do not feature of a GUI and only perform classical PSHA. For these reasons, a stand-alone software named REgional, Single-SitE and Scenario-based Seismic hazard analysis (REASSESS V2.0), provided with a GUI, was developed and presented in the chapter. The tool enables classical PSHA and the more advanced SPSHA and MSPSHA procedures. The definition of input is common to all the kinds of analysis. In particular, the user is required to define site(s) coordinates, GMPE (selected among an embedded database), intensity measures of interest, seismic sources (user-defined three-dimensional faults, area sources or sources selected from databases) and structure of logic tree, if any. In the case of single-site PSHA, REASSESS V2.0 is able to provide classical results such as hazard curves, even in terms of spectral-shape-based (i.e., advanced) ground motion intensity measures. Moreover, uniform hazard and conditional mean spectra, together with disaggregation distributions for the occurrence or the exceedance of the IM threshold, can be computed. Conditional hazard can also be computed for PGV or pseudo-spectral accelerations selected as secondary intensity measures. When SPSHA is of concern, available outputs are hazard curves, UHS, mainshock magnitude-distance disaggregation distribution and aftershock disaggregation. In the case of MSPSHA, given a vector of thresholds for a subset of sites of interest, REASSESS V2.0 is able to provide (i) the joint probability of observing, in the time interval, a given number of exceedances at the sites, (ii) the distribution of the total number of exceedances observed at the sites in the time interval and (iii) the distribution of the total number of exceedances observed at the sites given the occurrence of a generic earthquake. When SPSHA or MSPSHA are performed, the software also provides the classical PSHA outputs.

REASSES was optimized for accuracy of numerical computation, analysis time and ease of use. To this aim it also implements calculation shortcuts and provides a series of options of input/output management. It is finally to note that a practical user guide (tutorial) can be found online at http://wpage.unina.it/iuniervo/doc_en/REASSESS.htm, which is the same site where the software is available under a Creative Commons license: attribution—non-commercial—non derived.

Chapter 3 – THE EXCEEDANCE OF DESIGN ACTIONS FOR STRUCTURES: QUANTIFICATION AND EARTHQUAKE SCENARIOS ANALYSIS

This chapter is derived from the following papers:

Iervolino I, Giorgio M, Cito P (2018) The peak over the design threshold in strong earthquakes. Bull Earthq Eng http://dx.doi.org/10.1007/s10518-018-0503-9.

Iervolino I, Giorgio M, Cito P (2018) Which earthquakes are expected to exceed the design spectra? Earthq Spectra (in revision).

3.1. Introduction

In the framework of performance-based earthquake engineering, design actions are based on PSHA, which provides the ground motion intensity level of design with a certain probability to be exceeded in a given time interval at the site. In other words, design actions are derived from the UHS, that is, they have the same exceedance return period (T_r), which is determined based on the structural performance of interest (i.e., limit-state). For example, according to the Italian building code, the life-safety limit-state of an ordinary structure must be verified for actions deriving from UHS with $T_r = 475$ years. Nevertheless, the comparison of design spectra with those recorded in earthquakes indicates that situations in which structures are subjected to seismic actions larger than the design ones are not rare (e.g., Crowley, 2009). For example, in Italy exceedance of UHS has been observed in the near-source area of the seismic events of L'Aquila (2009), Emilia Romagna (2012), central Italy (2016), even if magnitudes were

not close to the maximum deemed possible (see Iervolino et al., 2010; Masi et al., 2011; Chioccarelli et al., 2012; Luzi et al., 2016). Iervolino and Giorgio (2018) illustrate that the exceedance of the design spectra is not sufficient to question PSHA, as the exceedance of hazard-based design actions is well expected around the source of moderate-to-high earthquakes, pointing out that design actions based on UHS are not conservative in the epicentral areas of earthquakes. Consequently, in these areas structural safety is left to other eventual margins beyond elastic design spectra which cannot be fully controlled.

The study presented in this chapter is intended to deepen this issue, with reference to Italy. In particular, two main results are presented:

- the expected acceleration over the design threshold if the exceedance occurs, which is related to the measure of the safety margins beyond the elastic design acceleration a structure should have to warranty the desired performance;
- the minimum magnitude of earthquakes that, occurring within a certain distance from the site, have a probability of exceeding the design spectrum larger than 0.5.

The study, which refers to two pseudo-accelerations with $T_r = 475$ years, is effectively a practical application of PSHA. In fact, for the purposes of this chapter the seismic hazard and disaggregation maps, calculated via the REASSESS V2.0 software (Chapter 2), are first introduced. Results of the expected exceedance and minimum magnitude of the earthquakes for which exceedance of the design actions is expected are also provided in form of maps. The effect of site-dependent soil conditions is also explored. Finally, the discussion is extended to a range of return periods of design interest for two sites, Milan and L'Aquila, located in regions of Italy characterized by low and high seismic hazard, respectively.

3.2. Seismic source model

For the purposes of the chapter, the seismic source zones and GMPE described in Stucchi et al. (2011) have been adopted to get the results introduced in the previous section. In fact, as mentioned in Section 2.5, the cited work describes the models and analyses assumed to develop the hazard assessment of Italy, which is at the basis of the definition of the structural seismic actions according to the enforced code in the country. Such analyses are carried out via a logic tree made of several branches. Among them, the branch identified as *921* is the one producing the results claimed to be the closest to those provided by the full logic tree.

Branch 921 considers the seismic source model of Meletti et al. (2008), which is made of thirty-six areal seismic source zones, numbered from 901 to 936, shown in Figure 3.1a (this model is common to all the branches of the cited logic tree). The seismicity of each zone is represented by the *activity rates*, that are annual rates of earthquakes occurrence associated to each bin of surface-waves magnitude; the width of the bins, is 0.3. The activity rates, which are published in Iervolino et al. (2018), are graphically shown in Figure 3.1b as a function of the central magnitude value of each bin. As shown, the lowest bin is generally centered on magnitude 4.3, but the zone 936, which is the Etna's volcanic area, has a central magnitude of the lowest bin equal to 3.7. The maximum magnitude depends on the zone of interest.

Finally, branch 921 adopts the Ambraseys et al. (1996) GMPE. The GMPE is applied within its definition ranges of magnitude and distance: these are, surface magnitude between 4.0 and 7.5 and the closest horizontal distance to the surface projection of the fault plane up to 200 km. The effects of earthquakes with magnitude and distance outside these intervals are neglected in the analyses. Assuming a uniform epicenter distribution in each seismogenic zone, epicentral distance is converted into the metric required by the GMPE, that is Joyner and Boore distance (Joyner and Boore, 1981), according to Montaldo et al. (2005). The style-of-faulting correction factors proposed by Bommer at

al. (2003) are also applied to the GMPE in accordance with the rupture mechanism associated to each seismic source zone in the model by Meletti et al. (2008). In accordance with branch 921, rock soil site class is always assumed herein.

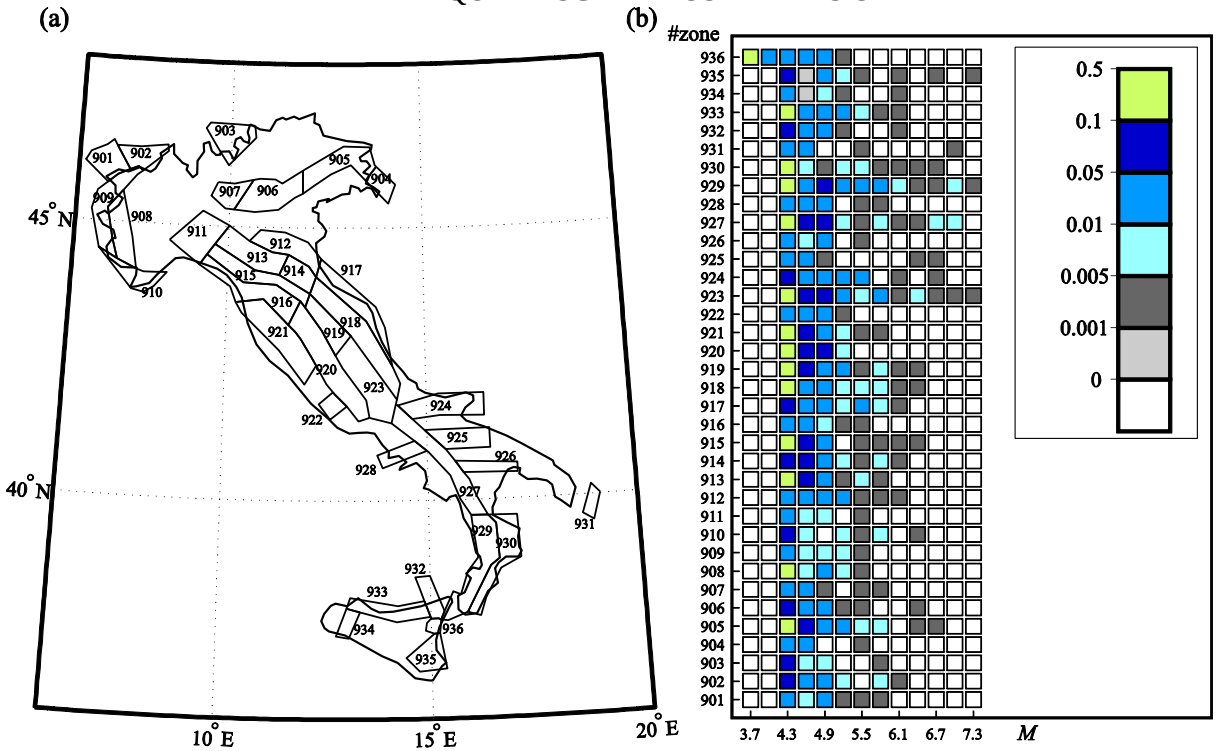

Figure 3.1. The seismic source zone model for Italy, according to the model of Meletti et al. (2008): (a) geographical distribution of the zones; (b) activity rates values for each bin of magnitude (from Chioccarelli et al., 2018).

3.3. Italian seismic hazard

Based on the model described in the previous section, in the next sub-sections the seismic hazard and disaggregation maps of peak ground acceleration (PGA) and $Sa(T=1s)$ with 475 years return period of exceedance at any site are illustrated. All the maps are obtained discretizing the whole national territory via a uniformly spaced grid of about ten-thousand point.

3.3.1. Hazard maps

The seismic hazard map of PGA and $Sa(T=1s)$, provided by the right and left panel of Figure 3.2, respectively, indicate that the design thresholds with 475 years return period (sa_{475}) are larger in central and southern Italy, along the Appenines mountain chain, and in north-east area. For example, with reference to PGA, accelerations greater than 0.25g can be observed in the most of zones 905, 923, 927 and 929. According to the map, the highest PGA which is exceeded, on average, every 475 years, is equal to 0.271g. The corresponding site is Aprigliano (16.36°E, 39.36°N), located in the district of Cosenza (southern Italy). In correspondence of Terratelle village (16.38°E, 39.24°N), less than 15km away from Aprigliano, the hazard map of $Sa(T=1s)$ shows its highest value (0.256g). Both the sites are enclosed by zone 929, which have the largest magnitude of the last bin equal to 7.3.

On the other hand, the lowest hazard levels correspond to 0.030g and 0.023g for PGA and $Sa(T=1s)$, respectively. For both the ordinates, the corresponding site is Pianosa (Pianosa island; 10.06°E, 42.58°N), located outside the source zones (Italian hazard model does not consider background seismicity).

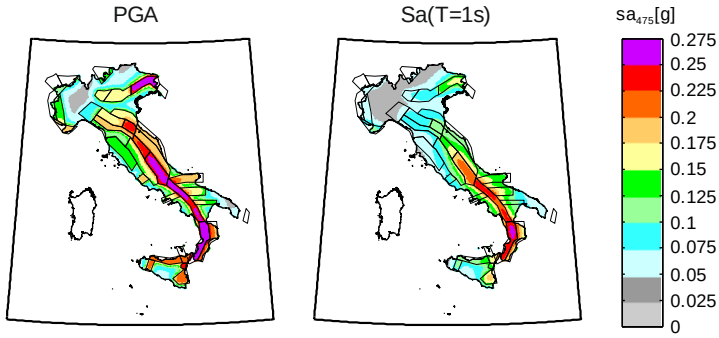

Figure 3.2. Seismic hazard maps of PGA and $Sa(T=1s)$ with $T_r = 475$ years on rock, according to the branch 921 of the logic tree described in Stucchi et al. (2011).

As stated in the introduction, Milan (9.12°E, 45.46°N) and L'Aquila (13.42°E, 42.34°N) are chosen to be representative of low and high hazard sites, respectively. Indeed, Table 3.1 provides the design thresholds with 475 years exceedance return period for the two sites, which will be recalled in the next sections.

Table 3.1. PGA and $Sa(T=1s)$ design thresholds with $T_r = 475$ for Milan and L'Aquila sites.

	Milan	**L'Aquila**
PGA [g]	0.050	0.253
$Sa(T=1s)$ [g]	0.035	0.208

3.3.2. Disaggregation of seismic hazard

As stated in Section 2.2.2, disaggregation of seismic hazard is a procedure that, given a spectral ordinate and return period of interest, allows the identification of the hazard contribution of each M, R and ε. In fact, a typical result of disaggregation is the joint pdf of $\{M, R, \varepsilon\}$ conditional to the exceedance of an IM threshold (see Equation 2.6). In the framework of this chapter, the maps of mean values of $\{M, R, \varepsilon\}$; i.e., $\overline{M}, \overline{R}$ (in terms of Joyner and Boore distance) and $\overline{\varepsilon}$, given the exceedance of sa_{475}, are given in Figure 3.3.

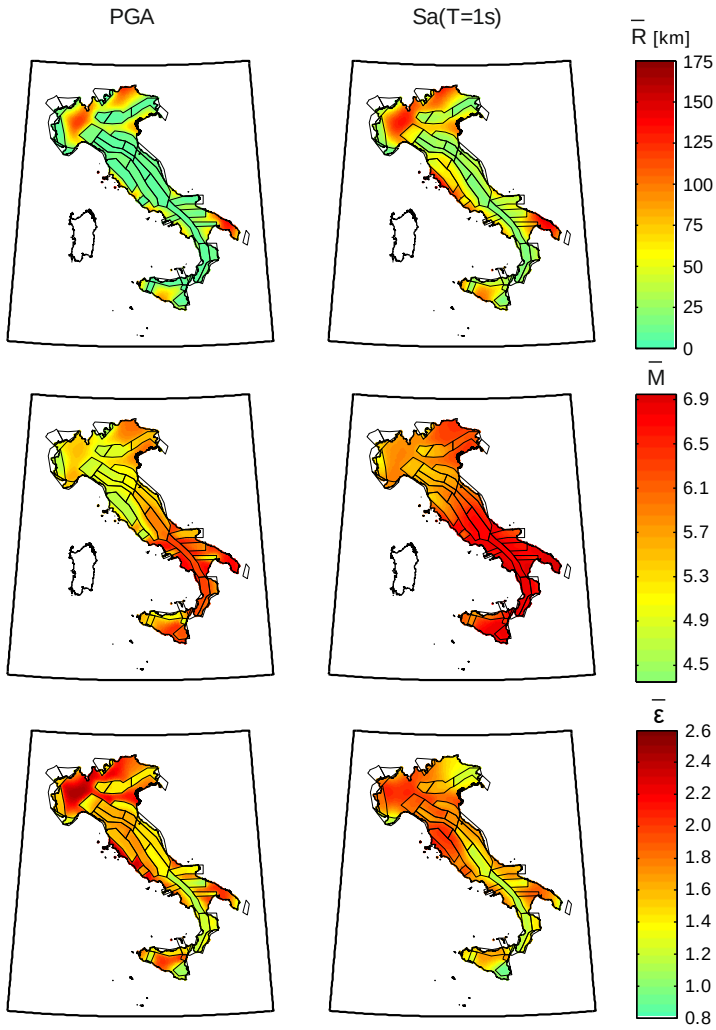

Figure 3.3. Maps of disaggregation in terms of average source-to-site distance, magnitude and ε, given the exceedance of the design PGA and $Sa(T=1s)$ with $T_r = 475$ years.

Even if the disaggregation of Italy is largely discussed in Barani et al. (2009) and Iervolino et al. (2011), some results are remarked. With reference to distance, maps show that the expected value in some cases is larger than 150km. This is related to the considered source model. In fact, there are several sites located in geographical areas (for example, part of the northern Italy) outside the seismic source zones. Conversely, the expected distance is, in general, smaller for the sites enclosed by source zones. In

particular, in the case of PGA the minimum and maximum values of $\overline{R}$ are equal to 6km (Caneso, enclosed by zone 915; 9.58°E, 44.50°N) and 152km (Pianosa), respectively. In the case of $Sa(T=1s)$, the minimum value is 14km (Alpi mountain chain, zone 902; 8.10°E, 46.26°N), while the maximum is 174km (Pianosa). With reference to the expected magnitude, in the case of PGA the minimum and maximum values are equal to 4.5 (Curon Venosta, zone 903; 10.56°E, 46.80°N) and 6.7 (Mezzatorre di San Mauro Cilento, outside any seismic source; 15.02°E, 40.20°N), respectively. With reference to $Sa(T=1s)$, the minimum value of $\overline{M}$ is 5.1 (near the Autaret lakes, on the Alpi mountain chain, zone 908; 7.12°E, 45.24°N), while the maximum is 6.9 (Marina di Pescoluse, outside any seismic source; 18.24°E, 39.84°N). Finally, the maps of the expected ε show that it can be greater than two for the sites outside the seismic sources, meaning that especially anomalous earthquakes are needed to cause the exceedance of sa_{475}. Differently, in the higher hazard regions of Italy lower values of the average ε can be observed. In particular, in the case of PGA the minimum and maximum values are equal to 1.061 (Corato, zone 925; 16.38°E, 41.12°N) and 2.588 (Pianosa), respectively. With reference to $Sa(T=1s)$, the minimum value of $\overline{\varepsilon}$ is equal to 0.896 (Giarratana, zone 935; 14.78°E, 37.06°N), while the maximum is 2.112 (near Donoratico, outside any seismic source; 10.56°E, 43.14°N).

Finally, Table 3.2 provides disaggregation results, in terms of $\overline{M}, \overline{R}$ and $\overline{\varepsilon}$,for Milan and L'Aquila, which will be recalled in the next sections.

Table 3.2. Expected magnitude, distance and ε from disaggregation given the exceedance of the design PGA and $Sa(T=1s)$ with $T_r = 475$ years for Milan and L'Aquila.

	Milan	**L'Aquila**
PGA	$\{\overline{M}=5.2, \overline{R}=76km, \overline{\varepsilon}=2.2\}$	$\{\overline{M}=5.9, \overline{R}=9km, \overline{\varepsilon}=1.4\}$
$Sa(T=1s)$	$\{\overline{M}=5.8, \overline{R}=117km, \overline{\varepsilon}=2.0\}$	$\{\overline{M}=6.7, \overline{R}=19km, \overline{\varepsilon}=1.2\}$

3.4. Maps of the expected exceedance

3.4.1. Methodology and results

If the exceedance of the UHS occurs, it could be worthwhile to assess the expected acceleration a structure is exposed to. In the framework of performance-based seismic design, this issue can be related to the capability a code-conformed structure should have in the case the occurring earthquake is causative for the exceedance of the design spectrum. In this section, given the exceedance of sa_{475}, the expected value of acceleration over the threshold, herein indicated as $E\left[Sa(T) \mid Sa(T) > sa_{475}\right]$ (Equation 3.1), is mapped for Italy.

$$E\left[Sa(T) \mid Sa(T) > sa_{475}\right] = \int_{sa_{475}}^{+\infty} sa \cdot f_{Sa(T)|Sa(T)>sa_{475}}(sa) \cdot dsa \tag{3.1}$$

Equation (3.1) can be rewritten according to Equation (3.2), which introduces earthquake magnitude and distance.

$$E\left[Sa(T) \mid Sa(T) > sa_{475}\right] = \int_{sa_{475}}^{+\infty} \int_{m_{\min}}^{m_{\max}} \int_{r_{\min}}^{r_{\max}} sa \cdot f_{Sa(T)|Sa(T)>sa_{475},M,R}(sa) \cdot f_{M,R|Sa(T)>sa_{475}}(m,r) \cdot$$

$$\cdot dr \cdot dm \cdot dsa \tag{3.2}$$

Since, recalling Equation (2.5), sa can be rewritten as $sa = e^{\mu_{m,r}+\sigma\cdot\varepsilon}$ (for rock soil conditions, it is $\theta = 0$), it follows that $f_{Sa(T)|Sa(T)>sa_{475},M,R}(sa) \cdot dsa = f_{\varepsilon|Sa(T)>sa_{475},M,R}(\varepsilon) \cdot d\varepsilon$ and Equation (3.3) applies.

$$E\left[Sa(T) \mid Sa(T) > sa_{475}\right] = \int_{\frac{\log(sa_{475})-\mu_{m,r}}{\sigma}}^{+\infty} \int_{m_{\min}}^{m_{\max}} \int_{r_{\min}}^{r_{\max}} e^{\mu_{m,r}+\sigma\cdot\varepsilon} \cdot f_{\varepsilon|Sa(T)>sa_{475},M,R}(\varepsilon) \cdot f_{M,R|Sa(T)>sa_{475}}(m,r) \cdot$$

$$\cdot dr \cdot dm \cdot d\varepsilon \tag{3.3}$$

It is easy to recognize that $f_{\varepsilon|Sa(T)>sa_{475},M,R}(\varepsilon)\cdot f_{M,R|Sa(T)>sa_{475}}$ is the disaggregation distribution from Equation 2.6, that is $f_{M,R,\varepsilon|Sa(T)>sa_{475}}(m,r,\varepsilon)$, whose results are mapped (in the form of mean values) in Figure 3.3. Therefore, the expected value of the acceleration over the threshold is finally computed according to Equation (3.4).

$$E\left[Sa(T)\,|\,Sa(T)>sa_{475}\right]=\int_{m_{\min}}^{m_{\max}}\int_{r_{\min}}^{r_{\max}} e^{\mu_{m,r}}\cdot\int_{\frac{\log(sa_{475})-\mu_{m,r}}{\sigma}}^{+\infty} e^{\sigma\cdot\varepsilon}\cdot f_{M,R,\varepsilon|Sa(T)>sa_{475}}(m,r,\varepsilon)\cdot d\varepsilon\cdot dr\cdot dm \tag{3.4}$$

The expected accelerations for Italy given the exceedance of PGA and $Sa(T=1s)$ with $T_r=475$ years (see Figure 3.2) are shown in the left- and right-top panel of Figure 3.4, respectively. The absolute (δ) and percentage (Δ) differences between the expected acceleration over the threshold and the threshold itself are also given in the middle and bottom panels, respectively. They are computed using Equation (3.5) and (3.6).

$$\delta=E\left[Sa(T)\,|\,Sa(T)>sa_{475}\right]-sa_{475} \tag{3.5}$$

$$\Delta=\frac{E\left[Sa(T)\,|\,Sa(T)>sa_{475}\right]-sa_{475}}{sa_{475}} \tag{3.6}$$

Results show that the largest expected accelerations over the threshold are equal to 0.460g in the case of PGA, and 0.509g in the case of $Sa(T=1s)$. They both occur within zone 929, at the sites of Aprigliano and Terratelle for PGA and $Sa(T=1s)$, respectively. One can note that these sites are the same where the thresholds are the highest ones (see Section 3.3.1). In other words, with reference to a structure with fundamental period equal to 1s and located in Terratelle, if the structural behavior beyond exceedance of the elastic actions is of interest, such a structure should be able to resist an acceleration exceeding the threshold by 0.251g in absolute terms and 98% in percentage, that is, about 2 times the threshold. However, still referring to $Sa(T=1s)$, the right-bottom panel of

Figure 3.4 shows a percentage difference greater than 150% occurring at Piano dell'Acqua (14.56°E, 37.10°N; located in the district of Ragusa), within zone 935; the corresponding expected acceleration is equal to 0.338g. This means that, in case of exceedance of the UHS, an acceleration exceeding 2.5 times the threshold should be expected if the above-considered structure is located in Piano dell'Acqua, even if the expected acceleration is smaller than Tarratelle. Across all the country, even if the expected PGA are mostly greater than the expected $Sa(T=1s)$, the former has a smaller exposure to exceedance than the latter. In fact, the average percentage difference between the expected acceleration over the threshold and the threshold itself is 50% for PGA and 70% for $Sa(T=1s)$. The maps in Figure 3.4 also reveal that the smallest differences can be found in the areas outside the seismic source zones. In case of exceedance, the lowest excursion over the $Sa(T=1s)$ design acceleration is about 45% in percentage terms and occurs close to Turin (northern Italy). Indeed, the structure with fundamental period equal to 1s would be subjected to an acceleration exceeding 1.5 times the design threshold.

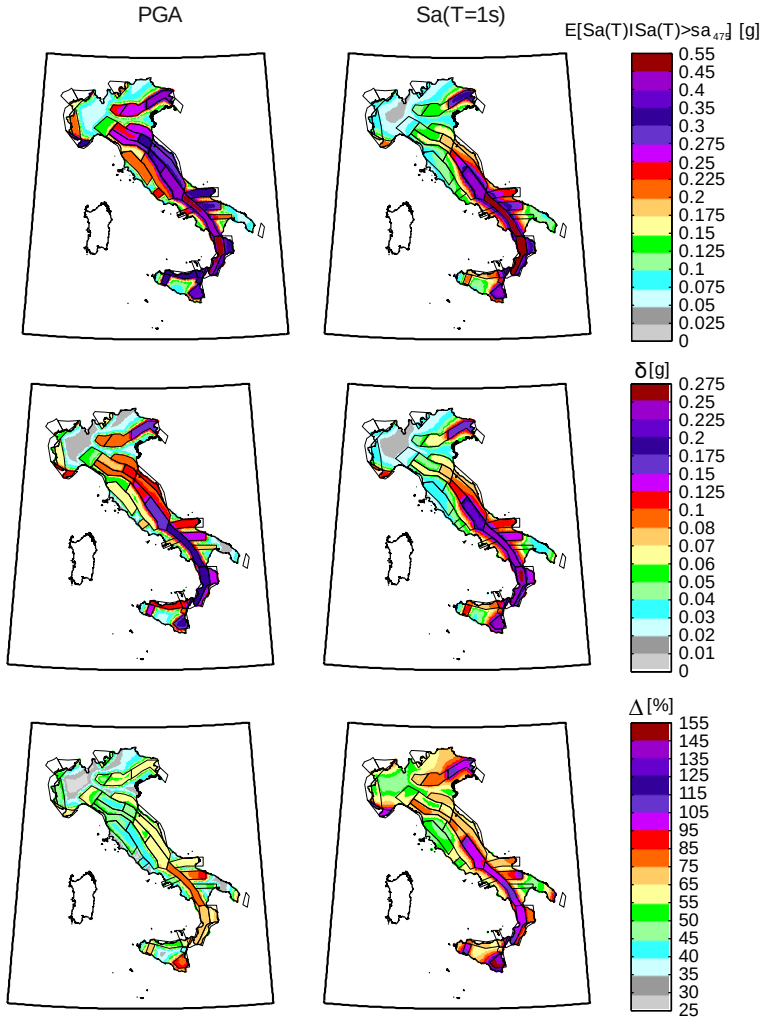

Figure 3.4. Maps of the expected accelerations over the PGA and $Sa(T=1s)$ design thresholds with $T_r = 475$ years. Top: expected value of the acceleration given the exceedance. Middle and bottom: absolute and percentage difference between the expected acceleration over the threshold and the threshold itself.

These observations can be related with the maps of the expected ε shown in the previous section (see Figure 3.3). In the areas outside the seismic sources, large values of $\bar{\varepsilon}$ and relatively small expected amount of exceedance can be observed. This is the case of Milan, for example. According to Table 3.2 the expected value of ε is 2.2 for PGA and

2.0 for $Sa(T=1s)$, while Table 3.3 reveals that excursions over the design acceleration, in percentage terms, are equal to 30% and 47% for PGA and $Sa(T=1s)$, respectively. On the other hand, in high hazard regions small values of $\bar{\varepsilon}$ and large expected amount of exceedance can be observed. With reference to L'Aquila, Table 3.2 indicates that the expected value of ε is 1.4, while accelerations up to 63% over the threshold are expected in case of exceedance of PGA (see Table 3.3). In the case of $Sa(T=1s)$, $\bar{\varepsilon}$ is equal to 1.2, while the percentage difference is 99%.

Table 3.3. Expected acceleration over the design PGA and $Sa(T=1s)$ with $T_r = 475$ years, absolute and percentage differences for Milan and L'Aquila.

	Milan		**L'Aquila**	
	PGA	$Sa(T=1s)$	PGA	$Sa(T=1s)$
$E\left[Sa(T) \mid Sa(T) > sa_{475}\right]$ [g]	0.065	0.051	0.412	0.413
δ [g]	0.015	0.016	0.159	0.205
Δ [%]	30	47	63	99

3.4.2. Influence of return period

With reference to the cases of the Milan and L'Aquila sites, this section shows the percentage differences between the expected acceleration and the threshold as a function of the return period of the threshold itself. The thresholds correspond to the spectral ordinates with the nine return periods the Italian building code refers to for design (between 30 and 2475 years). Equation (3.4) and (3.6) were used to compute the expected accelerations and percentage differences (with different subscript for return periods).

Figure 3.5 shows that Δ decreases with increasing return period. For PGA, the minimum values are 26% and 52% for Milan and L'Aquila, respectively. In the case of $Sa(T=1s)$, the minimum value of Δ is equal to 38% for Milan and 69% for L'Aquila. This means that, given the exceedance of the threshold with the highest return period

(among those the Italian code refers to), an acceleration clearly above the design threshold should be expected at the considered sites.

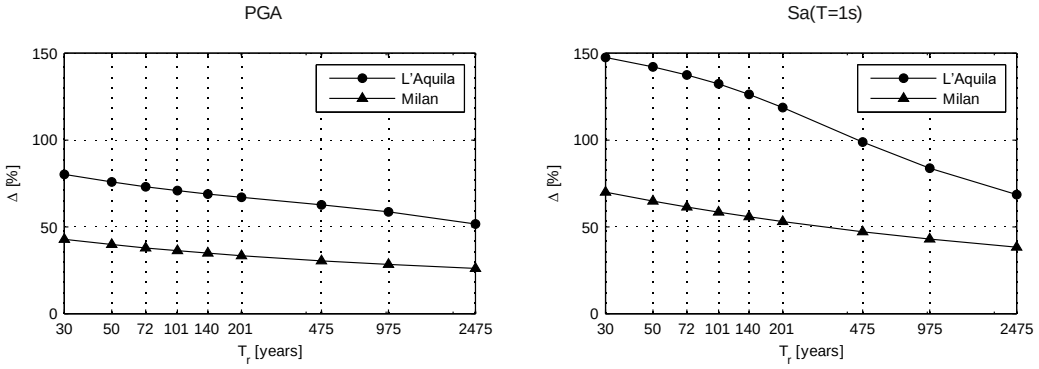

Figure 3.5. Percentage difference between the expected acceleration and the threshold for PGA and $Sa(T=1s)$ as a function of the return period in Milan and L'Aquila.

Table 3.4 and Table 3.5 provide the numerical values of the curves in Figure 3.5, including the expected accelerations and thresholds. One can clearly note that percentage differences are higher for $Sa(T=1s)$ than PGA for all the considered return periods, as the trend on national scale reflects for $T_r = 475$ years (see previous section).

Table 3.4. Expected acceleration over the design PGA and $Sa(T=1s)$ and percentage difference as a function of return period for Milan.

	Milan					
	PGA			$Sa(T=1s)$		
T_r [yrs]	sa_{T_r} [g]	$E\left[Sa(T) \mid Sa(T) > sa_{T_r}\right]$ [g]	Δ [%]	sa_{T_r} [g]	$E\left[Sa(T) \mid Sa(T) > sa_{T_r}\right]$ [g]	Δ [%]
30	0.022	0.031	43	0.011	0.019	70
50	0.026	0.037	40	0.014	0.023	65
72	0.029	0.040	38	0.016	0.026	61
101	0.033	0.044	36	0.019	0.030	59
140	0.036	0.048	35	0.022	0.034	56
201	0.040	0.053	33	0.025	0.038	53
475	0.050	0.065	30	0.035	0.051	47
975	0.060	0.077	28	0.045	0.064	43
2475	0.074	0.094	26	0.060	0.083	38

Table 3.5. Expected acceleration over the design PGA and $Sa(T=1s)$ and percentage difference as a function of return period for L'Aquila.

	L'Aquila					
	PGA			$Sa(T=1s)$		
T_r [yrs]	sa_{T_r} [g]	$E\left[Sa(T) \mid Sa(T) > sa_{T_r}\right]$ [g]	Δ [%]	sa_{T_r} [g]	$E\left[Sa(T) \mid Sa(T) > sa_{T_r}\right]$ [g]	Δ [%]
30	0.073	0.132	80	0.036	0.088	148
50	0.094	0.165	76	0.049	0.120	142
72	0.111	0.193	73	0.062	0.148	138
101	0.130	0.222	71	0.077	0.180	132
140	0.150	0.254	69	0.095	0.216	126
201	0.176	0.294	67	0.121	0.264	119
475	0.253	0.412	63	0.208	0.413	99
975	0.341	0.541	59	0.316	0.581	84
2475	0.496	0.753	52	0.515	0.869	69

3.4.3. Effect of soil conditions

As introduced in Section 3.2, the results discussed so far are carried out considering rock soil condition for all sites. It is now worthwhile to see the effects of the soil conditions on the expected acceleration over the threshold. In particular, the thresholds and the expected accelerations over the thresholds with $T_r = 475$ years on site-dependent soil conditions are calculated using the same source model and GMPE described in Section 3.2.

The structure of the Ambraseys et al. (1996) is such that the soil coefficient, θ, only affects the mean given magnitude and distance (see also Section 2.2.3). Therefore, according to Iervolino (2016) the thresholds for site-dependent soil classes ($sa_{475,soil}$) can be obtained via Equation (3.7).

$$sa_{475,soil} = sa_{475} \cdot e^{\theta} \tag{3.7}$$

The Ambraseys et al. (1996) GMPE considers three different soil classes according to $V_{S,30}$ intervals: *rock* ($V_{S,30} > 750m/s$), *stiff* ($360 < V_{S,30} \leq 750m/s$) and *soft* soil ($V_{S,30} \leq 360m/s$); for each of these intervals, the model adopts different soil coefficients for PGA and $Sa(T = 1s)$. The corresponding e^{θ} coefficients are reported in Table 3.6 (for rock soil condition it is $\theta = 0$):

Table 3.6. Soil coefficients according the model of Ambraseys et al. (1996).

	e^{θ}	
	stiff	*soft*
PGA	1.309	1.331
$Sa(T = 1s)$	1.343	1.656

The $V_{S,30}$ for each site is obtained via the SSC-Italy software (Forte et al., 2018). Applying Equation (3.7) to the threshold on rock of the hazard maps in Figure 3.2 provides the hazard maps on site-dependent soil conditions given in Figure 3.6.

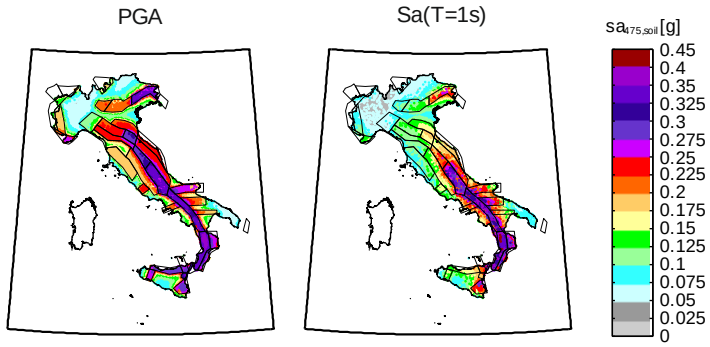

Figure 3.6. Seismic hazard maps of PGA and $Sa(T=1s)$ with $T_r=475$ years on site-dependent soil conditions.

Due to the soil effects, the average increments of PGA and $Sa(T=1s)$ across Italy are about 26% and 36%, respectively. The maximum acceleration which is exceeded, on average, every 475 years, is equal to 0.358g for PGA and 0.416g for $Sa(T=1s)$. The corresponding sites are Destre (16.28°E, 36.46°N) and Donnici Inferiore (16.28°E, 39.26°N), both located in the district of Cosenza and enclosed by zone 929. One can note that for both PGA and $Sa(T=1s)$ the design thresholds on rock soil condition for these sites are slightly smaller than the maximum ones, which are obtained for the Aprigliano and Terratelle sites (see Section 3.3.1). Nevertheless, according to the adopted classification, the soil amplification is such that the design thresholds on site-dependent soil conditions get larger for the Destre and Donnici Inferiore sites, for which the $V_{S,30}$ is equal to 326m/s.

Given the exceedance of the design spectral ordinates on a given soil condition, it is easy to recognize that from Equation (2.5) and (3.4) and profiting of the independence of disaggregation on θ (see Section 2.2.3), the expected acceleration over the thresholds on that soil condition, $E\left[Sa(T)\,|\,Sa(T)>sa_{475}\right]_{soil}$, can be computed by multiplying the corresponding $E\left[Sa(T)\,|\,Sa(T)>sa_{475}\right]$ on rock by e^{θ}. In fact, according to Equation (2.5), it is $sa_{soil}=e^{\mu_{m,r}+\theta+\sigma\cdot\varepsilon}$ and, as a consequence, Equation (3.3) can be rewritten as Equation (3.8).

$$E\left[Sa(T)\,|\,Sa(T)>sa_{475}\right]_{soil}=\int_{\frac{\log(sa_{475})-\mu_{m,r}}{\sigma}}^{+\infty}\int_{m_{\min}}^{m_{\max}}\int_{r_{\min}}^{r_{\max}} e^{\mu_{m,r}+\theta+\sigma\cdot\varepsilon}\cdot f_{\varepsilon|Sa(T)>sa_{475},M,R}(\varepsilon)\cdot \cdot f_{M,R|Sa(T)>sa_{475}}(m,r)\cdot dr\cdot dm\cdot d\varepsilon \tag{3.8}$$

Given the above-cited independence of disaggregation on θ, the product $f_{\varepsilon|Sa(T)>sa_{475},M,R}(\varepsilon)\cdot f_{M,R|Sa(T)>sa_{475}}(m,r)$ provides the same disaggregation distribution of Equation (3.3). Therefore, the expected acceleration over the threshold on a site-dependent soil condition is computed via Equation (3.9)

$$\begin{aligned}E\left[Sa(T)\,|\,Sa(T)>sa_{475}\right]_{soil}&=\int_{m_{\min}}^{m_{\max}}\int_{r_{\min}}^{r_{\max}} e^{\mu_{m,r}}\cdot e^{\theta}\cdot\int_{\frac{\log(sa_{475})+\theta-\mu_{m,r}-\theta}{\sigma}}^{+\infty} e^{\sigma\cdot\varepsilon}\cdot\\ &\cdot f_{M,R,\varepsilon|Sa(T)>sa_{475}}(m,r,\varepsilon)\cdot d\varepsilon\cdot dr\cdot dm=\\ &e^{\theta}\cdot\int_{m_{\min}}^{m_{\max}}\int_{r_{\min}}^{r_{\max}} e^{\mu_{m,r}}\cdot\int_{\frac{\log(sa_{475})+\theta-\mu_{m,r}-\theta}{\sigma}}^{+\infty} e^{\sigma\cdot\varepsilon}\cdot f_{M,R,\varepsilon|Sa(T)>sa_{475}}(m,r,\varepsilon)\cdot d\varepsilon\cdot dr\cdot dm=\\ &=e^{\theta}\cdot E\left[Sa(T)\,|\,Sa(T)>sa_{475}\right]\end{aligned} \tag{3.9}$$

The maps of the expected accelerations on site-dependent soil conditions are shown in the top panels of Figure 3.7. In both cases of PGA and *Sa(T = 1s)*, the largest $E\left[Sa(T)\,|\,Sa(T)>sa_{475}\right]_{soil}$ occurs in the Destre site, being equal to 0.610g and 0.830g, respectively. The absolute (δ_{soil}) and percentage (Δ_{soil}) differences between the expected acceleration over the threshold and the threshold itself on site-specific soil condition (middle and bottom panels) can be easily obtained from the corresponding differences for rock soil condition, as Equations (3.10) and (3.11) show.

$$\begin{aligned}\delta_{soil}&=E\left[Sa(T)\,|\,Sa(T)>sa_{475}\right]\cdot e^{\theta}-sa_{475}\cdot e^{\theta}=\\ &=e^{\theta}\cdot\left\{E\left[Sa(T)\,|\,Sa(T)>sa_{475}\right]-sa_{475}\right\}=e^{\theta}\cdot\delta\end{aligned} \tag{3.10}$$

$$\Delta_{soil} = \frac{E\left[Sa(T) \mid Sa(T) > sa_{475}\right] - sa_{475}}{sa_{475}} = \frac{E\left[Sa(T) \mid Sa(T) > sa_{475}\right] \cdot e^{\theta} - sa_{475} \cdot e^{\theta}}{sa_{475} \cdot e^{\theta}} = \Delta \tag{3.11}$$

In particular, according to Equation (3.11) the percentage differences are independent on θ. Indeed, in the case the site-dependent soil conditions are taken into account, the observations in Sections 3.4.1 and 3.4.2 on the amount of exceedance over the design thresholds still apply.

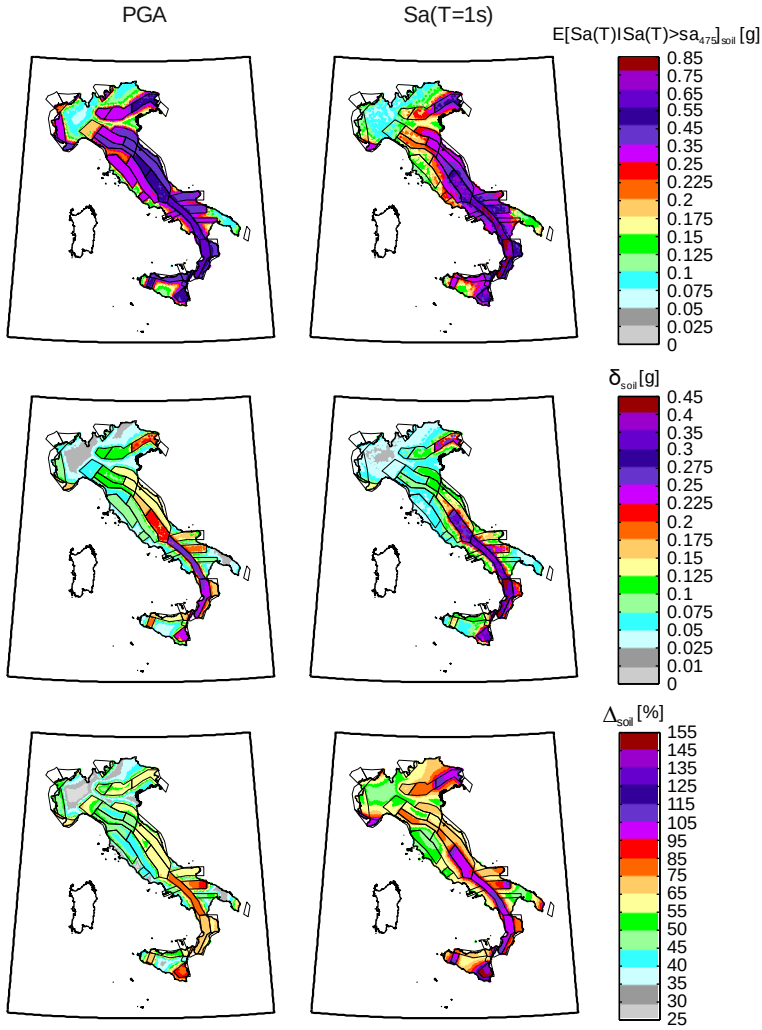

Figure 3.7. Maps of the expected accelerations over the PGA and $Sa(T=1s)$ design thresholds with $T_r = 475$ years on site-dependent soil conditions. Top: expected value of the acceleration given the exceedance. Middle and bottom: absolute and percentage difference between the expected acceleration over the threshold and the threshold itself.

To complete the discussion, results for Milan ($V_{S,30} = 379 m/s$) and L'Aquila ($V_{S,30} = 438 m/s$) are also shown in Table 3.7. According to the adopted classification, stiff soil is considered for both the sites.

Table 3.7. Expected acceleration over the design PGA and $Sa(T=1s)$ with $T_r=475$ years, absolute and percentage differences for Milan and L'Aquila on site-dependent soil conditions. Design thresholds are also given.

	Milan		**L'Aquila**	
	PGA	$Sa(T=1s)$	PGA	$Sa(T=1s)$
$sa_{475,soil}$ [g]	0.065	0.046	0.331	0.279
$E\left[Sa(T) \mid Sa(T) > sa_{475}\right]_{soil}$ [g]	0.085	0.068	0.539	0.555
δ_{soil} [g]	0.020	0.022	0.208	0.275
Δ_{soil} [%]	30	47	63	99

3.5. Map of the strong earthquakes

3.5.1. Methodology and results

In this section the maps of the minimum magnitude of earthquakes that, if occurring within a distance w from the site, have a probability larger than 0.5 of exceeding the design thresholds with $T_r=475$ years, are discussed. In particular, three ranges of distances are considered, that is, 5km, 15km and 50km. These earthquakes are herein indicated as strong earthquakes, meaning that they are supposed to be causative for the exceedance of the design spectral ordinates more likely than not. The maps presented herein aim to provide additional information to the maps of the expected acceleration over the threshold. In fact, while the latter account for all the earthquakes that can cause the exceedance of the design thresholds, the maps of minimum magnitude help to identify the earthquakes scenarios for which such exceedance is expected.

The minimum magnitude of the strong earthquakes occurring within a distance w from the site, herein indicated as $M_{Sa(T)>sa_{475},R\le w}$, is computed by calculating, for each magnitude, the probability of exceeding the threshold given the occurrence of an earthquake within a distance w from the site, $P\left[Sa(T)>sa_{475} \mid M=m, R\le w\right]$; thus,

$M_{Sa(T)>sa_{475},R\leq w}$ corresponds to the minimum magnitude for which $P\left[Sa(T)>sa_{475}\,|\,M=m,R\leq w\right]>0.5$. The analytical expression for $M_{Sa(T)>sa_{475},R\leq w}$ is given in Equation (3.12), where $P\left[Sa(T)>sa_{475}\,|\,M=m,R=r\right]$ is the probability of exceedance of the threshold with $T_r=475$ years conditional to the occurrence of the $\{M=m,R=r\}$ earthquake scenario, and $f_{R|R\leq w}(r)$ represents the distribution of source-to-site distance given the earthquake occurrence within w km.

$$M_{Sa(T)>sa_{475},R\leq w}=\min_{M}\left\{P\left[Sa(T)>sa_{475}\,|\,M=m,R\leq w\right]\right\}=$$
$$=\min_{M}\left\{\int_{0}^{w}P\left[Sa(T)>sa_{475}\,|\,M=m,R=r\right]\cdot f_{R|R\leq w}(r)\cdot dr>0.5\right\} \tag{3.12}$$

Figure 3.8 shows the maps of strong earthquakes occurring within 5km (top panels), 15km (middle panels) and 50km (bottom panels) from the sites, computed via Equation (3.12). With reference to earthquakes occurring within 5km, results show that, although the magnitudes result larger for $Sa(T=1s)$ than PGA, the largest value across the country is $M_{Sa(T)>sa_{475},R\leq 5km}=6.3$ for both the spectral ordinates. In particular, this value occurs in Calitri (15.44°E, 40.92°N), in the case of PGA, and Cerasi (15.76°E, 38.16°N) in the case of $Sa(T=1s)$. Both the sites are located in the most hazardous areas, being Calitri located in zone 927 and Cerasi in zone 929 (see also Figure 3.1 and Figure 3.2). The minimum magnitude of strong earthquakes tends to be smaller in the rest of Italy; in particular, the average $M_{Sa(T)>sa_{475},R\leq 5km}$ is equal to 5.2 for PGA and 5.7 for $Sa(T=1s)$. This is because short distant earthquakes have a more significant effect on PGA than $Sa(T=1s)$ hazard, which is mainly affected by more distant events (see also Iervolino et al., 2011). Therefore, considering the earthquakes occurring within 5km from the site, a greater magnitude is required to observe the exceedance in the case of $Sa(T=1s)$.

For earthquakes occurring within 15km, the average $M_{Sa(T)>sa_{475},R\leq 15km}$ is around 6 for both spectral ordinates, while the largest values are $M_{Sa(T)>sa_{475},R\leq 15km}=6.9$ for PGA, occurring at Mareneve (zone 936; 15.08°E, 37.80°N), and $M_{Sa(T)>sa_{475},R\leq 15km}=6.7$ for $Sa(T=1s)$, occurring at Lamezia Terme (zone 929; 16.30°E, 38.92°N).

Finally, considering 50km, for most of the Italian territory there is no magnitude having probability larger than 50% of exceeding the considered design spectral ordinates. This is because, on average, $M_{Sa(T)>sa_{475},R\leq 50km}\approx 7$, and earthquakes with such magnitude (or above) can occur in only few sources according to the adopted model (see Section 3.2). One can observe that in the case of PGA the non-affected areas (white colored) are larger than $Sa(T=1s)$. In fact, due to the faster attenuation of PGA than $Sa(T=1s)$ with the increasing distance, in the most of Italy a magnitude greater than the maximum possible is required to observe the PGA exceedance at a site 50km far away from the epicentre of the event.

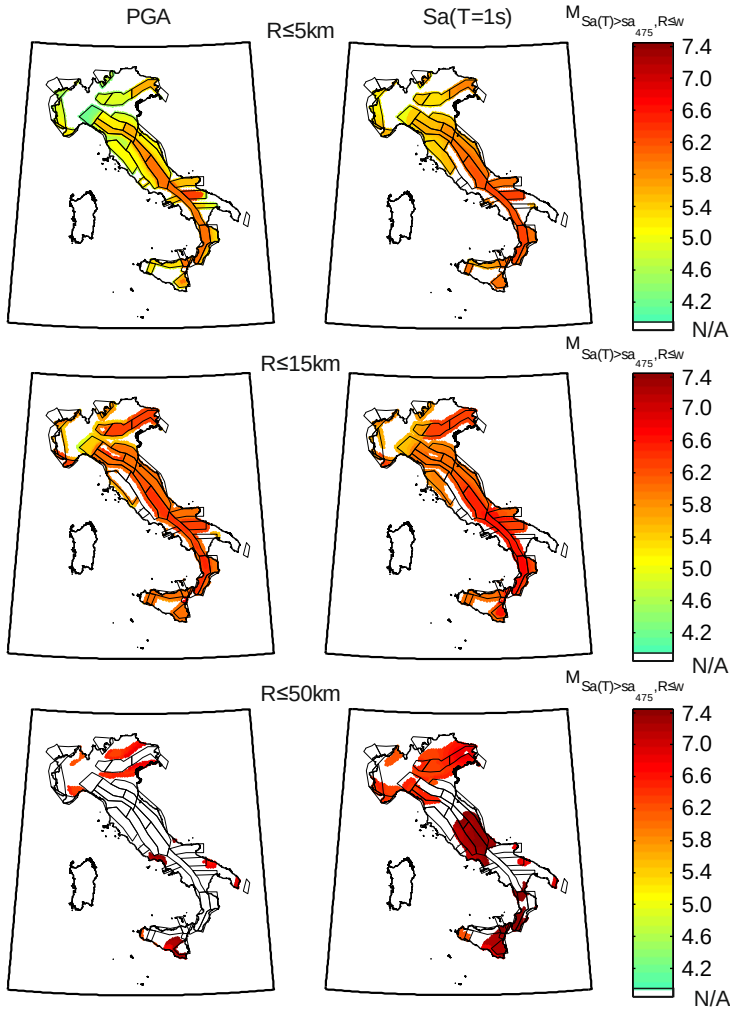

Figure 3.8. Maps of the minimum magnitude of the earthquakes with probability larger than 0.5 (strong earthquakes) of exceeding the PGA and $Sa(T=1s)$ design thresholds with $T_r = 475$ years in the case of occurrence within 5km (top), 15km (middle) and 50km (bottom).

The results in Figure 3.8 discussed so far indicate that the design threshold is not hard to be exceeded even for earthquakes of magnitude considered relatively moderate, if they occur close to the site of interest. In other words, the exceedance of the design spectrum is well expected in the epicentral areas of seismic events of magnitude even far from the maximum the site can be subjected. Conversely, the exceedance should be not expected

for distant earthquakes or those of relatively low magnitude among those occurring close to the site. For a more comprehensive understanding of these considerations, Figure 3.9 is given. In the top panels the maps of the maximum magnitude which can occur at each site (according to the source model described in Section 3.2) within each of the considered distance ranges, $M_{max,R\leq w}$, are shown. The mid and bottom panels, referring to PGA and $Sa(T=1s)$, respectively, provide the differences between $M_{max,R\leq w}$ and the minimum magnitude of strong earthquakes in Figure 3.8 corresponding to the same distance $(\Delta M = M_{max,R\leq w} - M_{Sa(T)>sa_{475},R\leq w})$. In accordance with the maps of the strong earthquakes and the previous considerations, the maps in Figure 3.9 show that, as the distance increases, the minimum magnitude of strong earthquakes tend to be closer to the maximum possible (in the areas where it can be identified) or, in other words, their difference decreases. In particular, the average values of ΔM, $\overline{\Delta M}$, can be observed in Table 3.8.

Table 3.8. Average differences between the maximum magnitude possible and minimum magnitude of strong earthquakes,

	$\overline{\Delta M}$	
w [km]	PGA	$Sa(T=1s)$
5	1.15	0.76
15	0.64	0.49
50	0.18	0.15

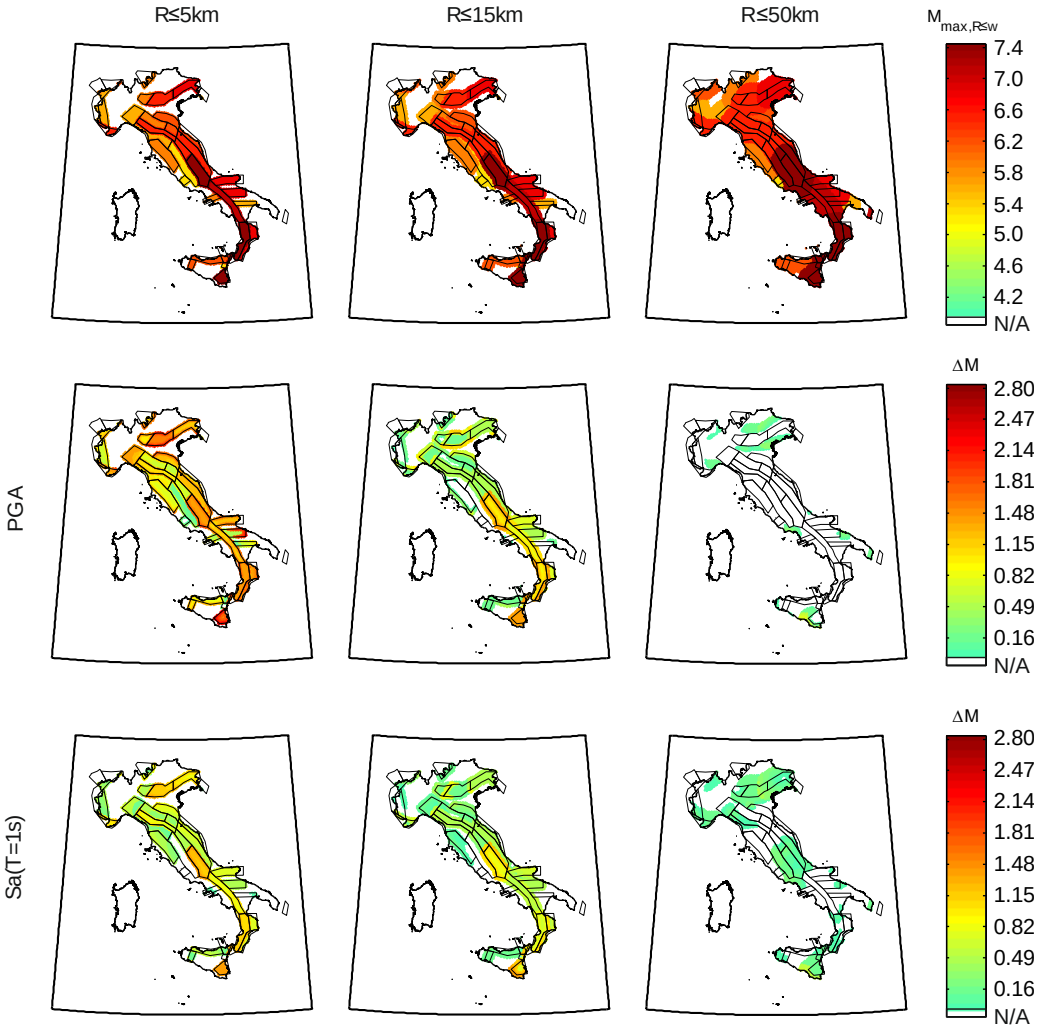

Figure 3.9. Top: maximum magnitudes which can occur at each site within 5km, 15km and 50km, according to the adopted source model; middle and bottom: difference of maximum magnitude and minimum magnitude of strong earthquakes for PGA and $Sa(T=1s)$, respectively.

3.5.2. Analysis of earthquake scenarios

The previous section focused on the identification of the earthquakes for which the exceedance of the design threshold should be expected. As an extension, the objective of this section is to discuss the contribution to seismic hazard of all the possible

magnitude-distance scenarios. To do so, it is worthwhile to rewrite the hazard integral considering finite magnitude $(m, m+\Delta m)$ and distance $(r, r+\Delta r)$ bins, as per Equation (3.13).

$$\lambda_{Sa(T)>sa} \approx \sum_M \sum_R P\left[Sa(T) > sa \mid M = m, R = r\right] \cdot \nu_{M=m,R=r} \cdot \Delta m \cdot \Delta r \approx$$
$$\approx \sum_M \sum_R \lambda_{Sa(T)>sa, M=m, R=r} \cdot \Delta m \cdot \Delta r \tag{3.13}$$

In the equation, $\lambda_{Sa(T)>sa,M=m,R=r} \cdot \Delta m \cdot \Delta r$ represents the rate of earthquakes from the considered magnitude-distance bin causing the exceedance of the threshold. The term $\nu_{M=m,R=r} \cdot \Delta m \cdot \Delta r$ is the rate of earthquakes of magnitude in the bin $(m, m+\Delta m)$ that occur at a distance from the site in the bin $(r, r+\Delta r)$, considering all seismic sources. In particular, noting that $\nu_{M=m,R=r} \cdot \Delta m \cdot \Delta r = \sum_{i=1}^{n_s} \nu_i \cdot P\left[M = m, R = r\right]_i$, it is easy to recognize that $\lambda_{Sa(T)>sa,M=m,R=r} \cdot \Delta m \cdot \Delta r$ derives from the magnitude-distance disaggregation multiplied by $\lambda_{Sa(T)>sa}$. Thus, the conditional probability that each $\{M = m, R = r\}$ scenario causes the exceedance of the threshold can be computed via the Equation (3.14), which derives from Equation (3.13).

$$P\left[Sa(T) > sa \mid M = m, R = r\right] = \frac{\lambda_{Sa(T)>sa, M=m, R=r}}{\nu_{M=m,R=r}} \tag{3.14}$$

Although the term on left-side is formally the GMPE, Equation (3.14) provides the site-specific conditional probability of exceeding the threshold. In fact, both the terms on right-side explicitly account for all seismic sources contributing to the hazard of the site, which can have, for example, different style-of-faulting.

At this point, the study of the earthquake scenarios contributing to hazard for Milan and L'Aquila, in terms of $Sa(T = 1s)$ hazard with $T_r = 475$ years, is explored. The latter,

which has the highest seismic hazard, is first considered. L'Aquila is enclosed by zone 923, which has maximum magnitude well above 7. Nevertheless, among the earthquakes that can occur close to the site; i.e., $R \leq 5km$, the maps in the top panels of Figure 3.8 reveal that the minimum magnitude of strong earthquakes is equal to 6 for PGA and 6.2 for $Sa(T=1s)$ (see also Table 3.9).

Table 3.9. Minimum magnitude of strong earthquakes occurring within 5km, 15km and 50km, which cause the exceedance of the design PGA and $Sa(T=1s)$ with $T_r = 475$ years for Milan and L'Aquila.

	Milan		**L'Aquila**	
	PGA	$Sa(T=1s)$	PGA	$Sa(T=1s)$
$M_{Sa(T)>sa_{475},R\leq 5km}$	N/A		6.0	6.2
$M_{Sa(T)>sa_{475},R\leq 15km}$			6.4	6.5
$M_{Sa(T)>sa_{475},R\leq 50km}$			N/A	7.3

With reference to the $Sa(T=1s)$ spectral ordinate, this result can be analyzed in detail in the left panel of Figure 3.10, which is the graphical representation of the probability of exceeding the considered design threshold (see Table 3.1) given the occurrence of the $\{M=m, R=r\}$ scenarios, computed via Equation (3.14). As expected, such probability increases with increasing magnitude and decreasing distance.

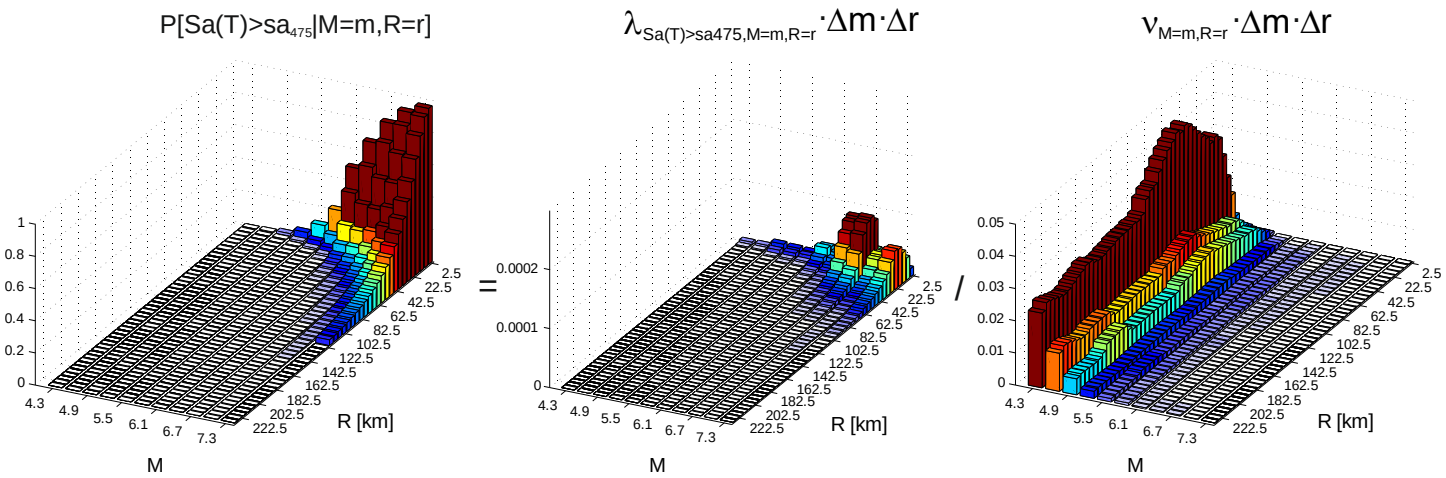

Figure 3.10. Analysis of the earthquake scenarios contributing to hazard for L'Aquila in terms of $Sa(T=1s)$ with $T_r = 475$ years. Left illustrates the probability of exceeding the design threshold conditional to the occurrence of each scenario; center provides the rate of earthquakes that, for each scenario, causes the exceedance of the threshold; right gives the rate of earthquakes occurring at the site, considering all seismic sources.

In particular, $P\left[Sa(T) > sa_{475} \mid M = m, R = r\right]$ starts to be larger than 0.1 at $M \approx 5.5, R \leq 5km$, it exceeds 0.5 at $M = 6.2, R \leq 5km$ (bin centred at $M = 6.1, R = 2.5km$) and it is even larger than 0.9 at $M \approx 7, R \leq 5km$. This implies that the exceedance of the threshold is almost certain in the case an earthquake of magnitude larger than 7 occurs within a distance smaller than 5km from L'Aquila. However, given the source-to-site distance, higher magnitude earthquakes are typically less frequent than lower magnitude, and this is in accordance with the magnitude-distance distribution of $\nu_{M=m,R=r} \cdot \Delta m \cdot \Delta r$ for L'Aquila, as shown in the right panel of Figure 3.10. In other words, protection of a code-conformed structure from earthquakes of high magnitude is only warranted by the rarity with which they occur in the epicentral area of the site in which the structure is located.

Furthermore, probabilities of exceeding the threshold larger than 0.2 can be found up to $R \approx 50km$ for the largest magnitudes. This means that the earthquakes within 50km are the most contributing to the hazard for L'Aquila, if the $Sa(T = 1s)$ spectral ordinate and $T_r = 475$ years are considered. This observation can be further illustrated through the central panel of Figure 3.10, which provides the magnitude-distance distribution of $\lambda_{Sa(T)>sa_{475},M=m,R=r} \cdot \Delta m \cdot \Delta r$. Obviously, the sum of these rates over all the bins is equal to $1/475 = 0.0021$ (the distribution of the rate of earthquakes causing the exceedance is obtained from the disaggregation multiplied by 0.0021, as mentioned). Indeed, summing up the values of the rates from all cells up to $R \leq 50km$ it results 0.00191, pointing that the earthquakes occurring within 50km from L'Aquila represent more than the 90% of the $Sa(T = 1s)$ hazard with $T_r = 475$ years.

Table 3.9 also provides the minimum magnitudes of strong earthquakes occurring within 15 and 50 km from L'Aquila. For $R \leq 15km$, $M_{Sa(T)>sa_{475},R\leq w}$ is still well below the maximum magnitude which can occur. In the case of $R \leq 50km$, there is no scenario having probability larger than 0.5 of exceeding the design PGA, while

$M_{Sa(T)>sa_{475},R\leq 50km} = 7.3$ for $Sa(T=1s)$. This is also related to the expected magnitude from disaggregation, which is larger for $Sa(T=1s)$ then PGA (see Table 3.2), and the propagation features of larger magnitude earthquakes.

In the case of Milan, Table 3.9 indicates that there is no scenario having $P\left[Sa(T)>sa_{475} \mid M=m,R=r\right]>0.5$. This is because the site is outside the source zones and the maximum magnitude which can occur within 50km is 5.9, according to the map in the top-right panel of Figure 3.9. In fact, the panels of Figure 3.11 clearly show that there are no contributions from earthquakes closer than 25km. In particular, the left panel of Figure 3.11 shows that $P\left[Sa(T)>sa_{475} \mid M=m,R=r\right]=0.5$ at $M\approx 6.4, R\approx 70km$, while the closest scenario, corresponding to $M\approx 5.8, R\approx 27km$, has $P\left[Sa(T)>sa_{475} \mid M=m,R=r\right]=0.49$.

The results discussed so far are in accordance with the expected value of ε from disaggregation (see Section 3.3.2). Still with reference to the $Sa(T=1s)$ spectral ordinate, $\bar{\varepsilon}$ is equal to 1.2 and 2 for L'Aquila and Milan, respectively (see Table 3.2). In fact, in the case of L'Aquila the exceedance is due to a relatively non-anomalous ground motion from one of the scenarios of moderate magnitude and close to the site. On the other hand, it has been shown that the threshold is hard to be exceeded for all the scenarios in the case of Milan, meaning that the exceedance can be only expected for relatively anomalous ground motion from one of the possible scenarios.

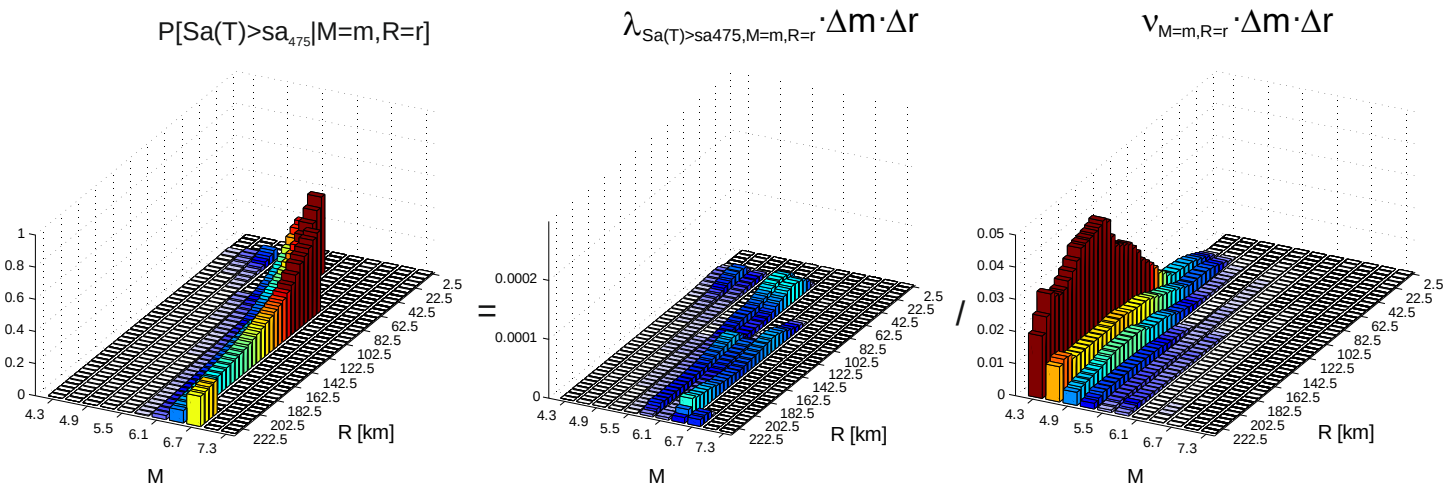

Figure 3.11. Analysis of the earthquake scenarios contributing to hazard for Milan in terms of $Sa(T=1s)$ with $T_r = 475$ years. Left illustrates the probability of exceeding the design threshold conditional to the occurrence of each scenario; center provides the rate of earthquakes that, for each scenario, causes the exceedance of the threshold; right gives the rate of earthquakes occurring at the site, considering all seismic sources.

To conclude, it is easy to recognize that all the results carried out in this section are soil-independent. In fact, looking at Equation (3.14), the $\lambda_{Sa(T)>sa_{475},M=m,R=r}$ term derives from the soil-independent disaggregation (see Section 3.4.3) and $\nu_{M=m,R=r}$ is related to the seismic sources affecting the sites. As a consequence, also the maps of the minimum magnitude of strong earthquakes shown in the previous section are soil-independent.

3.5.3. Influence of return period

In this section, the influence of the return period of the threshold on the minimum magnitude of the strong earthquakes is explored. Similarly to Section 3.4.2, with reference to Milan and L'Aquila the minimum magnitude with probability larger than 0.5 of exceeding the design PGA and $Sa(T=1s)$, for the nine return periods the Italian building code refers to, are given. Results are obtained by using Equation (3.12) again and plotted in Figure 3.12.

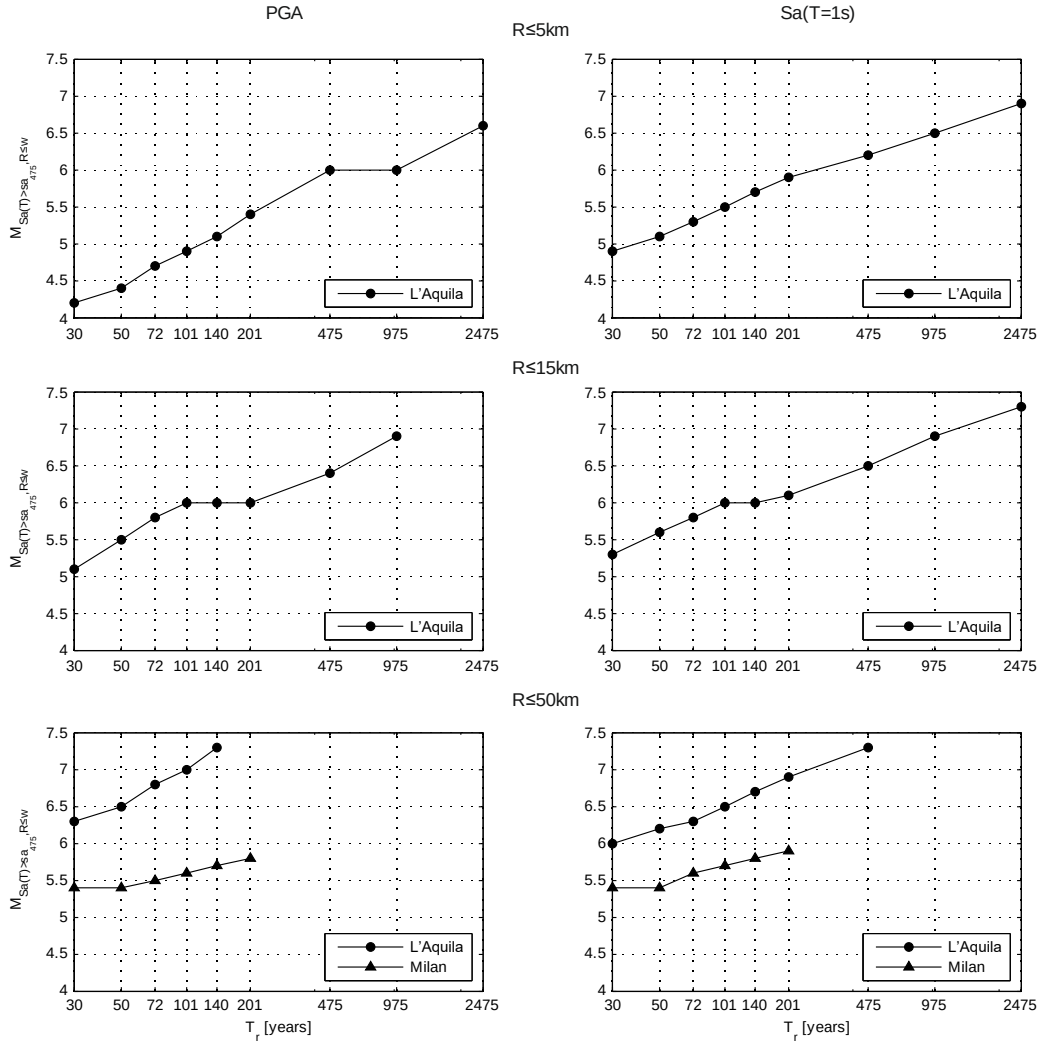

Figure 3.12. Minimum magnitude of earthquakes causing the exceedance of the PGA and $Sa(T=1s)$ design thresholds as a function of return period for Milan and L'Aquila, in the case of occurrence within 5km (top), 15km (middle) and 50km (bottom).

The panels in figure refer to the same distance ranges considered in the section 3.5.1. In general, $M_{Sa(T)>sa_{475},R\leq w}$ increases with return period, because the threshold also increases with T_r. Considering Milan, the top and middle panels show that there are no curves. In fact, as discussed in the previous section, there are no earthquakes occurring

within 25km from the site. Considering all the events within 50km, the bottom panels point out that the minimum magnitude of strong earthquakes is below 6 referring to any return period. In particular, with reference to $Sa(T=1s)$, it is $M_{Sa(T)>sa_{201},R\leq 50m}=5.9$, which is the maximum possible for the site, according to the previous section. This is because Milan is located in a very low hazardous area; therefore, the exceedance of the design threshold can be caused by an event of relatively low-moderate magnitude. In the case of L'Aquila, for both PGA and $Sa(T=1s)$ spectral ordinates and for distances up to 15km, it is required a return period equal to well-above 2000 years to get the minimum magnitude of strong earthquakes close the maximum magnitude which can occur (see also Table 3.10; for completeness, the thresholds for the different return periods shown in Table 3.9, are provided again). This means that the exceedance of the design threshold with $T_r=2475$ years should be expected in the epicentral areas of earthquakes of magnitude almost equal to the maximum possible. Looking at $Sa(T=1s)$, for $R\leq 50km$ the maximum T_r for which the minimum magnitude of strong earthquakes can be defined is 475 years (see also Table 3.11). In other words, according to the adopted source model, the exceedance of the design threshold with $T_r>475$ should be not expected in the case a distant earthquake occurs.

Table 3.10. Minimum magnitude of strong earthquakes occurring within 5km, 15km and 50km, which cause the exceedance of the design PGA and $Sa(T=1s)$ as a function of return period for Milan. The design thresholds are also given.

	Milan							
	PGA				$Sa(T=1s)$			
T_r [yrs]	sa_{T_r} [g]	$R \le 5km$	$R \le 15km$	$R \le 50km$	sa_{T_r} [g]	$R \le 5km$	$R \le 15km$	$R \le 50km$
30	0.022	N/A	N/A	5.4	0.011	N/A	N/A	5.4
50	0.026			5.4	0.014			5.4
72	0.029			5.5	0.016			5.6
101	0.033			5.6	0.019			5.7
140	0.036			5.7	0.022			5.8
201	0.040			5.8	0.025			5.9
475	0.050			N/A	0.035			N/A
975	0.060			N/A	0.045			N/A
2475	0.074			N/A	0.060			N/A

Table 3.11. Minimum magnitude of strong earthquakes occurring within 5km, 15km and 50km, which cause the exceedance of the design PGA and $Sa(T=1s)$ as a function of return period for L'Aquila. The design thresholds are also given.

	L'Aquila							
	PGA				$Sa(T=1s)$			
T_r [yrs]	sa_{T_r} [g]	$R \le 5km$	$R \le 15km$	$R \le 50km$	sa_{T_r} [g]	$R \le 5km$	$R \le 15km$	$R \le 50km$
30	0.073	4.2	5.1	6.3	0.036	4.9	5.3	6
50	0.094	4.4	5.5	6.5	0.049	5.1	5.6	6.2
72	0.111	4.7	5.8	6.8	0.062	5.3	5.8	6.3
101	0.130	4.9	6.0	7	0.077	5.5	6.0	6.5
140	0.150	5.1	6.0	7.3	0.095	5.7	6.0	6.7
201	0.176	5.4	6.0	N/A	0.121	5.9	6.1	6.9
475	0.253	6.0	6.4	N/A	0.208	6.2	6.5	7.3
975	0.341	6.0	6.9	N/A	0.316	6.5	6.9	N/A
2475	0.496	6.6	N/A	N/A	0.515	6.9	7.3	N/A

3.6. Conclusions

In performance-based earthquake engineering the design elastic seismic actions derive from UHS, the return period of which is based on the limit-state of interest. In case an earthquake occurs close to the site, the design thresholds of the UHS are not hard to be exceeded, even if the event magnitude is far from the maximum possible. From the structural engineering point of view, given the violation of the limit-state of interest, the structural safety is left to other factors beyond the elastic behavior which, generally, are not controlled in design.

In this context, this chapter proposed a single-site PSHA study aiming to (i) quantify the amount of exceedance of the UHS in case of exceedance, which is related to the margin in terms of elastic spectral acceleration a structure should have to resist exceedance, and (ii) the minim magnitude of earthquakes occurring within a given distance for which such exceedance is expected, herein indicated as strong earthquakes.

With reference to Italy and considering two spectral ordinates, PGA and $Sa(T=1s)$, with 475 years return period of exceedance, results of the expected accelerations over the design thresholds and the minimum magnitude of strong earthquakes were given in form of maps. Furthermore, the Milan and L'Aquila sites, located in low and high hazard regions, respectively, allowed to investigate these results as a function of the return period of the design thresholds. The seismic hazard and disaggregation maps, which are useful to the discussions of results, were also given. The seismic source model used to define the design thresholds according to the Italian building code was considered.

With reference to the expected accelerations given the exceedance of the design thresholds, it was found that the largest values are observed in the most hazardous sites and, in general, are larger for PGA than $Sa(T=1s)$. Nevertheless, the largest excursions over the spectrum are expected for $Sa(T=1s)$, indicating a larger exposure of the higher natural vibration periods to exceedance. In case of exceedance of the UHS, the expected

elastic acceleration a structure should resist can be up to 2.5 times the threshold. In the areas outside the seismic source zones, the expected value above the UHS can be smaller than 1.5 times. It was also shown that, given the threshold, the amount of exceedance over the UHS is related to the expected ε from disaggregation. In fact, in the high hazard regions the exceedance is expected from non-anomalous ground motion (lower $\bar{\varepsilon}$) and the expected amount of exceedance is large. Conversely, in the less hazard regions more anomalous event (higher $\bar{\varepsilon}$) are expected to be causative for the exceedance of the threshold, and the expected amount of exceedance is small.

The investigation of the trend of the expected amount of exceedance over the UHS as a function of the return period for Milan and L'Aquila revealed that, even considering the largest return period the code allows, the elastic seismic actions affecting a structure could be in the range between 26%-69% larger than the considered spectrum.

Similarly to the design thresholds, the expected accelerations on a given soil condition given the exceedance of the UHS on that specific soil condition were easily obtained by amplifying those on rock through the soil coefficient. Furthermore, it was shown that the expected amount of exceedance (in relative terms) is independent on the soil condition.

With reference to the soil-independent maps of the minimum magnitude of the strong earthquakes, it was found that for the lowest distance range considered for earthquakes occurrence (5km), on average, it is equal to 5.2 and 5.7 for PGA and $Sa(T=1s)$, respectively. In the most hazardous regions, even the earthquakes of magnitude far from the maximum possible and occurring within a short distance from the site can be causative of the exceedance of the UHS with 475 years return period. In fact, the comparison of the minimum magnitude of strong earthquakes with the maximum magnitude each site can experience revealed that the largest differences are obtained for the sites with high seismic hazard and decrease with the increasing distance range. The analysis of the earthquakes scenarios for which the exceedance of the threshold is expected for L'Aquila and Milan showed that, in general, the design spectrum is hard to be exceeded by close earthquakes of small magnitude and those distant even of high

magnitude. On the other hand, given the occurrence of an earthquake of high magnitude near the site, the conditional probability of exceeding the threshold can be even larger than 0.9. However, given the source-to-site distance, the occurrence of earthquakes of high magnitude decreases with increasing magnitude. In other words, from the structural engineering point of view, the protection of a code-conformed structure in the epicentral areas of strong earthquakes is only warranted by the rarity with which such events occur. According to the study of the minimum magnitude of strong earthquakes as a function of return period for L'Aquila and Milan, one can see that in the most hazardous areas the minimum magnitude of strong earthquakes occurring close to the site is below the maximum magnitude which can occur even for largest return period the code allows.

Chapter 4 – SEQUENCE-BASED PSHA: STUDY OF THE CONTRIBUTION OF AFTERSHOCKS TO SEISMIC HAZARD

Sections 4.3 and 4.4 of this chapter are derived from the following paper:

Chioccarelli E, Cito P, Iervolino I (2018) Disaggregation of sequence-based seismic hazard. In: Proc of the 16th european conference on earthquake engineering, Thessaloniki.

4.1. Introduction

At the state-of-the-art of most advanced structural engineering codes, design seismic accelerations are derived from PSHA. In fact, although earthquakes generally occur in time-space clusters, only mainshocks, typically the largest magnitude events within each cluster, are usually considered in the assessment of the seismic threat at long-term time scale. As stated in Section 2.3, SPSHA includes the effect of aftershocks in PSHA by combining this latter with the APSHA of Yeo and Cornell (2009). As a result, SPSHA provides the annual rate of mainshock-aftershock sequences that cause the exceedance of the threshold at the site (see Equation 2.15). Similarly to PSHA, disaggregation of seismic hazard can be performed in the case of SPSHA. As discussed in Section 2.3.1, given the exceedance of the IM threshold during the mainshock-aftershock sequence, two kinds of disaggregation can be carried out: the joint pdf of mainshock magnitude and distance (Equation 2.19) and the aftershock disaggregation, which provides the probability that the exceedance is caused by an aftershock rather than by a mainshock (Equation 2.20).

With reference to Italy, this chapter first recalls the differences existing between PSHA and SPSHA maps of PGA and $Sa(T=1s)$ with $T_r=475$ years on rock conditions, introduced in Iervolino et al. (2018). The SPSHA maps on site-dependent soil conditions are also shown and compared with the PSHA counterparts.

Subsequently, SPSHA results are presented in detail and compared with those of PSHA for two Italian sites, Frosinone and Messina, selected to be representative of two different typical cases of PSHA disaggregation, and located in medium- and high-seismicity areas. In particular, the chapter focuses on both the kinds of SPSHA disaggregation. Indeed, starting from the comparison of aftershock disaggregations for Frosinone and Messina, the influence on results of the source-to-site distance and aftershock modeling hypotheses is discussed first. Then, the differences in magnitude and distance disaggregation of the seismic hazard when PSHA or SPSHA are of concern are deepened on a national scale. Subsequently, due to strong variability of the contribution of aftershocks to hazard with the considered threshold for a given site, emerged from the presented case-studies, the chapter deepens the general trend of aftershock disaggregation with return period for Italy, which can be monotonically increasing, monotonically decreasing or non-monotonic. To do so, three results in the form of maps are given, with reference to a range of return periods between ten and one-hundred-thousand years: (i) the return period for which the highest probability that the exceedance is caused by an aftershock is obtained, (ii) the highest probability that an aftershock causes the exceedance and (iii) the trend of aftershock disaggregation. These results are re-evaluated with reference to a range of return periods of interest according to the Italian building code, that is those between 50 and 2475 years. Finally, in order to investigate the difference of aftershock disaggregation between different sites for a given return period, the maps of the probabilities that an aftershock causes the exceedance of the threshold for fixed return periods, among those the Italian code refers to for design, are given. All the results presented in this chapter are obtained via the REASSESS V2.0 software described in Chapter 2.

4.2. Sequence-based PSHA for Italy

In Iervolino et al. (2018) the results of SPSHA and the PSHA counterparts are presented in terms of hazard maps on the national scale for fixed return periods and two spectral periods. The cited study focused the attention on the hazard increments when the aftershocks' effect is considered. It was shown that the absolute hazard increments due to SPSHA with respect to PSHA increase with the return period in average on national scale, while percentage increments have a non-monotonic trend with T_r (depending on the considered site). In this section the hazard maps of PGA and $Sa(T=1s)$ with $T_r=475$ years on rock are given in the top panels of Figure 4.1. They provide the design threshold at each site when the effect of aftershocks is taken into account ($sa_{475,SPSHA}$). The maps are carried out by discretizing the whole territory via the same uniformly spaced grid of about ten-thousand point adopted to elaborate the maps of Chapter 3. The seismic source model and GMPE adopted for the analyses are the same discussed in Section 3.2. It is also assumed that the same GMPE is able to describe the ground motion propagation of both mainshock and aftershocks. In the case of aftershocks, the style of faulting is maintained equal to the one used for the mainshock. The model describing the occurrence of aftershocks is the one of Lolli and Gasperini (2003) for the generic Italian aftershocks sequence. According to it, the parameter of the model describing the occurrence of aftershocks (see Equation 2.17) are $a=-1.66$, $b=0.96$, $c=0.03$ $p=0.93$, $\Delta T_A=90$ (in days). Moreover, it is assumed that the minimum magnitude of generated aftershocks corresponds to the minimum mainshock magnitude of the seismic source zones, whit the exception of the zone 936, for which $m_{A,min}=4$, that is the minimum magnitude allowed by the Ambraseys et al. (1996) GMPE. The minimum magnitude of the triggering mainshock is equal to 4.3.

Regarding the geographical distribution of aftershocks, it is assumed that they are located, with uniform probability, in a circular area centred on the mainshock location.

The size of this area, S_A, depends on the magnitude of the mainshock $(m = x)$ via Equation (4.1), in squared kilometres (Utsu, 1970).

$$S_A = 10^{x-4.1} \tag{4.1}$$

The middle panels of Figure 4.1 show the hazard increments due to aftershocks in terms of absolute differences between SPSHA and PSHA thresholds, $\delta_{475,SPSHA}$, computed via Equation (4.2); the bottom panels show the hazard increment in percentage terms, $\Delta_{475,SPSHA}$, computed via Equation (4.3).

$$\delta_{475,SPSHA} = sa_{475,SPSHA} - sa_{475} \tag{4.2}$$

$$\Delta_{475,SPSHA} = \frac{sa_{475,SPSHA} - sa_{475}}{sa_{475}} \tag{4.3}$$

As indicated in Section 3.3.1, the term sa_{475} in the equations denotes the threshold from PSHA maps shown in Figure 3.2.

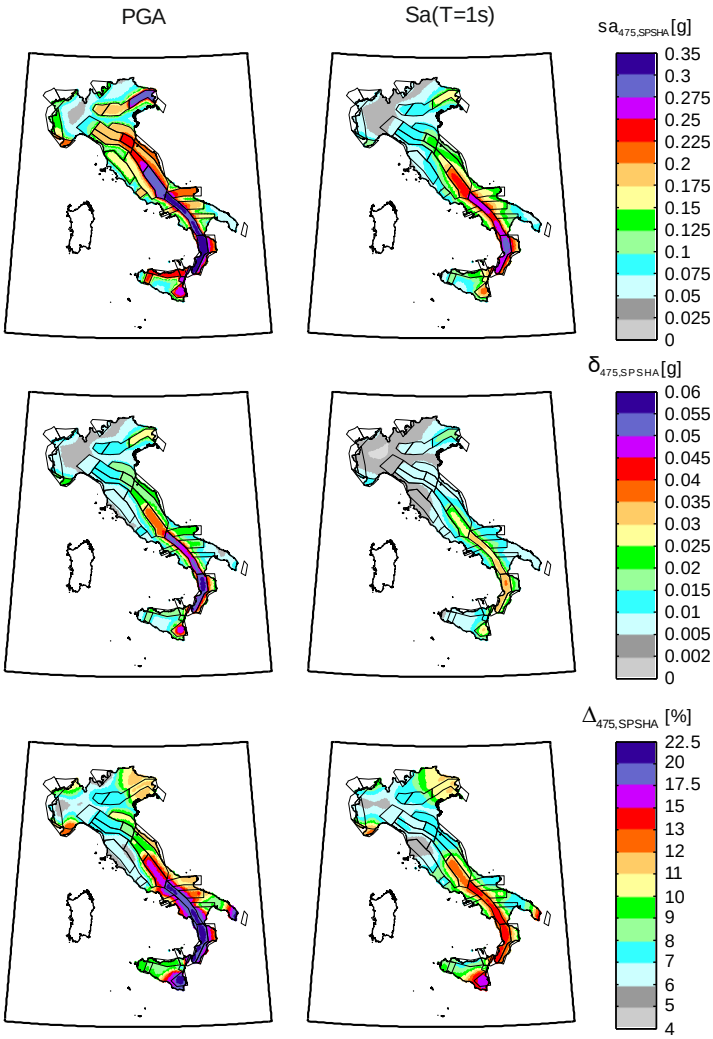

Figure 4.1. Top: SPSHA maps of PGA and $Sa(T=1s)$ with $T_r = 475$ years on rock. Middle and bottom: absolute and percentage differences between SPSHA and PSHA thresholds.

The maps show that absolute and percentage differences for PGA are larger than those for $Sa(T=1s)$. In fact, due to the aftershocks' effect the average absolute increments of PGA and $Sa(T=1s)$ across Italy are 0.0151g and 0.001g, respectively. In percentage terms, the average increments are 10.0% for PGA and 8.7% for $Sa(T=1s)$. For both spectral ordinates, the largest differences can be observed in the most hazardous regions

of the country. SPSHA results show that the highest values of the PGA and $Sa(T=1s)$ which are exceeded, on average, every 475 years, are equal to 0.330g for Aprigliano and 0.291g for Terratelle, respectively. These sites are enclosed by zone 929 and are the same where the design thresholds from PSHA map are the highest, as discussed in Section 3.3.1. The hazard increment due to aftershocks is $\delta_{475,SPSHA}=0.0584g$ in absolute terms and $\Delta_{475,SPSHA}=21.5\%$ in percentage terms for Aprigliano. In the case of Terratelle, the differences are $\Delta_{475,SPSHA}=13.7\%$ and $\delta_{475,SPSHA}=0.0351g$. The differences at the sites in absolute terms are almost equal to the maximum values observed across all the country. In fact, the highest $\delta_{475,SPSHA}$ are equal to 0.0585g and 0.0352g for PGA and $Sa(T=1s)$, respectively; for both the spectral ordinates the corresponding sites are in the district of Cosenza, less than 10km away from Aprigliano and Terratelle and enclosed by zone 929. With reference to the percentage increase, the highest $\Delta_{475,SPSHA}$ are equal to 22.4% and 16.8% for PGA and $Sa(T=1s)$, respectively; for both the spectral ordinates the corresponding site is Ferla (14.92°E, 37.14°N), which is located in the district of Siracusa and enclosed by zone 935.

4.2.1. Effect of site-dependent soil conditions on SPSHA

In Section 3.4.3 the PSHA maps on site-dependent soil conditions are given. The accelerations on soil are obtained via Equation (3.7), which takes advantage of the structure of the adopted GMPE. It is easy to recognize that Equation (3.7) implies that, in the logarithmic scale, the threshold on a particular soil condition can be obtained by adding the soil coefficient to the logarithm of the threshold on rock, as shown in Equation (4.4). This derives from the consideration that, under the hypothesis that θ does not affect the standard deviation of the residual of the GMPE, the hazard curve for a given soil condition (e.g., soft soil) is exactly the hazard curve for rock horizontally moved by θ in the logarithmic scale of the abscissa (see Iervolino, 2016, for demonstration). In

this framework, this section aims to show that the same consideration is valid in the case of SPSHA.

$$log(im_{SPSHA,\theta}) = log(im_{SPSHA}) + \theta \tag{4.4}$$

In other words, if λ_{SPSHA} and $\lambda_{SPSHA,\theta}$ are the rates of exceedance of im_{SPSHA} and $im_{SPSHA,\theta}$ at the same site on rock and on a different soil condition, respectively, and if Equation (4.4) applies, then the hypothesis is that, also in the case of SPSHA, the two rates of exceedance are the same (Equation 4.5).

$$\lambda_{SPSHA} = \lambda_{SPSHA,\theta} \tag{4.5}$$

Equation (4.5), recalling Equation (2.15) and Equation (2.16), can be rewritten as in Equation (4.6) (for simplicity of notation, a single source with unitary rate is considered, and it is assumed that the expected number of aftershocks in the time interval is also equal to 1, that is $E[N_{A|m}(0,\Delta T_A)] = 1$):

$$\begin{aligned}
&\int_M \int_X \int_Y P\left[IM \le im_{SPSHA,\theta} \mid m,x,y,\theta\right] \cdot e^{-\int_{M_A}\int_{X_A}\int_{Y_A} P\left[IM_A > im_{SPSHA,\theta} \mid m_A,x_A,y_A,\theta\right] \cdot f_{M_A,X_A,Y_A \mid M,X,Y}(m_A,x_A,y_A)\cdot dm_A \cdot dx_A \cdot dy_A} \cdot \\
&\cdot f_{M,X,Y}(m,x,y) \cdot dm \cdot dx \cdot dy + \\
&-\int_M \int_X \int_Y P\left[IM \le im_{SPSHA} \mid m,x,y\right] \cdot e^{-\int_{M_A}\int_{X_A}\int_{Y_A} P\left[IM_A > im_{SPSHA} \mid m_A,x_A,y_A\right] \cdot f_{M_A,X_A,Y_A \mid M,X,Y}(m_A,x_A,y_A)\cdot dm_A \cdot dx_A \cdot dy_A} \cdot \\
&\cdot f_{M,X,Y}(m,x,y) \cdot dm \cdot dx \cdot dy = 0
\end{aligned} \tag{4.6}$$

For the distributive property of the integrals, Equation (4.6) can be rewritten as in Equation (4.7):

$$\begin{aligned}
&\int_M \int_X \int_Y \Bigg\{ P\left[IM \le im_{SPSHA,\theta} \mid m,x,y,\theta\right] \cdot e^{-\int_{M_A}\int_{X_A}\int_{Y_A} P\left[IM_A > im_{SPSHA,\theta} \mid m_A,x_A,y_A,\theta\right] \cdot f_{M_A,X_A,Y_A \mid M,X,Y}(m_A,x_A,y_A)\cdot dm_A \cdot dx_A \cdot dy_A} + \\
&-P\left[IM \le im_{SPSHA} \mid m,x,y\right] \cdot e^{-\int_{M_A}\int_{X_A}\int_{Y_A} P\left[IM_A > im_{SPSHA} \mid m_A,x_A,y_A\right] \cdot f_{M_A,X_A,Y_A \mid M,X,Y}(m_A,x_A,y_A)\cdot dm_A \cdot dx_A \cdot dy_A} \Bigg\} \cdot \\
&\cdot f_{M,X,Y}(m,x,y) \cdot dm \cdot dx \cdot dy = 0
\end{aligned} \tag{4.7}$$

The integral in Equation (4.7) is null because the term in the brace is null $\forall(m,x,y)$ and $\forall(m_A,x_A,y_A)$. To recognize this, the difference in Equation (4.7) can be rewritten according to Equation (4.8), where Φ is the Gauss function:

$$\Phi\left[\frac{log(im_{SPSHA,\theta})-(\mu_{m,x,y}+\theta)}{\sigma}\right]\cdot \cdot e^{-\int_{M_A}\int_{X_A}\int_{Y_A}1-\Phi\left[\frac{log(im_{SPSHA,\theta})-(\mu_{m_A,x_A,y_A}+\theta)}{\sigma}\right]\cdot f_{M_A,X_A,Y_A|M,X,Y}(m_A,x_A,y_A)\cdot dm_A\cdot dx_A\cdot dy_A} + -\Phi\left[\frac{log(im_{SPSHA})-\mu_{m,x,y}}{\sigma}\right]\cdot e^{-\int_{M_A}\int_{X_A}\int_{Y_A}1-\Phi\left[\frac{log(im_{SPSHA})-\mu_{m_A,x_A,y_A}}{\sigma}\right]\cdot f_{M_A,X_A,Y_A|M,X,Y}(m_A,x_A,y_A)\cdot dm_A\cdot dx_A\cdot dy_A} \quad (4.8)$$

Therefore, Equation (4.9) can be obtained by replacing Equation (4.4) in Equation (4.8):

$$\Phi\left[\frac{log(im_{SPSHA})+\theta-(\mu_{m,x,y}+\theta)}{\sigma}\right]\cdot \cdot e^{-\int_{M_A}\int_{X_A}\int_{Y_A}1-\Phi\left[\frac{log(im_{SPSHA})+\theta-(\mu_{m_A,x_A,y_A}+\theta)}{\sigma}\right]\cdot f_{M_A,X_A,Y_A|M,X,Y}(m_A,x_A,y_A)\cdot dm_A\cdot dx_A\cdot dy_A} + -\Phi\left[\frac{log(im_{SPSHA})-\mu_{m,x,y}}{\sigma}\right]\cdot e^{-\int_{M_A}\int_{X_A}\int_{Y_A}1-\Phi\left[\frac{log(im_{SPSHA})-\mu_{m_A,x_A,y_A}}{\sigma}\right]\cdot f_{M_A,X_A,Y_A|M,X,Y}(m_A,x_A,y_A)\cdot dm_A\cdot dx_A\cdot dy_A} = \Phi\left[\frac{log(im_{SPSHA})-\mu_{m,x,y}}{\sigma}\right]\cdot e^{-\int_{M_A}\int_{X_A}\int_{Y_A}1-\Phi\left[\frac{log(im_{SPSHA})-\mu_{m_A,x_A,y_A}}{\sigma}\right]\cdot f_{M_A,X_A,Y_A|M,X,Y}(m_A,x_A,y_A)\cdot dm_A\cdot dx_A\cdot dy_A} + -\Phi\left[\frac{log(im_{SPSHA})-\mu_{m,x,y}}{\sigma}\right]\cdot e^{-\int_{M_A}\int_{X_A}\int_{Y_A}1-\Phi\left[\frac{log(im_{SPSHA})-\mu_{m_A,x_A,y_A}}{\sigma}\right]\cdot f_{M_A,X_A,Y_A|M,X,Y}(m_A,x_A,y_A)\cdot dm_A\cdot dx_A\cdot dy_A} = 0 \quad (4.9)$$

This implies that Equation (4.6) is true. In other words, the logarithms of im_{SPSHA} and $im_{SPSHA,\theta}$ have the same rate of exceedance. Therefore, the hazard curve for a given soil condition can be obtained by horizontally translating by θ in the logarithmic scale of the abscissa the hazard curve for rock also in the case of SPSHA. Furthermore, similarly to the case of PSHA, SPSHA magnitude and distance disaggregations (Equation 2.19)

and aftershock disaggregations (Equation 2.20) on two different soil conditions are equal. In fact, the denominator in the disaggregation equations for the two soil is the same, by hypothesis, and the numerators coincide according to Equation (4.9). Similarly to PSHA, in the case of logic tree featuring different GMPEs, the discussed translation of hazard curves has to be applied to each branch (see Section 2.2.3).

At this point the SPSHA maps of PGA and $Sa(T=1s)$ with $T_r=475$ years on site-dependent soil conditions (top panels of Figure 4.2) can be introduced. In fact, the thresholds $(sa_{475,soil,SPSHA})$ are computed according to Equation (3.7), similarly to Section 3.4.3. The absolute $(\delta_{475,soil,SPSHA})$ and percentage $(\Delta_{475,soil,SPSHA})$ differences with the PSHA counterparts (for site-dependent soil conditions) are also given according to Equation (4.10) and (4.11), respectively.

$$\delta_{475,soil,SPSHA} = sa_{475,SPSHA} \cdot e^{\theta} - sa_{475} \cdot e^{\theta} = e^{\theta} \cdot \delta_{475,SPSHA} \tag{4.10}$$

$$\Delta_{475,soil,SPSHA} = \frac{sa_{475,SPSHA} \cdot e^{\theta} - sa_{475} \cdot e^{\theta}}{sa_{475} \cdot e^{\theta}} = \Delta_{475,SPSHA} \tag{4.11}$$

Equations show that, if the site-dependent soil conditions are considered, the absolute increments due to aftershocks can be easily obtained by multiplying those for rock by the exponential of the soil coefficient, while the percentage differences are independent on θ. In Figure 4.2, the map of the absolute differences on site-dependent soil conditions are given in the middle panels, while the bottom panels are the same of Figure 4.1.

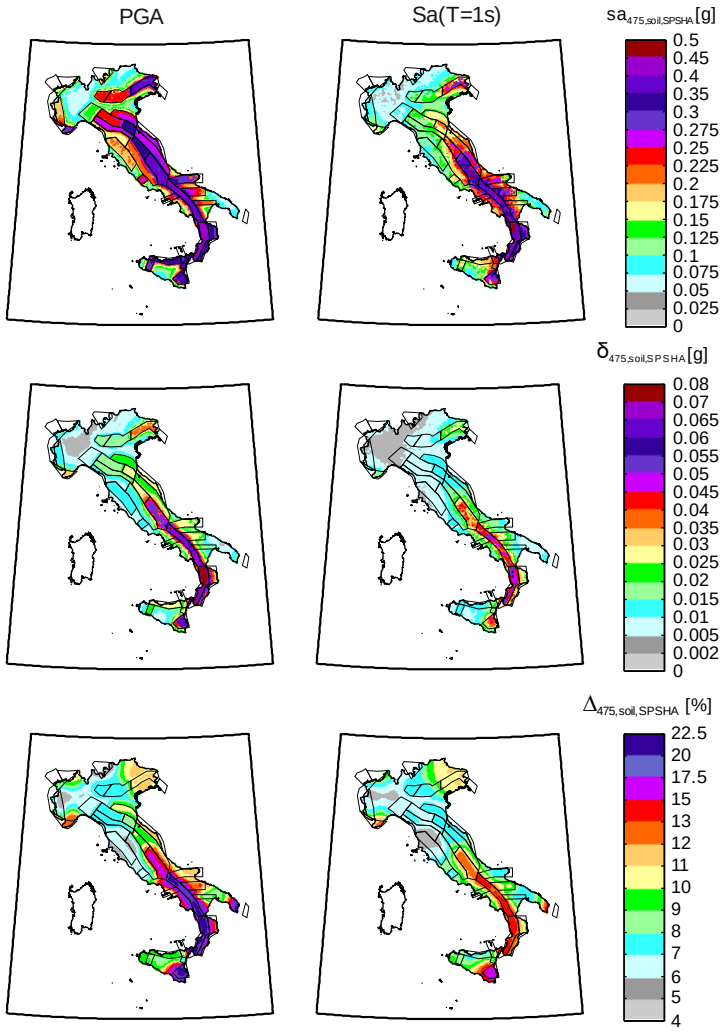

Figure 4.2. Top: SPSHA maps of PGA and $Sa(T=1s)$ with $T_r = 475$ years on site-dependent soil conditions. Middle and bottom: absolute and percentage differences between SPSHA and PSHA thresholds.

Since the soil coefficients are those of Table 3.6, due to soil effects the average increments of PGA and $Sa(T=1s)$ are about 26% and 36%, respectively, as in the case of PSHA (see Section 3.4.3). However, since the percentage increment is soil-independent, the amount of exceedance over the PSHA thresholds is, on average, larger for PGA than $Sa(T=1s)$. The absolute differences are, on average, 0.0190g for PGA

and 0.0129g for $Sa(T=1s)$. In particular, in the case of PGA the highest value is 0.435g, while it is equal to 0.473g for $Sa(T=1s)$. The corresponding sites are those where the PSHA maps on site-dependent soil conditions (Figure 3.6) have the highest values, that is Destre and Donnici Inferiore, located in the district of Cosenza and enclosed by zone 929. As discussed in Section 3.4.3, the soil amplification for these sites is such that the thresholds on soil are larger than those for the Aprigliano and Terratelle sites. The absolute differences due to aftershocks increase to 0.0766g for PGA and 0.0567g for $Sa(T=1s)$ when soil effects are taken into account. It can be observed that, in the case of PGA, the site is the same where the highest value of $\delta_{475,SPSHA}$ is obtained (see the previous section), while for $Sa(T=1s)$ the soil amplification is such that for the site (classified as soft soil) where the maximum $\delta_{475,soil,SPSHA}$ is obtained is not the same (classified as stiff soil) where $\delta_{475,SPSHA}$ is the largest.

4.3. SPSHA disaggregation

In this section, the attention is focused on the both types of hazard disaggregations presented in Section 2.3.1, with the twofold aim of deepen the trend of aftershock disaggregation as a function of the return period and discuss the differences between magnitude-distance disaggregation distributions in the case of PSHA and SPSHA.

For the intended purposes, two sites are selected: Frosinone in central Italy (13.37°E, 41.64°N) and Messina in southern Italy (15.55°E, 38.19°N). The selection of these two sites is motivated by two reasons. First, they are representative of the medium- (Frosinone) and high-seismicity (Messina) Italian sites. Then, their geographical location with respect to the seismic sources makes the two sites representative of two typical situations in terms of earthquakes most contributing to the hazard. Indeed, Messina is enclosed into zone 929, one of three Italian zones with largest maximum magnitude (see Figure 3.1). As a consequence, according to the source model, the site

could be hit by very strong events (up to magnitude equal to 7.45) at zero source-to-site distance. The other seismic zones potentially affecting the hazard of the site may produce weaker (or equal magnitude, in the case of zone 935) and more distant earthquakes. Thus, it can be anticipated that hazard contributions of the other zones are comparatively smaller with respect to the contribution of zone 929 (see also Iervolino et al. 2011). This will result unimodal magnitude-distance disaggregation to follow.

On the other hand, the site of Frosinone is within the zone 920 (central magnitude of the highest magnitude equal to 5.2) and is close to the more seismically active zone 923 (central magnitude of the highest magnitude equal to 7.3). Thus, the zero-distance events for Frosinone are characterized by a maximum magnitude that is much lower than the more distant events generated by the zone 923 (the minimum distance of Frosinone from the boundaries of the zone 923 is about 22 km). This suggests that both zones have significant effects on the hazard of the site and the magnitude-distance disaggregation distributions may be bimodal. Further details are presented in the following section.

For both the sites, all the results are carried out considering rock soil conditions.

4.3.1. Frosinone

Results of hazard assessment for Frosinone are given in Figure 4.3. More specifically, Figure 4.3a shows the site location and the twelve seismogenic zones within 200 km (in terms of R_{jb}; i.e., the definition range of the adopted GMPE). Uniform hazard spectra in terms of pseudo-acceleration for the four return periods of 50, 475, 975 and 2475 years are reported in Figure 4.3b. The spectra, indicated as PSHA_{Tr} and SPSHA_{Tr}, are computed considering the forty-seven natural vibration (spectral) periods, T, between zero and two seconds provided by the GMPE. Increments between SPSHA and PSHA for the selected return periods are reported in Figure 4.3c as a function of the spectral period. Hazard increments are within 7% and 13% for all the vibration periods and the largest values of increments are associated to the lowest return period.

Aftershock disaggregation is reported in Figure 4.3d as a function of the increasing return period. The considered spectral ordinates are PGA and $Sa(T=1s)$. As discussed, aftershock disaggregation according to Equation (2.20) provides the probability that, once exceedance of the threshold is observed, it is caused by an aftershock rather than a mainshock; in this sense, it may help in assessing the contribution of aftershock to hazard. These curves show a monotonic shape: the longer the return period, the higher the probability that aftershocks are causative of the exceedance of the threshold. Such a trend looks reasonable recalling that increasing the return period (i.e., increasing the threshold), the magnitude of earthquakes most contributing to the hazard tend to increase (see for example Iervolino et al., 2011) and larger magnitude mainshocks generate longer and with larger magnitudes aftershock sequences. However, the trend of aftershock disaggregation is not common to all the Italian sites (see also Section 4.6). In fact, the disaggregation in Figure 4.3d is different with respect to the case of Messina (see the next section). The reason behind these differences will be explained in Section 4.4.

The second line of panels in Figure 4.3 is dedicated to the magnitude-distance disaggregation distributions. Such distributions are reported discretized per bins of magnitude and distance. The dimension of each bin is 0.5 and 10km, respectively (but the first bin of distance is from 0 to 5km). The figures show such disaggregations computed for PGA (Figure 4.3e and Figure 4.3f) and $Sa(T=1s)$ (Figure 4.3g and Figure 4.3h). In the panel, Figure 4.3e and Figure 4.3g are from Equation (2.6) while Figure 4.3f and Figure 4.3h are from Equation (2.19). In the plots, the symbols $f_{M,\mathrm{R}|IM>im}(m,\mathrm{r})$ and $f_{M,R|IM>im\cup IM_{\cup A}>im}(m,r)$ are replaced by $P\left[M_E,R_E\left|IM_E>im\right.\right]$ and $P\left[M_E,R_E\left|IM_E>im\cup IM_{\cup A}>im\right.\right]$, respectively, because the continuous magnitude and distance random variables are represented in a discretized form; the subscript (E) indicates that the variables are referred to mainshock. To maximize the possible difference among SPSHA and PSHA disaggregations, the selected return period is 10000 years, which corresponds to the maximum of the aftershock disaggregation, shown in

Figure 4.3d. However, it should be noted that aftershock disaggregation keeps increasing for return periods larger than those considered here and so differences among magnitude-distance disaggregations.

Figure 4.3e shows two modal bins corresponding to $\{4.5 \le M_E \le 5; 0 \le R_E \le 5\}$ and $\{7.0 \le M_E \le 7.5; 15 \le R_E \le 25\}$. The former is due to the zone 920 while the latter is from zone 923. Comparison among Figure 4.3e and Figure 4.3g confirms one of the results of Iervolino et al. (2011): the disaggregation is dependent on the considered spectral period and, in case of bimodal disaggregation distribution, when the spectral period increases, the hazard contribution of stronger and more distant seismic events may increase. The novel result can be derived by the comparison of the PGA disaggregations in Figure 4.3e (PSHA) and Figure 4.3f (SPSHA). Although the two distributions are characterized by the same two modal values, it is apparent that when the aftershocks' effect to the hazard is considered, the modal value associate to higher magnitude-distance events becomes comparatively more significant. This is because clusters generated by higher magnitude events are more likely exceeding the threshold.

On this issue, it can be added that comparison of the magnitude-distance disaggregations of PGA for return period equal to 10000 years, shows that, in the case of SPSHA, the first modal value become equal to $\{7.0 \le M_E \le 7.5; 15 \le R_E \le 25\}$, while it remains $\{4.5 \le M_E \le 5; 0 \le R_E \le 5\}$ for PSHA. When $Sa(T = 1s)$ is of concern (Figure 4.3g and Figure 4.3h), the differences among PSHA and SPSHA are less significant because, as recalled, the stronger and more distant events are the most contributing to hazard even in the PSHA case.

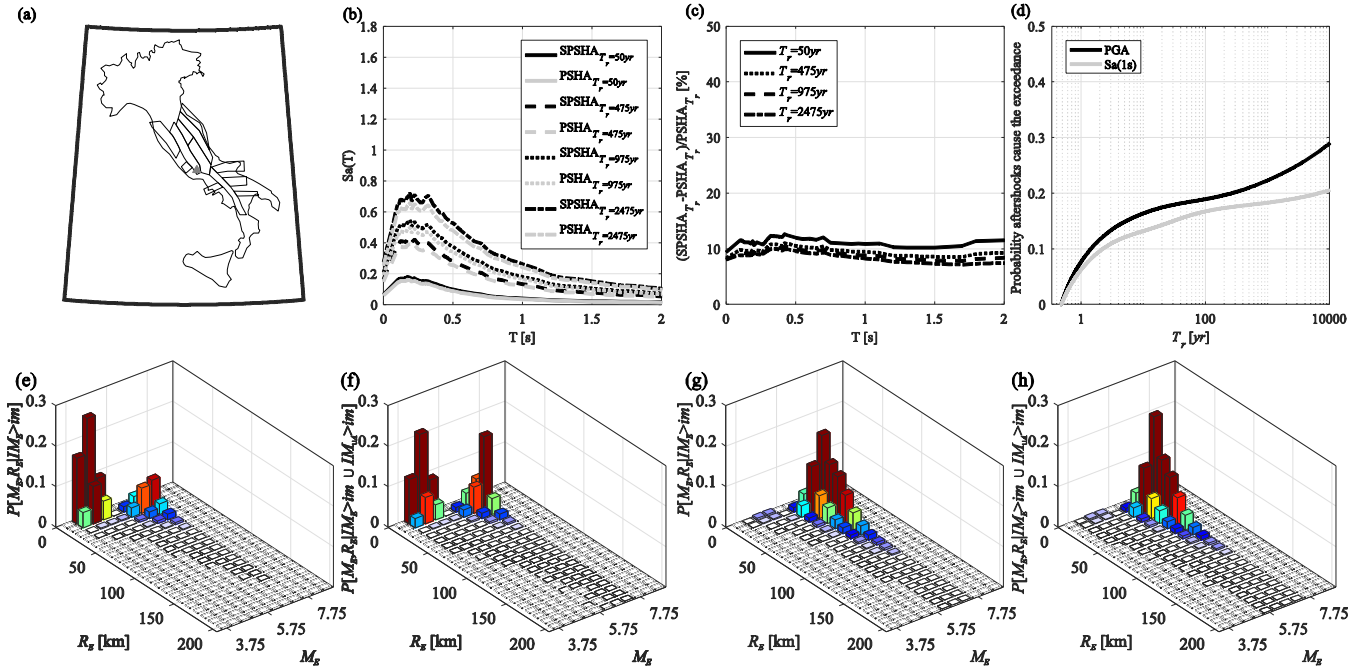

Figure 4.3. Results of hazard analyses for Frosinone: (a) location of the site and seismic areal zones contributing to its hazard; (b) UHS' for 50years, 475 years, 975 years and 2475 years; (c) hazard increments as a function of the spectral period and for fixed return periods; (d) aftershock disaggregations for PGA and $Sa(T=1s)$; (e) and (g) magnitude and distance disaggregation distributions according to PSHA for PGA and $Sa(T=1s)$ respectively and $T_r=10000$ years; (f) and (h) magnitude and distance disaggregation distributions according to SPSHA for PGA and $Sa(T=1s)$ respectively and $T_r=10000$ years.

4.3.2. Messina

The results for the site of Messina are reported in Figure 4.4. The site is on the boundary of zone 929 and the eight zones reported in Figure 4.4a are those within the distance definition range of the GMPE. UHS' for the four return periods are shown in Figure 4.4b. Hazard increments (Figure 4.4c) due to SPSHA with respect to PSHA are, for this site, between about 12% and 25% for vibration periods up to one second and between 10% and 13% for higher spectral periods. Hazard disaggregation is reported in Figure 4.4d. Its trend is completely different with respect to Frosinone. Indeed, aftershock disaggregation increases with the return period until it reaches a maximum equal to 0.32 for PGA and 0.18 for $Sa(T=1s)$. Then, for both the IMs, it starts decreasing. The return period corresponding to the maximum is 1150 and 1350 years for PGA and $Sa(T=1s)$, respectively.

Magnitude-distance disaggregation distribution are reported in the same figure for PGA and $Sa(T=1s)$. Similarly to the previous case, Figure 4.4e and Figure 4.4g are computed via Equation (2.6) while Figure 4.4f and Figure 4.4h are from Equation (2.19). The considered return periods are those for which the aftershock disaggregations of Figure 4.4d are maximum, that is, 1150 and 1350 years. All the four distributions have a single modal value equal to $\{7.0 \le M_E \le 7.5; 5 \le R_E \le 15\}$ indicating that the earthquakes most contributing to the hazard are from the zone 929. Comparison between PSHA and SPSHA magnitude-distance disaggregation for PGA (Figure 4.4e and Figure 4.4f, respectively) shows that considering aftershocks reduce the conditional probabilities of low magnitudes and increases the ones of high magnitude. This is in accordance with what observed for Frosinone, even if applied to the case of unimodal disaggregations. In accordance with what discussed for Frosinone is also the comparison between disaggregations when $Sa(T=1s)$ is of concern: differences between PSHA and SPSHA are minor.

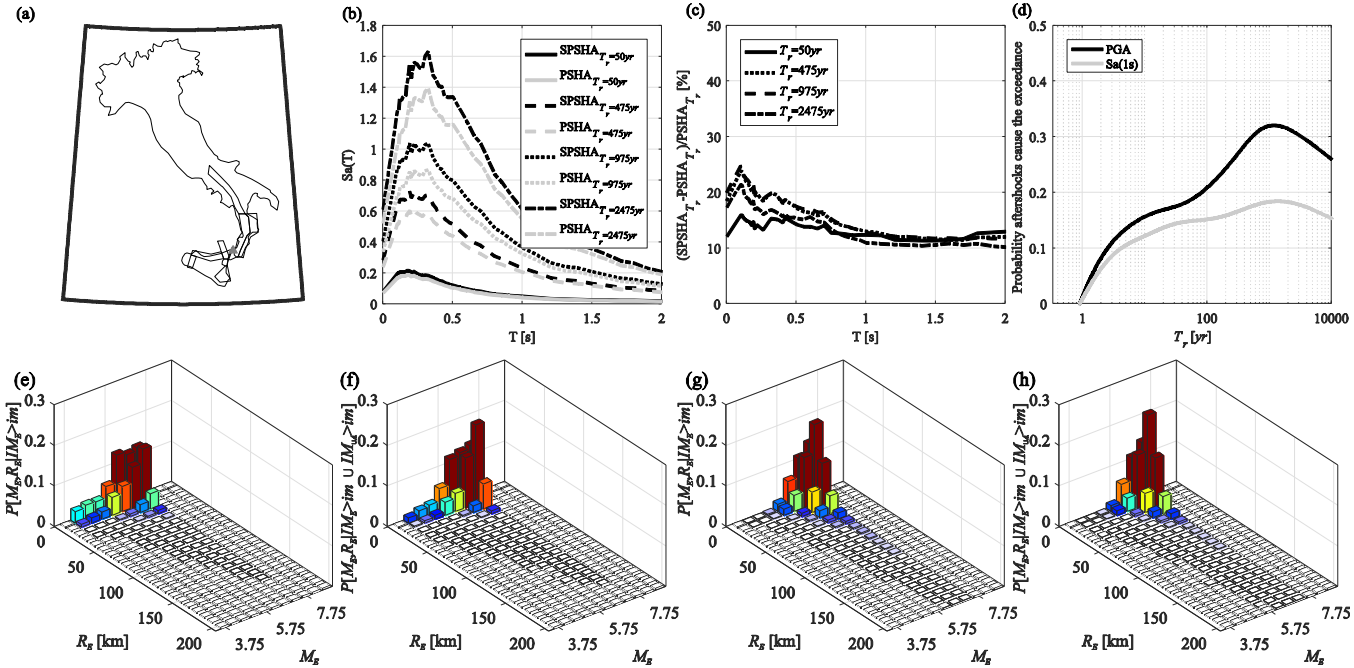

Figure 4.4. Results of hazard analyses for Messina: (a) location of the site and seismic areal zones contributing to its hazard; (b) UHS' for 50years, 475 years, 975 years and 2475 years; (c) hazard increments as a function of the spectral period and for fixed return periods; (d) aftershock disaggregations for PGA and $Sa(T=1s)$; (e) and (f) magnitude and distance disaggregation distributions for PGA and $T_R=1150$ years according to PSHA and SPSHA, respectively; (g) and (h) magnitude and distance disaggregation distributions for $Sa(T=1s)$ and $T_R=1350$ years according to PSHA and SPSHA, respectively.

4.4. Source-to-site distance effect on aftershocks disaggregation

According to the results obtained for Frosinone and Messina (see previous sections), the trend of aftershock disaggregation as a function of the increasing return period may be significantly different from site to site (see Figure 4.3d and Figure 4.4d). The thesis addressed in this section is that such differences are due to the adopted hypothesis about the spatial distribution of aftershocks around the mainshock. This is discussed considering two simplified scenarios in which the hazard of the site is assumed to be affected by one point-like seismic source producing mainshocks of single magnitude, $M_E = 7.3$. The sole difference between the two scenarios is the relative site-source location. This is chosen in order to be representative of the distance modal value of the magnitude-distance SPSHA disaggregation of the Messina and Frosinone sites, when a high return period is disaggregated. Thus, in the scenarios here analysed, the mainshock source-to-site distance, R_E, equals to zero and twenty kilometres, respectively. It should also be noted that, the constant magnitude here selected is equal to the mean value of the largest bin of magnitude generated by both the zones 923 and 929.

The two scenarios are represented in Figure 4.5: the site is represented as a triangle in the figure while the point-like seismic source is the red star. Because the GMPE and aftershocks' distribution models here adopted are the same described above for the case of Italy, the circular geographical area on which aftershocks are uniformly distributed is known via Equation (4.1) and is equal to about 1600 square kilometres with a radius of about 22km; this area is represented shaded in the figure.

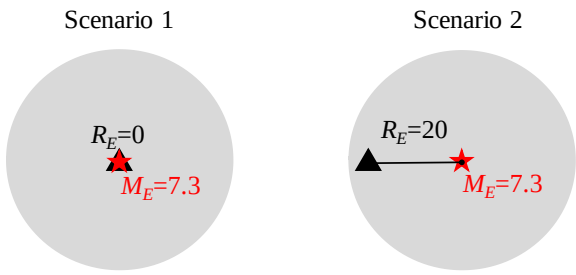

Figure 4.5. Simplified source-to-site cases.

For each scenario, the PGA aftershock disaggregation is computed as a function of the return period. The resulting plots are reported in Figure 4.6a. When $R_E = 0$, the maximum probability from hazard disaggregation is lower than 0.10 and correspond to a very short return period (about one year). Increasing the return period, aftershock disaggregation monotonically decreases being all the possible aftershocks of lower magnitude and at larger distance than the mainshock. This means that, given that the threshold is exceeded (at least once) during a sequence, the probability that the exceedance is due to an aftershock tends to zero when the threshold (i.e., the return period) increases. This case is, in fact, representative of the aftershock disaggregations of sites enclosed in seismic source with high seismicity (e.g., the site of Messina).

The opposite trend of aftershock disaggregation is observed in the $R_E = 20$ scenario. In this case, the site is at the boundary of the aftershock geographical distribution thus the distance from the mainshock is (almost) the maximum that allows the occurrence of aftershocks at zero distance. In this condition, with the increasing return period, aftershock disaggregation monotonically increases toward the asymptotic limit of one. This means that the higher is the threshold, the higher the probability that the exceedance of the threshold during the cluster is due to an aftershock. The results shown in Figure 4.3d are, in fact, a combination of the two scenarios discussed in this section.

To complete the discussion, an alternative hypothesis on the aftershock geographical distribution is considered: it is assumed that all the aftershocks occur at the mainshock

location, $R_A = R_E$. The aftershock disaggregations resulting in these cases are shown in Figure 4.6b for the same two values of R_E. As apparent, the two plots have a common trend, that is the disaggregation is only slightly influenced by R_E value. This result validates the thesis formulate at the beginning of this section that the observed differences in aftershock disaggregation are due to the hypothesis on the spatial distribution of aftershocks around the mainshock.

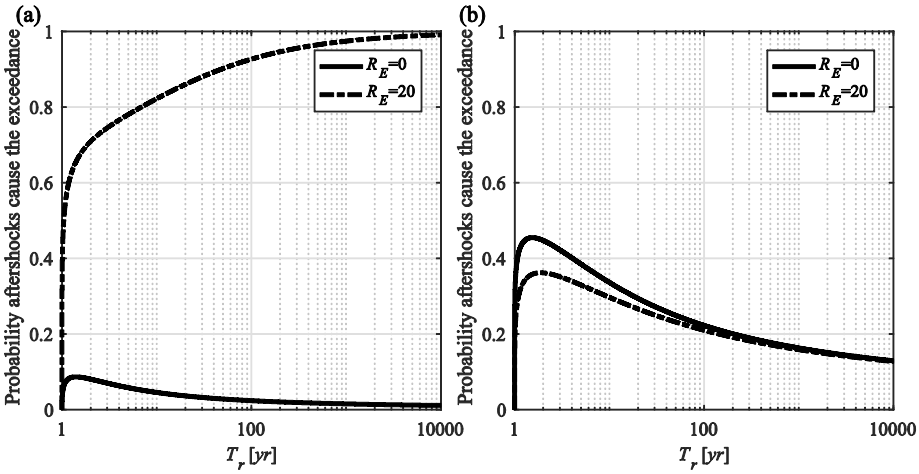

Figure 4.6. Aftershocks disaggregations for the two seismic scenarios of Figure 4.5: (a) according to the geographical aftershock distribution of Utsu (1970); (b) assuming all the aftershocks located at the epicenter of the mainshock.

4.5 Magnitude and distance disaggregation maps

As stated in Section 2.3.1, disaggregation of seismic hazard can be performed also in the case of SPSHA. In fact, given that the exceedance of the threshold has been observed during the mainshock-aftershock sequence, Equation (2.19) provides the joint pdf of mainshock magnitude and distance, $f_{M,R|IM>im\cup IM_{\bigcup A}>im}(m,r)$. Similarly to Section 3.3.2, the mean values of magnitude and distance conditional to the exceedance of $sa_{475,SPSHA}$,

herein indicated as $\overline{M}_{SPSHA}$ and $\overline{R}_{SPSHA}$, respectively, are computed and mapped for Italy as shown Figure 4.7.

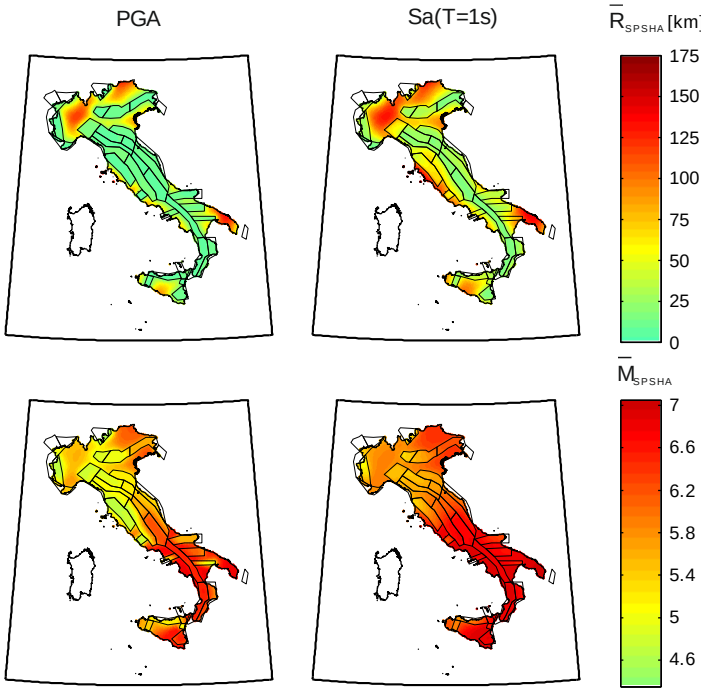

Figure 4.7. Maps of disaggregation in terms of average source-to-site distance and magnitude, given the exceedance of the PGA and $Sa(T=1s)$ threshold with $T_r = 475$ years according to SPSHA.

A first comparison of the maps in Figure 4.7 with their PSHA counterparts introduced in Section 3.3.2 (see Figure 3.3) reveals that there are not significant differences for both the considered spectral ordinates. In fact, with respect to the maps of the average distance, the colours scale from the PSHA counterpart is kept (see Figure 3.3) due to the slight differences of the maximum values. In particular, with reference to PGA the minimum and maximum values of $\overline{R}_{SPSHA}$ are equal to 7km (Spinaceto, enclosed by zone 922; 12.44°E, 41.78°N) and 153km (Pianosa), respectively. In the case of $Sa(T=1s)$ the minimum value is 14km (Alpi mountain chain, zone 902; 8.10°E, 46.26°N), while the maximum is 174km (Pianosa). It is recalled that, when PSHA is of

concern, the minimum and maximum values of the expected distance are equal to 6km and 152km, in the case of PGA; with reference to $Sa(T=1s)$, the minimum value of $\overline{R}_{PSHA}$ is 14km, while the maximum is 174km (see Section 3.3.2). On the other hand, with reference to magnitude, the colours scale is slightly different with respect to the PSHA counterpart. In fact, the minimum and maximum values of $\overline{M}_{SPSHA}$ are equal to 4.6 (Curon Venosta, zone 903; 10.56°E, 46.80°N) and 6.8 (Baia di Gallipoli, outside any seismic source; 18.08°E, 40°N) in the case of PGA. With reference to $Sa(T=1s)$, the minimum value of $\overline{M}_{SPSHA}$ is equal to 5.1 (near the Autaret lakes, on the Alpi mountain chain, zone 908; 7.12°E, 45.24°N), while the maximum is 7.0 (Torre Pali, outside any seismic source; 18.22°E, 39.86°N). In the case of PSHA, the minimum and maximum values of the expected magnitude are equal to 4.5 and 6.7, respectively; in the case of $Sa(T=1s)$ the minimum $\overline{M}_{PSHA}$ is 5.1, while the maximum is 6.9 (see Section 3.3.2). However, to further investigate the differences between the SPSHA and PSHA mean values of magnitude and distance, it is worthwhile to look at Figure 4.8. The top panels provide, for each site, the percentage variation of the mainshock mean distance when the effects of aftershocks to hazard are considered, $\Delta_{\overline{R}}$, calculated according to Equation (4.12). Similarly, the bottom panels show the percentage variation of mainshock mean magnitude, $\Delta_{\overline{M}}$, according to Equation (4.13). It is recalled that, in the mentioned equations, $\overline{R}$ and $\overline{M}$ are the average distance and magnitude from PSHA disaggregation maps (Figure 3.3).

$$\Delta_{\overline{R}} = \frac{\overline{R}_{SPSHA} - \overline{R}}{\overline{R}} \tag{4.12}$$

$$\Delta_{\overline{M}} = \frac{\overline{M}_{SPSHA} - \overline{M}}{\overline{M}} \tag{4.13}$$

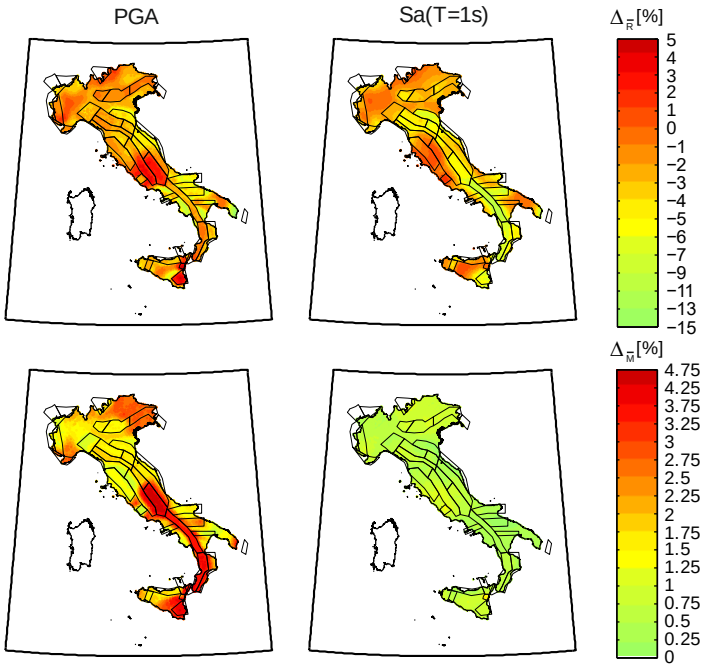

Figure 4.8. Differences between PSHA and SPSHA magnitude and distance disaggregation, given the exceedance of the PGA and $Sa(T=1s)$ threshold with $T_r = 475$, in term of average distance (top) and magnitude (bottom).

The maps of $\Delta_{\bar{R}}$ show that when the effects of aftershocks to hazard are considered, at most of the sites the average distance from the mainshock is smaller with respect to the case of PSHA. In fact, $\bar{R}_{SPSHA} < \bar{R}$ in the 89.3% and 95.4% of the territory for PGA and $Sa(T=1s)$, respectively. The maps of $\Delta_{\bar{M}}$ show that in the case of SPSHA the mean magnitude of the mainshocks causing the exceedance of $sa_{475,SPSHA}$ is larger with respect to the case of PSHA. On average, $\Delta_{\bar{M}}$ is equal to 1.98% for PGA and 0.56% for $Sa(T=1s)$. In particular, with reference to PGA, the maximum percentage increment is equal to 4.57%, occurring at Villetta Barrea (enclosed by zone 923; 13.90°E, 41.80°N). In the case of $Sa(T=1s)$, the maximum value of $\Delta_{\bar{M}}$ is 1.54%, occurring at Linera (enclosed by zone 936; 15.12°E, 37.66°N). These observations are in accordance to what observed for Frosinone and Messina (see Section 4.3.1 and Section 4.3.2). In

fact, even if these results only consider the mean values of the joint pdf of mainshock magnitude and distance (i.e., not distinguishing between uni- and bi-modal distributions), it can be argued that, when the effect of aftershocks is considered, the mean magnitude of the mainshock causing the exceedance of the threshold is larger than the case of PSHA on the national scale. This is because high magnitude mainshocks generate aftershocks which can also have a high magnitude (at least equal to the mainshock one). Thus, the whole mainshock-aftershock can have a not-negligible probability of causing the exceedance of the threshold.

4.6 Aftershock disaggregation maps

4.6.1. Contribution of aftershocks to hazard

In Section 2.3.1 it is shown that, given the exceedance of a threshold of interest, the contribution to hazard of aftershocks can be quantified via Equation (2.20). In fact, the recalled equation provides the probability that such exceedance is caused by an aftershock rather than by a mainshock, $P\left[IM \le im \cap IM_{\cup A} > im \middle| IM > im \cup IM_{\cup A} > im \right]$. The case-studies proposed in Section 4.3.1 and Section 4.3.2 point out that, given the site, this probability can strongly vary with the considered threshold, that is, return period. This would mean that, in the framework of performance-based earthquake engineering, the contribution of aftershocks to hazard varies with the design structural performance of interest. Section 4.3.1 and Section 4.3.2 also reveal that, given the return period, the probability that an aftershock is causative for the exceedance of the threshold can be very different from site to site and, as stated in Section 4.4, such differences are related to the adopted hypothesis about the spatial distribution of aftershocks around the mainshock. For these reasons, this section is intended to deepen the general trend of aftershock disaggregation with return period, on a national scale. In fact, it is shown that, for a range of return periods, three possible trends can be identified, that is, monotonically increasing, monotonically decreasing and non-monotonic. For example,

in each of the panels of Figure 4.9 the continuous curves represent, for a given site, the probability that the aftershock is causative for the exceedance of the threshold as a function of the return period in the range between 50 and 2475 years, The bounds of the range are not casual. In fact, according to the Italian building code, the former is the lowest return period which is typically considered for design (e.g., verification of damage limit-state for an ordinary structure), while the latter is the maximum considered. The sites are chosen to be representative of different disaggregation trends. In fact, Figure 4.9a shows one of the rare cases in which the contribution of aftershocks to hazard decreases with increasing return period for both the spectral ordinates (Alagna site; 8.86°E, 45.18°N). Conversely, Figure 4.9b shows the less unusual case where both PGA and $Sa(T=1s)$ disaggregations increase with return period (Salino site; 13.12°E, 46.50° N). Figure 4.9c considers another rare case in which aftershock disaggregation monotonically increases with return period for PGA, while it decreases for $Sa(T=1s)$ (Barberino di Mugello site; 11.22°E, 44.0°N). Finally, in Figure 4.9d the general case in which both PGA and $Sa(T=1s)$ disaggregations have a not-monotonic trend is shown (Resiga site; 8.66°E, 46°N).

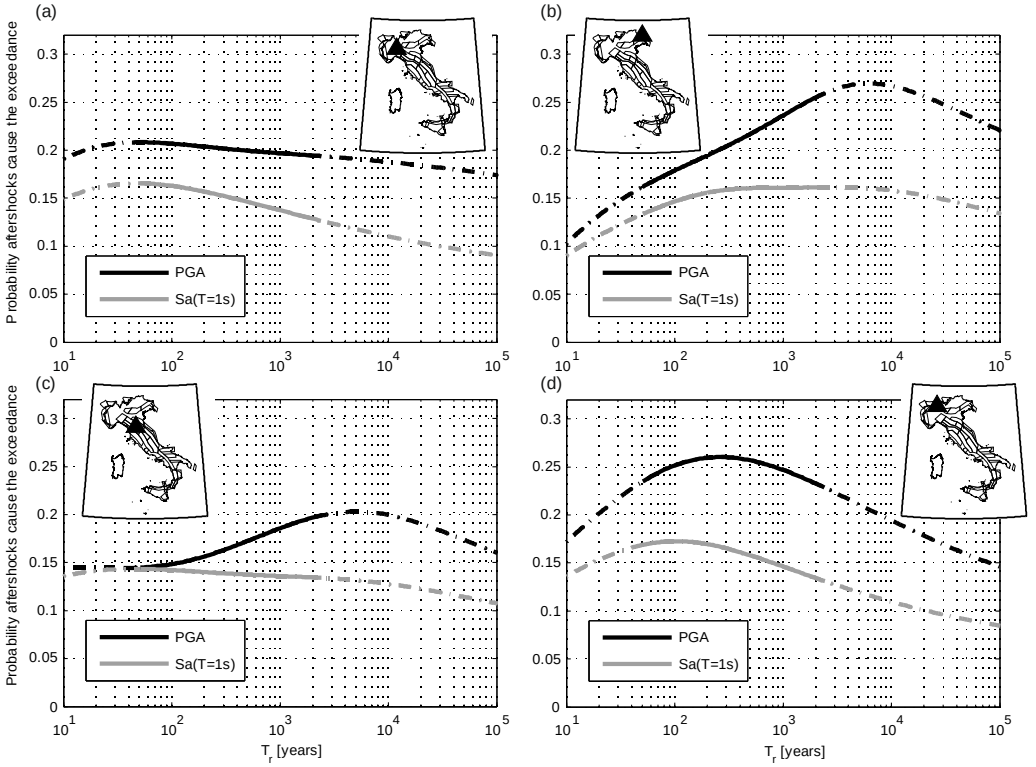

Figure 4.9. Aftershock disaggregations for PGA and $Sa(T=1s)$ as a function of return period: (a) Alagna (8.86°E, 45.18°N); (b) Salino (13.12°E, 46.50° N); (c) Barberino di Mugello (11.22°E, 44.0°N); (d) Resiga (8.66°E, 46°N).

The dotted curves represent the contribution of aftershocks to hazard for return periods out of the range envisioned by the Italian code. Overall, a range of return periods between ten and one-hundred-thousand years is considered. It can be easily observed that the monotonic trend of the aftershock disaggregation tends to be non-monotonic with the increasing return period in the larger range (see Figure 4.9a-c).

In order to investigate the general trend of the aftershock disaggregation with return period on the national scale, Figure 4.10 is given. With reference to a range of return periods between ten and one-hundred-thousand years, the top panels provide the return period for which the highest probability that the exceedance is caused by an aftershock is obtained; in the middle panels the largest value of the probability that the exceedance

is caused by an aftershock is mapped; the bottom panels indicate, for each site, the trend of aftershock disaggregation.

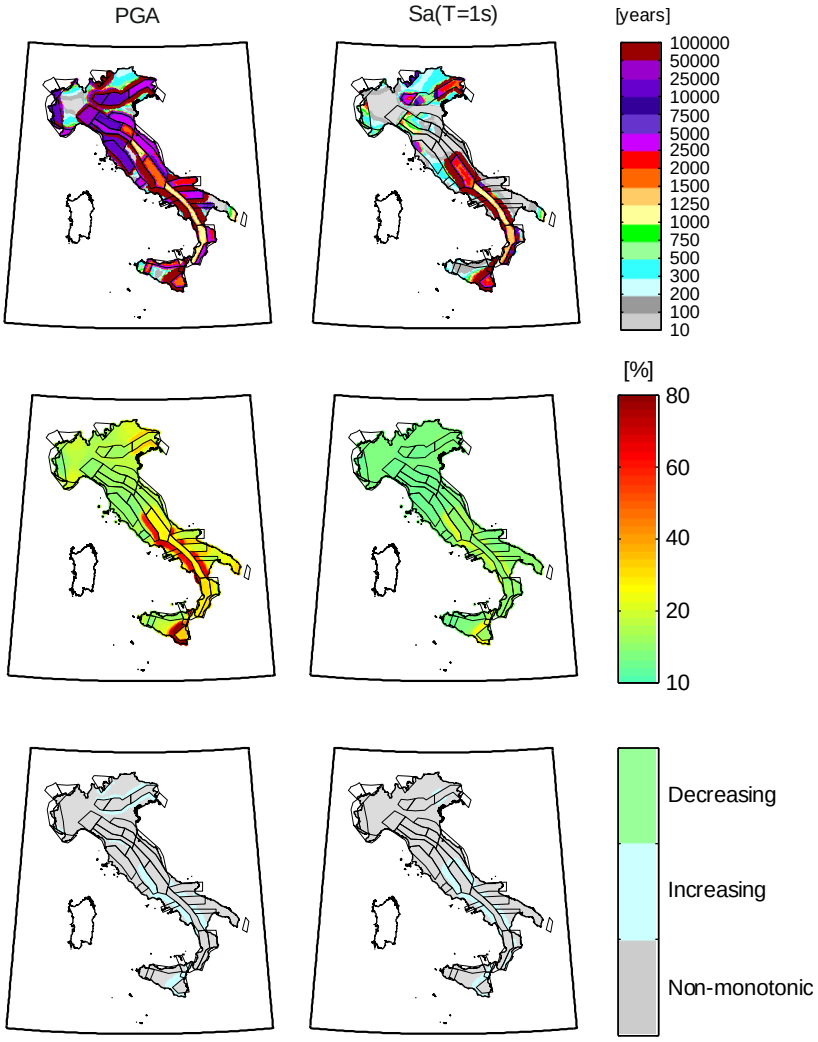

Figure 4.10. Study of the trend of the aftershock disaggregation as a function of return period in the range between ten and one-hundred-thousand years for PGA and $Sa(T = 1s)$. Top: maps of the return periods for which the probability that an aftershock causes the exceedance of the threshold is maximum. Middle: maps of the maximum probabilities that the exceedance is caused by an aftershock. Bottom: trend of disaggregation for each site.

It is interesting to note that in the 14.2% and 7.7% of the sites for PGA and $Sa(T=1s)$, respectively, the return period, for which the maximum probability that an aftershock causes the exceedance of the threshold is obtained, is in the range between fifty- and one-hundred-thousand years (top panels); in fact, the probability values for these sites are in the range 50%-80% in the case of PGA and 20%-30% for $Sa(T=1s)$ (middle panels). However, the trend of the aftershock disaggregation is non-monotonic in large areas, which cover the 90.7% and 94.2% of the territory for PGA and $Sa(T=1s)$, respectively. It can be also observed that there are no sites where the disaggregation monotonically decreases with the increasing return period. This means that, even considering return periods up to one-hundred-thousand years, there are small areas where the disaggregation is monotonically increasing (bottom panels), which cover the remaining 9.3% in the case of PGA and 5.8% in the case of $Sa(T=1s)$. It is noted that these areas surround the borders of the sources with the high maximum magnitude (see also Figure 3.1) for both PGA and $Sa(T=1s)$. This result reflects, on a national scale, what is discussed with reference to the simplified $R_E = 20$ scenario in Section 4.4.

According to the maps in Figure 4.10, in the high-seismicity regions the return period for which the maximum contribution of aftershocks is obtained is of the same order of magnitude for the considered spectral ordinates, even if the maximum values of the probability are larger in the case of PGA (see middle panels). For example, in the areas enclosed by zone 923, 927, 929, and 935, the return period varies in the range between 1000 and 2000 years for both spectral ordinates. Even if in the medium-seismicity regions the maximum values of the probability are slightly larger in the case of PGA, the corresponding return periods are between one and two orders of magnitude larger with respect to the case of $Sa(T=1s)$. It is the case, for example, of the areas enclosed by zones 901, 902 and 908; in fact, in the case of PGA the return period is larger than 5000 years, while it is smaller than 750 years in the most of these areas for $Sa(T=1s)$. In small areas with low-seismicity and outside any seismic source, the maximum values of

the probability are still slightly larger in the case of PGA, while the return period corresponding to the maximum contribution of aftershocks is lower than 200 years for both the considered spectral ordinates.

4.6.2. Trend of aftershock disaggregation in the range of return periods of interest according to the Italian code

Figure 4.9 of previous section highlights that, for a given site, the general trend of the aftershock disaggregation within a range of return periods between ten and one-hundred-thousand years can vary in the case different lower and upper return periods are considered. Therefore, it could be also worthwhile to explore the general trend of the contribution of aftershocks to hazard from the structural design perspective, that is considering return periods in the range between 50 and 2475 years. With this aim, similarly to Figure 4.10, but with reference to the new range of return periods, the top panels of Figure 4.11 provide the return period for which the probability that the exceedance is caused by an aftershock is maximum; the middle panels give the maps of the largest probability that an aftershock causes the exceedance; the trend of the contribution of aftershocks to hazard as a function of return period is given in the bottom panels.

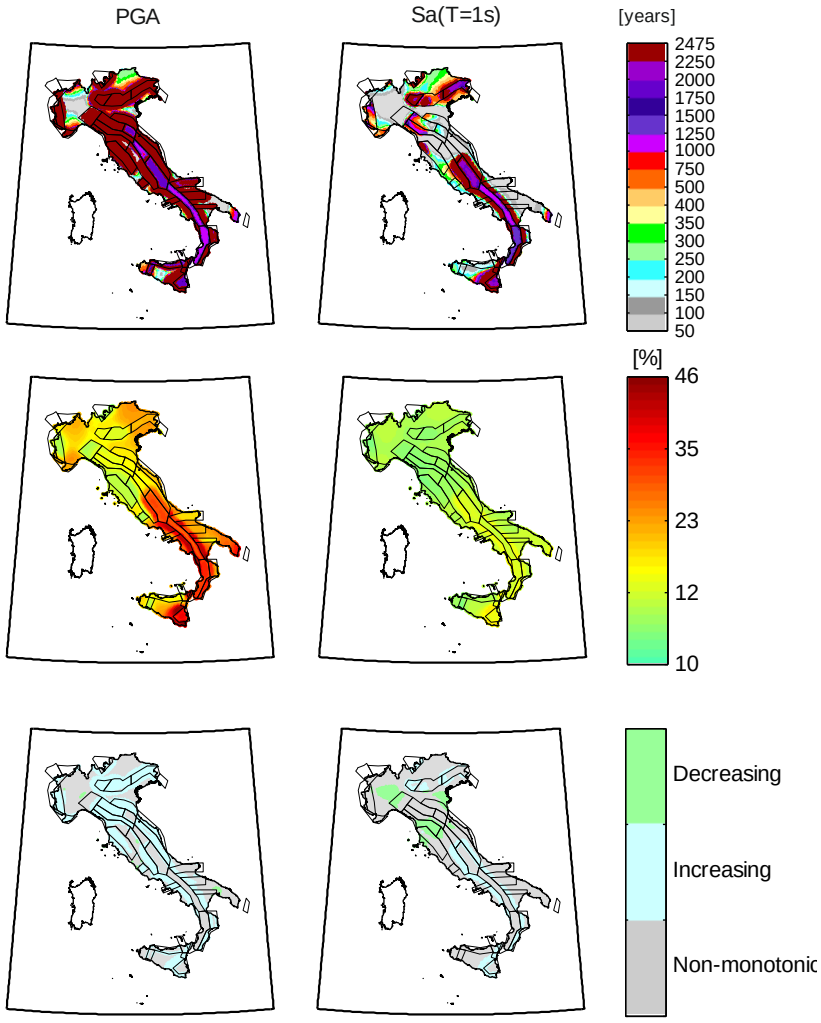

Figure 4.11. Study of the trend of the aftershock disaggregation as a function of return period in the range between 50 and 2475 years for PGA and $Sa(T=1s)$. Top: maps of the return periods for which the probability that an aftershock causes the exceedance of the threshold is maximum. Bottom: maps of the maximum probabilities that the exceedance is caused by an aftershock. Bottom: trend of disaggregation for each site.

With reference to PGA, the top panel shows that there are large areas where the return period for which the aftershock disaggregation is in the range between 2250 and 2475 years, which is the maximum the Italian building code refers to for design. In particular, these areas cover the 55.1% of the territory and, according to the middle panel, the values

of maximum probability can be very different. The map of the trend of the disaggregation (bottom panel) shows that in most of these areas, which are representative of the most of medium- and high-seismicity regions of Italy, the aftershock disaggregation monotonically increases; overall, these areas cover the 40.5% of the whole territory. On the other hand, the disaggregation is shown to be non-monotonic in the 59.0% of the country. The interested areas cover both the low- and high- seismicity regions. Finally, the aftershock disaggregation monotonically decreases with the increasing return period in the 0.5% of the territory.

With reference to $Sa(T=1s)$, the areas where the return period for which the contribution of aftershocks to hazard is maximum is in the range between 2250 and 2475 years cover the 14.4% of the country. The aftershock disaggregation monotonically increases only in the 13%. In fact, the contribution of aftershocks to hazard has a non-monotonic trend in the 78.4% of the territory. In the remaining 8.6%, the aftershock disaggregation monotonically decreases with increasing return period.

Results also show that the maximum contributions of aftershocks to hazard for PGA are higher than $Sa(T=1s)$. However, for both the spectral ordinates, the maximum values of the probability that an aftershock is causative for exceedance are significantly lower in low-seismicity regions with respect to the case of high-seismicity regions.

Thus, even if in the range of return periods between 50 and 2475 years, for both PGA and $Sa(T=1s)$, the aftershock disaggregation is shown to be monotonically increasing in areas which, overall, are larger than those observed when the range between ten and one-hundred-thousand is considered (see previous section), a non-monotonic trend is still found in the most of the sites.

Finally, the results discussed so far do not allow to compare the contribution that aftershocks give to hazard at the different sites for a given return period. For this reason, Figure 4.12 is provided. It shows the maps of the probabilities that an aftershock causes the exceedance of the threshold for fixed return periods, with reference to PGA (top panels) and $Sa(T=1s)$ (bottom panels). In particular, four return periods, among the

ones the Italian code considers for design, are considered, that is, 50, 475, 975 and 2475 years.

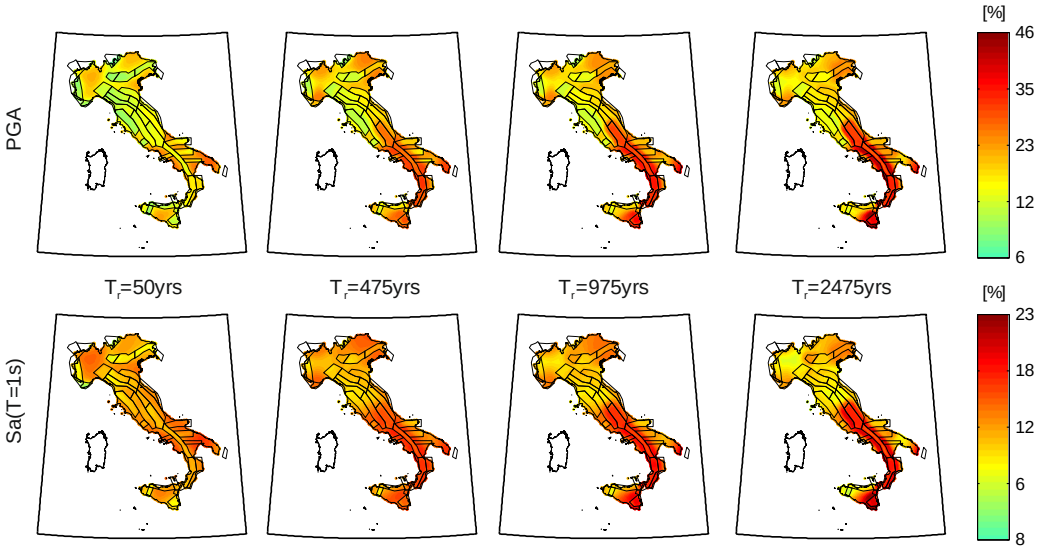

Figure 4.12. Maps of the probabilities that an aftershock causes the exceedance of the threshold for different return periods. Top: PGA. Bottom: $Sa(T=1s)$.

Maps reveal that, given the return period, the contribution of aftershocks to hazard can be very different from site to site. For PGA the probability values are larger than $Sa(T=1s)$. These results reflect, on a national scale, what observed in detail for Frosinone and Messina (see Figure 4.3 and Figure 4.4), Alagna, Salino, Barberino di Mugello and Resiga (see Figure 4.9). Furthermore, with reference to both the spectral ordinates, it can be observed that differences between the different areas of the country tend to be higher with the increasing return period. This is related to the effects of the adopted hypothesis about the spatial distribution of aftershocks around the mainshock. In particular, disaggregation is a combination of the two simplified scenarios discussed in Section 4.4 in most of the sites, with the exception of those near the border of high seismicity zones (see previous section). In these zones, due to the high magnitude, sites are exposed to aftershocks which are closer than the triggering mainshock. Thus, with the increasing threshold in the range of return periods up to 2475 years, for these sites

the probability that the exceedance is caused by an aftershock increases faster than the sites located in low-seismicity areas.

4.7 Conclusions

Sequence-based probabilistic seismic hazard analysis allows to include the aftershocks' effect in probabilistic seismic hazard assessment. The modified hazard integral relies on the modified Omori law and is probabilistically rigorous in the framework of the considered models. The SPSHA stochastic model was introduced in 2014; herein it is applied at national scale first, using Italy as case study. Adopting the source model discussed in Chapter 3 and considering the same spectral ordinates with return period equal to 475 years, the seismic hazard maps on rock site conditions were introduced and compared with the PSHA counterparts discussed in Chapter 3. Thus, the hazard increase due to aftershocks was evaluated in absolute and percentage terms. The SPSHA maps on site-dependent soil conditions and the increments due to aftershocks were also illustrated. Subsequently, SPSHA results were discussed in detail for two Italian sites. The considered sites are Frosinone and Messina. They were chosen because representative of the medium- and high- seismicity areas in Italy and also because they are representative of two typical conditions characterizing the hazard disaggregations. For each of the sites, the uniform hazard spectra with four return periods of exceedance between 50 and 2475 years on rock site conditions were shown. Then, the discussion was focused on the comparison between the magnitude and distance disaggregation distributions when SPSHA or PSHA are of concern, and on the trend of aftershock disaggregation with the return period. Regarding the former, it was shown that including the aftershocks' effect (i.e., in the case of SPSHA) may produce significant effects especially when short vibration periods are considered. More specifically, disaggregations of SPSHA, with respect to the PSHA counterparts, are characterized by higher probability associated to the high magnitude events. The analyses of aftershock

disaggregations showed that the trend with return period can be monotonic or non-monotonic depending on the geographical location of the seismic area contributing to the hazard of the site. It was also demonstrated that this result is strongly influenced by the adopted hypothesis on the symmetrical distribution of aftershock around the mainshock location.

Similarly to PSHA, the magnitude and distance disaggregation of SPSHA allowed to evaluate, for each site, the mainshock average magnitude and distance, given the exceedance of the threshold during the subsequent cluster. The contribution of aftershocks to hazard as a function of the return period in the range between ten and one-hundred-thousand years was analysed, with the aim to investigate the general trend at a national scale. In particular, the study was carried out in terms of (i) return period corresponding to the maximum probability of exceeding due to an aftershock, (ii) maximum value of the probability that an aftershock causes the exceedance, (iii) trend of aftershock disaggregation. With reference to a range of return periods of interest according to the Italian code (between 50 and 2475 years), results were re-evaluated. Overall, results from the analyses allows to point out the following issues:

- hazard increase, for the return period of 475 years, can be as high as about 0.06g in absolute terms and 22% in percentage terms for PGA. In the case of $Sa(T=1s)$, the maximum absolute and percentage increments are bout 0.035g and 17%, respectively;
- similarly to PSHA, the SPSHA maps on site-dependent soil conditions can be easily obtained as a function of the soil coefficient. It is shown that the maximum absolute differences increase to about 0.08g and 0.06g for PGA and $Sa(T=1s)$, respectively, while the percentage difference are independent on soil conditions;
- the maps of mainshock average distances and magnitudes according to SPSHA are not very different from the PSHA counterparts. With reference to distance,

the average values in the case of SPSHA are smaller than those of PSHA for most of the sites and for both the considered spectral ordinates. With reference to magnitude, the average values in the case of SPSHA are greater than the PSHA counterparts for all the sites;

- generally, the trend of aftershocks disaggregation as a function of the return period is non-monotonic across all the country, with the exception of the sites located on the borders of seismic sources with high seismicity;
- according to the maps of the probabilities that an aftershock causes the exceedance of the threshold for the four selected return periods, it can be observed that, given the return period, the aftershock disaggregation can be very different from site to site, as the results observed in detail for the different sites considered in the chapter also showed. Furthermore, they reveal that the differences between low- and high- seismicity areas increase with the increasing threshold in the range of return periods up to 2475 years.

Chapter 5 - MULTI-SITE PSHA: THE ROLE OF SPATIAL DEPENDENCE IN HAZARD VALIDATION

This chapter is derived from the following paper:

Iervolino I, Giorgio M, Cito P (2017) The effect of spatial dependence on hazard validation. Geophys Journ Int 209:1363–1368.

5.1. Introduction

Probabilistic seismic hazard analysis studies are often questioned. For example, due to the damaging earthquakes recently occurred (recalled in Section 3.1), in Italy the adequacy of the national hazard map, which is at the basis of the definition of the structural seismic actions, is at the center of an ongoing debate. In this context, it can be observed that, in the last years, PSHA has been quantitively confirmed or disproved in several studies based on observed ground motions over time. The most of them adopts the theory of hypothesis testing. With the aim of validating hazard estimates at a single site, these studies need to collect a large number of earthquake observations, which are not easily available due to the very long time required to collect them (see, for example, Iervolino, 2013). Thus, given the time span, these researches tend to create a sample of observations by pooling seismic records at different sites.

Given a return period of interest, hazard maps provide the corresponding site-specific value of a ground motion intensity measure. This implies that, for statistical validation purposes, multiple earthquake records should be collected at each site. Nevertheless, due to their rarity, strong ground motion records need to be collected from different sites in

the region covered by the map. For this reason, according to Giorgio and Iervolino (2016) and Iervolino and Giorgio (2015), ground motion IMs occurring at different sites due to a given event cannot be assumed stochastically independent, even if the effect of multiple events at a given site are considered independent. This is a crucial point in hazard validation studies via collected data from different sites. In fact, if the stochastic dependence is not considered, erroneous conclusions on the adequacy of PSHA can be achieved. In this framework, this chapter is intended to provide a quantitative interpretation of the importance of spatial dependence of ground motion IMs in hazard validation studies. To do so, the causes and effects of spatial dependence of IMs are recalled first. Subsequently, a MSPSHA study is presented with the aim to revise the hazard validation study of Albarello and D'Amico (2008), which assumes stochastic independence between ground motion IMs. In particular, it is shown that accounting for spatial dependence can change the result of the statistical test used by Albarello and D'Amico (2008) to validate the hazard map.

The presented MSPSHA study is carried out through the REASSESS V2.0 software, which is able to account for the above-mentioned spatial dependence (see Chapter 2).

5.2. The stochastic dependence of IMs in MSPSHA

As stated in Section 2.2, the main result of PSHA is λ_{im}, that is, the annual rate of earthquakes causing the exceedance of the *im* threshold at the site of interest (Equation 2.3). Since classical PSHA profits of the HPP, knowing λ_{im} allows to compute the probability that the number of exceedances in the $\Delta T = (t, t + \Delta t)$ time interval at the site, $N_{im}(t, t + \Delta t)$, results exactly equal to n (Equation 2.2).

As mentioned in Section 2.4.1, the outcomes of MSPSHA can be various. For example, given a set of n_{sts} sites, starting from the simulated realizations of GRF it is possible to compute the rate of earthquakes causing exceedance jointly at the sites, $\lambda_{im_{s_1} \cap im_{s_2} \cap \ldots \cap im_{n_{sts}}}$

. In the simple case that two sites are of interest, say $\{s_1, s_2\}$, the analytical expression for such a rate is given by Equation (5.1), which is written considering a single seismic source for the sake of simplicity.

$$\lambda_{im_{s_1} \cap im_{s_2}} = \nu \cdot \int_M \int_X \int_Y P\left[IM_{s_1} > im_{s_1} \cap IM_{s_2} > im_{s_2} \middle| m,x,y \right] \cdot f_{M,X,Y}(m,x,y) \cdot dm \cdot dx \cdot dy \tag{5.1}$$

The term $P\left[IM_{s_1} > im_{s_1} \cap IM_{s_2} > im_{s_2} \middle| m,x,y \right]$ represents the probability of exceeding simultaneously the thresholds at the sites, given magnitude and location of the event.
At this point it has to be recalled that, according to Giorgio and Iervolino (2016), the probabilistic characterization of the effects of a common earthquake at different sites is at the basis of the stochastic dependence among the site-specific counting processes over time. In particular, in order to better comprehend the correlation among the IMs, it is worthwhile to rewrite Equation (2.5) according to Equation (5.2), in which the inter- and intra-events components of the residual explicitly appear.

$$\log\left(im_{s_j,i} \right) = \mu\left(m_i, r_{s_j,i}, \theta \right) + \psi_i + \varsigma_{s_j,i} \tag{5.2}$$

Given an IM of interest (e.g., PGA), the ψ_i term denotes the inter-event residual. It is constant for all sites in the i-th earthquake. In particular, given a magnitude and distance value, ψ_i accounts for the fact that the mean of the logarithms of IM is different from event to event. On the other hand, $\varsigma_{s_j,i}$ represents the intra-event residual at site s_j in earthquake i. Given the event, $\varsigma_{s_j,i}$ considers the variability of IMs at different sites which are at the same distance from the source; it also accounts for the fact that close sites experience similar IM values. It is typically assumed that ψ_i and $\varsigma_{s_j,i}$ are stochastically independent normal RVs with zero mean and standard deviation equal to

σ_{inter} and σ_{intra}, respectively. For this reason, the standard deviation of the total residual is $\sigma = \sqrt{{\sigma_{\text{inter}}}^2 + {\sigma_{\text{intra}}}^2}$, as stated in Section 2.2.2.

As mentioned in Section 2.4.1, it is generally assumed that, given magnitude and location of the event, the logs of IMs at multiple sites form a GRF (see also Park et al., 2007; Malhotra, 2008). With reference to the simple case in which a single $IM_1 = Sa(T_1)$ is considered (which is the case of the study of this chapter, as the next sections show; however, see Section 2.4.1 for the more complex case in which multiple IMs are of concern), the components of the mean vector of the GRF are given by the $\mu\left(m_i, r_{s_j,i}, \theta\right)$ terms (one for each site) and the covariance matrix is provided by Equation (5.3).

$$\Sigma = \sigma_{\text{inter}}^2 \begin{bmatrix} 1 & 1 & \cdots & 1 \\ 1 & 1 & \cdots & 1 \\ \vdots & \vdots & \ddots & \vdots \\ 1 & 1 & \cdots & 1 \end{bmatrix} + \sigma_{\text{intra}}^2 \begin{bmatrix} 1 & \rho_{\text{intra}}\left(T_1,T_1,h_{s_1,s_2}\right) & \cdots & \rho_{\text{intra}}\left(T_1,T_1,h_{s_1,s_{n_{sts}}}\right) \\ \rho_{\text{intra}}\left(T_1,T_1,h_{s_2,s_1}\right) & 1 & \cdots & \vdots \\ \vdots & \vdots & \ddots & \vdots \\ \rho_{\text{intra}}\left(T_1,T_1,h_{s_{n_{sts}},s_1}\right) & \rho_{\text{intra}}\left(T_1,T_1,h_{s_{n_{sts}},s_2}\right) & \cdots & 1 \end{bmatrix} \tag{5.3}$$

The $\rho_{\text{intra}}\left(T_1,T_1,h_{s_1,s_2}\right)$ term has already been defined in Section 2.4.1. Given the structure of the GRF, Giorgio and Iervolino (2016) illustrate that correlation among IMs derive by the fact that all the components of the mean vector share the rupture's features. Furthermore, as Equation (5.3) shows, inter-event residuals are the same at all sites given the event. Therefore, they also generate (perfect) correlation among IMs. Finally, given the event, there is also a correlation between intra-event residuals, which decreases with inter-site distance (e.g., Loth and Baker, 2013). For these reasons, the processes counting the number of exceedances at the sites over time are stochastically dependent. Such a dependency implies that, in the same hypothesis of HPP of earthquakes occurrence on the source, the process counting the total number of exceedances at the sites is, in general, not a Poisson process. In particular, Giorgio and Iervolino (2016) demonstrate that the counting processes at the two above-considered sites are independent only if

$P\left[IM_{s_1} > im_{s_1} \cap IM_{s_2} > im_{s_2} \middle| m,x,y \right] = 0$. The latter condition can be satisfied only if the two sites are distant enough. However, also in the case the sites are not close each other, spatial dependence should always be considered in the case of risk assessment of spatially distributed systems (e.g., pipelines) or hazard validation studies, as shown in the next sections.

5.3. The hazard validation study of Albarello and D'Amico (2008)

The study of Albarello and D'Amico (2008) aims to validate, via observed ground motions, the Italian hazard map of PGA with return period equal to 285 years (PGA_{285} hereafter) on A local site conditions (according to the Eurocode 8, CEN, 2004). In other words, they considered the PGA with 10% exceedance probability in 30 years. For this scope, data were derived from sixty-eight stations across the country (see Figure 5.1) operating in a time span of 30 years. The authors counted the number of exceedances of the official PGA_{285} values (i.e., those from Italian hazard map), herein indicated as $n_{exc,PGA_{285}}$. In particular, for each site they compared the maximum recorded PGA with the PGA_{285} and observed that, overall, the former was greater than the latter in correspondence of thirteen stations, that is $n_{exc,PGA_{285}} = 13$.

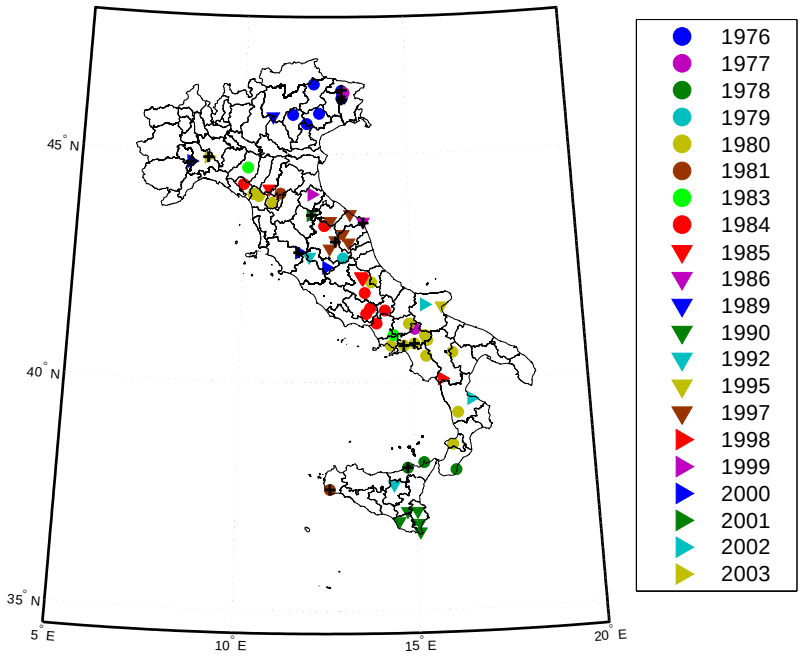

Figure 5.1. Seismic stations continuously operating for 30 years considered by Albarello and D'Amico (2008), with earthquake occurrence years and observed exceedances of PGA_{285} (crosses).

Due to high average inter-site distance, Albarello and D'Amico (2008) developed the hazard validation study under the hypothesis of independence of the exceedances observed at the sites. In particular, they considered two methodologies. For the purpose of the chapter, it is only recalled the first one. In this approach, the event exceeding the PGA_{285} at each site is considered as a Bernoulli RV with success probability equal to 10%, which is equal to zero if exceedance is not observed, and one if at least one exceedance is observed at the site in 30 years. Indeed, since each RV has probability to observe the exceedance of PGA_{285} equal to 10% (deriving from the fact that the exceedance of PGA_{285} at each site in 30 years is investigated), under the independence hypothesis the probability that at exactly n_k sites, among the considered sixty-eight, is observed at least one exceedance in 30 years, herein indicated as $P(n_k)$, is computed

via the binomial PMF, as per Equation (5.4), for which the number of trials is 68 and the probability of success for each trial is 0.1.

$$P(n_k) = \binom{68}{n_k} 0.1^{n_k} 0.9^{68-n_k} \tag{5.4}$$

As a consequence, the mean of the distribution counting the number of sites experiencing at least one exceedance of the PGA_{285} in 30 years is $\mu_{binomial} = 0.1 \cdot 68 = 6.8$, while the variance is $var_{binomial} = s \cdot p \cdot (1-p) = 68 \cdot 0.1 \cdot (1-0.1) = 6.12$. At this point, Albarello and D'Amico (2008) carried out a statistical test to verify the hypothesis that the probability of exceeding the PGA_{285} in 30 years at the generic site is equal to 10% (null hypothesis), according to the Italian code, against the hypothesis that such probability has a different value. In particular, considering that the observed data revealed that $n_{exc,PGA_{285}} = 13$ and recalling that according to the central limit theorem (via a Gaussian approximation; e.g. Mood et al., 1974), it can be assumed that $P\left[| n_{exc,PGA_{285}} - \mu_{binomial} | > 1.96\sqrt{var_{binomial}} \right] \cong 0.05$, the authors rejected the hypothesis that the probability of exceedance at the generic site is equal to 10% at the 0.05 significance level. In fact, it resulted $13 - 6.8 = 6.2 > 1.96\sqrt{6.12} = 4.85$. Indeed, the work of Albarello and D'Amico (2008) concludes that the PGA_{285} values from the hazard map are not conservative, because they tend to underestimate the actual hazard. It is also worthwhile to note that the upper limit of the acceptance region of the hypothesis test at 0.05 significance level is $6.8 + 1.96\sqrt{6.12} = 11.65$. This means that, under the hypothesis of Albarello and D'Amico (2008), the null hypothesis that observed exceedances are in agreement with hazard map has to be rejected in the case $n_{exc,PGA_{285}} \geq 12$.

5.3.1. Exceedance data from observed ground motions

According to the previous section, if the number of observed exceedances is smaller than twelve, the statistical test leads to not reject the null hypothesis. For this reason, a careful evaluation of the collected data is of primary importance in the hazard validation studies. In this context, this section is intended to explore in detail the observed exceedances, which are given in Table 5.1. In particular, the second column provides the maximum recorded PGA according to Albarello and D'Amico (2008); the third column shows the maximum recorded PGA according to the Italian accelerometric archive (ITACA; Luzi et al., 2008) online database (http://itaca.mi.ingv.it/; last accessed December 2018); finally, the last column shows the PGA_{285} values from the Italian hazard map. Looking at the table, it can be observed that the accelerations from the second and third column are not exactly the same. Although the differences seem to be not significative, they cannot be neglected in the study. In fact, in the case of RASRL station (Sirolo, central Italy; 43.52°N, 13.61°E), the PGA_{285} is equal to 0.140g. The maximum recorded PGA according to Albarello and D'Amico (2008) is equal to 0.143g, while the one from ITACA is 0.137g. Moreover, the exceedance observed in Sirolo is due to an earthquake of magnitude equal to 3.7. On the other hand, the seismic hazard assessment for Sirolo, according to the model of Stucchi et al. (2011), only accounts for earthquakes of magnitude larger than 4.15 (in fact, zone 936 does not contribute to the hazard of the site; see Figure 3.1). For these reasons, the exceedance observed at RASRL station results doubtful.

Table 5.1 also gives the actual soil conditions for the considered sites, which can also have an impact on the hazard validation study. In fact, recalling Equation 3.7, the PGA_{285} values on site-dependent soil conditions are larger than those on A-type soil class. Therefore, one or more exceedances could be not considered in the study. It is the case of RANAS and RASRL stations, for example, being the PGA_{285} on site-dependent

soil condition equal to 0.193g and 0.186g, respectively. However, for the purposes of the chapter, A-type soil is assumed in the study for all the sites.

Table 5.1. Exceedance data in the study of Albarello and D'Amico (2008) and PGA (10/30) from the hazard map.

Station ID	Max recorded PGA (g)	Max recorded PGA (g) (ITACA)	Event ID (ITACA)	ML (Mw) (ITACA)	Soil (ITACA)	PGA(10/30) (g) A-type soil
RATLM1	0.342	0.346	IT-1976-0002	6.4	B	0.193
SRC0	0.249	0.250	IT-1976-0030	6.0	B[a]	0.202
FRC	0.352	0.349	IT-1976-0030	6.0	B	0.202
RANAS	0.149	0.148	IT-1978-0004	5.5 (6.0)	C	0.145
RAMRT	0.140	0.141	IT-1980-0012	6.5 (6.9)	B	0.115
RABGI	0.189	0.187	IT-1980-0012	6.5 (6.9)	B	0.153
RAMZR	0.193	0.193	IT-1981-0006	(4.9)	B	0.051
RASRL	0.143	0.137	IT-1986-0001	3.7	C	0.140
RANCR	0.500	0.502	IT-1997-0006	5.8 (6.0)	E	0.193
RAPNC	0.160	0.150	IT-2000-0001	3.0 (4.5)	B[a]	0.117
RANZZ	0.131	0.132	IT-2000-0008	4.3 (4.8)	C	0.041
RAPVS	0.196	0.186	IT-2001-0041	4.4 (4.7)	B	0.179
RATRT	0.087	0.086	IT-2003-0023	4.7 (4.8)	E	0.067

[a]Local site condition inferred from large-scale geology rather than measured average shear wave velocity in the upper 30m of soil.

5.4. The effect of dependence of IMs in hazard validation

This section discusses the effect of the stochastic dependence among the ground motion IMs at different sites on the hazard validation study of Albarello and D'Amico (2008). To do so, the same Bernoulli RVs of Section 5.3 are considered, that is, with reference to a specific site, the one that at each site is equal to one if the exceedance of the corresponding PGA_{285} is observed at least once in 30 years, zero otherwise. The only difference with Albarello and D'Amico (2008) is that, in the proposed study, the stochastic dependence between the site-specific Bernoulli RVs is considered. The sum of the considered RVs allows to carry out the distribution of the number of sites, among the sixty-eight considered, experiencing at least one exceedance of the corresponding PGA_{285} in 30 years. Thus, the obtained distribution is compared with the binomial distribution of Equation 5.4 which Albarello and D'Amico (2008) obtained under the hypothesis of independence among the Bernoulli RVs (the former is hereinafter indicated as non-binomial distribution).

To compute the non-binomial distribution, the realizations of GRF for PGA at the sites have to be simulated. Coherently with the work of Albarello and D'Amico (2008), the same seismic source model and GMPE discussed in Section 3.2 are herein adopted. With reference to the GMPE, it should be noted that the Ambraseys et al. (1996) has only one residual term, not distinguishing between inter- and intra-event. It is treated herein as an intra-event residual with $\sigma_{\text{intra}} = 0.25$. Moreover, no spatial correlation is introduced among the residuals (e.g., Esposito and Iervolino 2011). This means that the only source of dependence is related to the fact that ground motions at the sites share the same rupture's features (see Section 5.2). The seismic history spanning over 30 years at the sixty-eight sites was simulated one-hundred-thousand times via the two-step procedure implemented in REASSESS and described in Section 2.4.2 (see Figure 2.1). The distribution of the number of sites experiencing at least one exceedance of a vector of

thresholds in a given time interval is not an output among those the software provides (see Section 2.6.2). Indeed, the sought distribution is computed by post-processing simulations. In particular, starting from the simulated dataset of PGA, for each seismic history spanning 30 years, the number of sites experiencing at least one exceedance of the corresponding PGA_{285} is counted. The collection of the one-hundred-thousand n_k -values allows to build the (non-binomial) distribution of the number of sites experiencing at least one exceedance of PGA_{285} in 30 years. This distribution is the PMF of a discrete random variable taking values between zero and sixty-eight and it is shown in Figure 5.2, along with the binomial distribution of Albarello and D'Amico (2008).

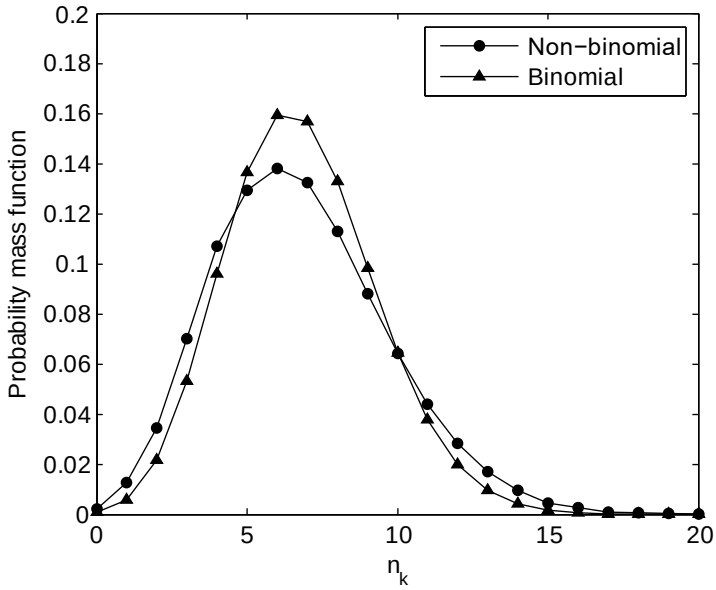

Figure 5.2. Probability distribution of the number of sites with at least one exceedance of PGA_{285} in 30 years on A-type soil.

Since the stochastic dependence existing between IMs does not have effect on the average number of sites experiencing at least one exceedance in a given time interval, both the non-binomial and binomial distributions have the same mean, that is $\mu_{binomial} = \mu_{non-binomial} = 6.8$. It is found that the above-mentioned dependence only

increases the variance of the investigated distribution, in accordance with Giorgio and Iervolino (2016). In fact, it is $var_{non-binomial} = 8.43 > var_{binomial} = 6.12$. Then, the non-binomial distribution is adopted to perform the same statistical test at the 0.05 significance level carried out by Albarello and D'Amico (2008). In particular, the upper limit of the acceptance region of the test results $6.8 + 1.96\sqrt{8.43} = 12.49$. This means that, also under the hypothesis of dependence between IMs, the hypothesis that observed exceedances are in agreement with the hazard map has to be rejected at the 0.05 significance level, being $n_{exc,PGA_{285}} = 13$. Nevertheless, as stated in Section 5.3.1, the exceedance observed at the RASRL station is doubtful. If it was not considered, it would be $n_{exc,PGA_{285}} = 12$, a number which is still greater than the upper limit of the acceptance region of the test according to the binomial distribution (11.65), but in the acceptance region according to the non-binomial distribution, due to the variance increase (the lower limit of the acceptance region is $6.8 - 1.96\sqrt{8.43} = 1.11$). Thus, in the case that $n_{exc,PGA_{285}} = 12$, the decision whether the observed exceedances are in agreement with the hazard map would be reverted. Furthermore, it is worthwhile to highlight the following two issues, which may have also impact on the hazard validation study:

- according to Giorgio and Iervolino (2016), the variance increase would be more significant considering a GMPE modeling inter-event residuals and the spatial correlation of intra-event residuals. As a consequence, adopting a similar GMPE would imply a greater number for the upper limit of the acceptance region of the statistical test;
- if the actual soil conditions were considered, the PGA_{285} would increase for all the sites (none of the sites is classified as A-type; see Table 5.1) and, as a consequence, the number of observed exceedances from collected data would reduce.

For these reasons, even if the sites are on average distant enough, the spatial dependence among IMs may have a not-negligible impact on the hazard validation study and it should be always accounted for.

5.5. Conclusions

The stochastic dependence existing between ground motion IMs at multiple sites generated by a common earthquake implies that the site-specific processes, each counting the number of exceedances of an intensity measure threshold over time, are also dependent. For this reason, under the same hypothesis of HPP of earthquakes occurrence on the source, the process counting the total number of exceedances at the sites is, in general, not a Poisson process.

In this framework, the chapter focused on the importance of the spatial dependence of IMs in hazard validation studies via observed ground motions at multiple sites over time. In particular, the work of Albarello and D'Amico (2008) was revised. It considers sixty-eight sites across all Italy and the corresponding PGA with 10% probability to be exceeded in 30 years from the official hazard map. The authors observed overall thirteen exceedances in 30 years. Profiting of a statistical test, and under the hypothesis that exceedances at sites are stochastically independent, they found that the hypothesis that that the probability of exceeding the PGA_{285} in 30 years at the generic site is equal to 10% has to be rejected at the 0.05 significance level. Under the same hypothesis of Albarello and D'Amico (2008), with the exception of the stochastic independence, the MSPSHA study proposed in this chapter provided the results to performs the same statistical test. It was found that, even if the effect of spatial dependence could be considered negligible at a first glance, it could be relevant. In fact, it was shown that one of the observed exceedances is doubtful. If it is not considered, the hypothesis that the observed exceedances are in agreement with the hazard map has not to be rejected. Finally, there are other factors that can strongly influence the results of hazard validation,

such as considering a GMPE modeling inter- and spatial correlation of intra-event residuals or considering the actual soil conditions of the sites. For these reasons, it is recommended to always account for the spatial dependence of IMs in hazard validation studies, even if sites may appear far enough from each other.

Chapter 6 - SUMMARY AND CONCLUSIONS

In the framework of performance-based earthquake engineering, the definition of seismic actions for the design of structures is based on probabilistic seismic hazard analysis, which is the consolidated procedure for the characterization of the seismic threat. Indeed, in the most advanced countries design seismic actions are derived from a uniform hazard spectrum which is, in fact, a typical result of PSHA. Nevertheless, PSHA has been often debated over the years; this is also due to the actually-observed seismic actions on structures, that in some cases exceed those derived from uniform hazard spectra. Furthermore, at the state-of-the-art worldwide seismic codes implicitly exclude the possibility that the exceedance of design actions can be due to an aftershock rather than by a mainshock. Another relevant issue is that PSHA has been confirmed or disproved through statistical tests via observed ground motions at multiple sites over time, whose results depend on both the adopted hypothesis on spatial dependence/independence between ground motions at the sites and collected data.

Not questioning PSHA, this thesis dealt with the above-introduced issues profiting of recent hazard assessment methodologies which were also recalled. In fact, in the recent years, sequence-based and multi-site PSHA have been developed. SPSHA considers the effect of aftershocks in the hazard assessment. MSPSHA accounts for the existence of stochastic dependence among the site-specific counting processes over time, which is shown to be required in the case of risk assessment of building portfolios, for example. These advanced probabilistic seismic hazard analysis methodologies have been implemented in an engineering-oriented software named REgionAl, Single-Site and Scenario-based Seismic hazard analysis (REASSESS V2.0), which is one main results of the thesis. This tool has been used to develop the studies proposed in the thesis which,

as mentioned, aim to deepen some PSHA aspects under three points of view, with reference to the case-study Italy.

In Chapter 2 the basics of PSHA were recalled first. Then, SPSHA and MSPSHA were introduced, and the algorithms for their implementation in REASSESS V2.0 were shown. The functionalities, along with the input and output of the analyses the software is able to perform, were finally illustrated.

Chapter 3 discussed what to expect for code-conforming structures in the case of exceedance of the design seismic actions derived from uniform hazard spectrum. In particular, with reference to PGA and $Sa(T=1s)$ spectral ordinates with $T_r=475$ years and assuming the seismic source model used to define elastic seismic actions according to the current Italian building code, two main results were given: (i) expected acceleration over the design threshold if the exceedance occurs, and (ii) the minimum magnitude of earthquakes that, occurring within a certain distance from the site, have a probability of exceeding the design spectrum larger than 0.5 (strong earthquakes). With reference to (i), results revealed that higher natural vibration periods are more exposed to exceedance and the largest accelerations over the thresholds are observed in the most hazardous areas. In particular, it was shown that the amount of exceedance can be up to 2.5 times the design acceleration while, outside seismic sources, it can be 1.5 times the UHS. With reference to (ii), it was found that, in the epicentral areas of earthquakes of relatively moderate magnitude, the design threshold is not hard to be exceeded while, in the case of distant events, or those close to the site of low magnitude, such exceedance should be not expected. This means that, in the epicentral areas of an even moderate magnitude event, protection of structures is only warranted by the rarity with which such event occurs. With reference to two sites, chosen to be representative of high (L'Aquila) and low seismic hazard exposure (Milan), these observations were further explored through the study of the contribution to seismic hazard, in terms of $Sa(T=1s)$, of all possible magnitude-distance scenarios. In fact, it was shown that if an earthquake of high magnitude (larger than 7) occurs within 5km from L'Aquila, the probability of exceeding

the design threshold with $T_r = 475$ years is larger than 0.9. In the case of Milan, which is located outside any seismic source, it was found that there is no scenario for which the exceedance of the threshold should be expected. In fact, according to the adopted source model, there is no contribution from earthquakes closer than 25km, while the maximum magnitude which can occur within 50km is equal to 5.9.

For the same sites, the influence of return period on the proposed results was also investigated. In particular, the nine return periods the Italian building code refers to for design were considered. It was found that the amount of exceedance over the UHS decreases with increasing return period. However, even considering the largest return period, increment varies in the range between 26% and 69%. Furthermore, it was shown that the minimum magnitude of earthquakes occurring within 5km from L'Aquila remains below the maximum deemed possible also for the highest return period.

In Chapter 4, assuming the seismic source model of Chapter 3, the SPSHA maps of PGA and $Sa(T = 1s)$ with $T_r = 475$ years were first recalled. It was found that, across Italy, due to aftershocks the hazard can be subjected to increments up to 22% for PGA and 17% for $Sa(T = 1s)$. Subsequently, SPSHA results were discussed in detail for Frosinone and Messina, which are characterized by two different PSHA disaggregations. In particular, with reference to magnitude-distance disaggregation, it was found that, with respect to the PSHA counterparts, SPSHA disaggregations are characterized by higher probability associated to the high magnitude events. With reference to the trend of aftershocks contribution to hazard with return period, the study revealed that it is strongly influenced by both the geographical location of the seismic area contributing to the hazard of the site and the adopted hypothesis on the symmetrical distribution of aftershock around the mainshock location.

With reference to the same spectral ordinates, the chapter then focused on the two kinds of SPSHA disaggregation discussed in Chapter 2. Thus, the maps of mainshock average magnitude and distance disaggregation given the exceedance of the threshold during the mainshock-aftershock sequence were presented and compared with the PSHA

counterparts illustrated in Chapter 3. It was shown that the average distance in the case of SPSHA is smaller than PSHA for most of the sites, while average SPSHA magnitude is greater than PSHA for all the sites. Subsequently, the contribution of aftershocks to hazard as a function of the return period in the range between ten and one-hundred-thousand years was explored. It was found that the general trend of disaggregation is non-monotonic in more than 90% of the country for both the considered spectral ordinates. Finally, the maps of the the probabilities that an aftershock causes the exceedance of the threshold for four return periods; i.e., 50, 475, 975 and 2475 years, pointed out that, given the return period, the aftershock disaggregation can be very different on a national scale, reflecting what was observed for the case-studies presented in the chapter.

In Chapter 5 the fundamental role of MSPSHA in hazard validation studies was shown, as it accounts for the spatial correlation existing among the site-specific processes, each counting the number of exceedances at each site in time. In particular, to quantitatively assess the effect of spatial correlation, the chapter revised a previous hazard validation study, in which sixty-eight Italian sites with the corresponding PGA with $T_r = 285$ years from the official hazard map are considered. It was shown that the effect of spatial dependence is not irrelevant, even if the considered sites are, on average, distant enough. In fact, if one questionable counted exceedance is not taken into account, considering correlation among IMs would lead to conclude that the hypothesis that observed exceedances are in agreement with the hazard map has not to be rejected at the level of significance 0.05, while it would be rejected if such correlation is not considered.

In conclusion, with reference to the encountered issues concerning PSHA, the study presented in this thesis points out that the well-expected exceedance of design actions in the epicentral areas of earthquakes of even moderate magnitude is not a disproof of PSHA. Furthermore, classical PSHA results do not change significantly if the effect of aftershocks is considered, even if they imply a not negligible maximum hazard increase equal to around 22% (for the considered spectral accelerations and return period);

however, the contribution of aftershocks to hazard strongly vary with return period and, in general, it is non-monotonic. Finally, spatial dependence of IMs should be always considered in hazard validation studies via observed ground motions at multiple sites over the years, to avoid fallacious conclusions about the inadequateness of PSHA.

6.1. Future developments

This short section illustrates the ongoing developments of the software presented in the Chapter 2 of the thesis. The first one is related to the possibility of implementing user-defined GMPEs; in fact, several recent GMPEs adopt functional forms differing from those of the models embedded in REASSESS (see also Stafford et al., 2017). The second topic concerns the implementation of the expected exceedance over the threshold when faults are included in the source model. In fact, as illustrated in Chapter 3, the computation of $E\left[Sa(T)\,|\,Sa(T)>sa\right]$ requires the disaggregation of magnitude, distance and epsilon, given the exceedance of sa (see Equation 3.4). As stated in Chapter 2, the current version of REASSESS provides the joint distribution of $\{M,R,\varepsilon\}$ according to Equation (2.6), in the case seismogenic zones are considered in the analysis. On the other hand, when tridimensional faults are included in the model, disaggregation only provides the magnitude-distance disaggregation and, therefore, the software is not able to compute $E\left[Sa(T)\,|\,Sa(T)>sa\right]$. Thus, to overcome this limit, the disaggregation of $\{M,R,\varepsilon\}$ is being implemented. This will allow to discuss, for example, the effect of dominating faults on the results presented in Chapter 3.

APPENDIX

This appendix provides a short scientific curriculum vitae with the aim to illustrate the personal contribution to the published articles from which Chapters from 2 to 5 are derived:

- *Chioccarelli E, Cito P, Iervolino I, Giorgio M (2018) REASSESS V2.0: Software for single- and multi-site seismic hazard analysis. Bull Earthq Eng http://dx.doi.org/10.1007/s10518-018-00531-x:* implementation of the illustrated procedures for PSHA, SPSHA and MSPSHA; development of the REASSESS software; elaboration of the illustrative examples presented in the paper.
- *Iervolino I, Giorgio M, Cito P (2018) The peak over the design threshold in strong earthquakes. Bull Earthq Eng http://dx.doi.org/10.1007/s10518-018-0503-9:* implementation of the illustrated procedure for the evaluation of the expected exceedance; elaboration of the results and figures presented in the paper.
- *Iervolino I, Giorgio M, Cito P (2018) Which earthquakes are expected to exceed the design spectra? Earthq Spectra (in revision):* implementation of the illustrated procedure for the evaluation of the minimum magnitude of strong earthquakes; elaboration of the results and figures presented in the paper.
- *Chioccarelli E, Cito P, Iervolino I (2018) Disaggregation of sequence-based seismic hazard. In: Proc of the 16th european conference on earthquake engineering, Thessaloniki:* elaboration of the illustrative examples presented in the paper

- *Iervolino I, Giorgio M, Cito P (2017) The effect of spatial dependence on hazard validation. Geophys Journ Int 209:1363–1368:* implementation of the illustrated procedure for simulating spatially correlated ground motion fields; post-processing of simulations and elaboration of the non-binomial distribution (indicated as “exact” in the paper); review of the data concerning the observed exceedances at the sites

REFERENCES

Aki K, Richards P (1980) Quantitative Seismology: theory and methods. Freeman, San Francisco, 932 pp

Akkar S, Bommer JJ (2010) Empirical equations for the prediction of PGA, PGV and spectral accelerations in Europe, the Mediterranean region and the Middle East. Seismol Res Lett 81:195-206

Albarello D, D'Amico V (2008) Testing probabilistic seismic hazard estimates by comparison with observations: an example in Italy. Geophys Journ Int 175: 1088–1094

Ambraseys NN, Simpson KA, Bommer JJ (1996) Prediction of horizontal response spectra in Europe. Earthq Eng Struct Dyn 25:371–400

Baker JW (2007) Probabilistic structural response assessment using vector-valued intensity measures. Earthq Eng Struct Dyn 36:1861–1883

Baker JW (2011) Conditional Mean Spectrum: Tool for ground motion selection. Journ of Struct Eng 137(3):322-331

Baker JW, Cornell CA (2006a) Spectral shape, epsilon and record selection. Earthq Eng Struct Dyn 35:1077-1095

Baker JW, Cornell CA (2006b) Vector-Valued Ground Motion Intensity Measures for Probabilistic Seismic Demand Analysis. PEER Technical Rept

Baker JW, Jayaram N (2008) Correlation of spectral acceleration values from NGA ground motion models. Earthq Spectra 24:299–317

Barani S, Spallarossa D, Bazzurro P (2009) Disaggregation of probabilistic ground-motion hazard in Italy. Bull Seismol Soc Am 99:2638–2661

Bazzurro P, Cornell CA (1999) Disaggregation of seismic hazard. Bull Seismol Soc Am 89:501-520Bazzurro P, Cornell CA (2002) Vector-valued probabilistic seismic hazard analysis (VPSHA). In: Proc of the 7th US national conference on earthquake engineering, Boston, MA, July 21–25

Bender B, Perkins DM (1987) Seisrisk III: A Computer Program for Seismic Hazard Estimation. US Geol Surv Bull 1772

Bianchini M, Diotallevi P, Baker JW (2009) Prediction of inelastic structural response using an average of spectral accelerations. In: Proc of the 10th international conference on structural safety and reliability (ICOSSAR 09), Osaka, Japan

Bindi D, Pacor F, Luzi L, Puglia R, Massa M, Ameri G, Paolucci R (2011) Ground motion prediction equations derived from the Italian strong motion database. Bull Earthq Eng 9(6):1899-1920

Bojórquez E, Iervolino I (2011) Spectral shape proxies and nonlinear structural response. Soil Dyn and Earthq Eng 31(7):996-1008

Bommer JJ, Douglas J, Strasser FO (2003) Style-of-faulting in ground-motion prediction equations. Bull Earthq Eng 1:171–203

Boyd OS (2012) Including foreshocks and aftershocks in time-independent probabilistic seismic-hazard analyses. Bull Seismol Soc Am 102:909–917

Bradley BA (2012) Empirical Correlations between Peak Ground Velocity and Spectrum-Based Intensity Measures. Earthq Spectra 28:17-35

Castanos H, Lomnitz C (2002) PSHA: is it a science? Eng Geol 66:315-317

Cauzzi C, Faccioli E, Vanini M, Bianchini A (2015) Updated predictive equations for broadband (0.01–10 s) horizontal response spectra and peak ground motions, based on a global dataset of digital acceleration records. Bull Earthq Eng 13:1587-1612

Chioccarelli E, Cito P, Iervolino I (2018) Disaggregation of sequence-based seismic hazard. In: Proc of the 16th european conference on earthquake engineering, Thessaloniki

Chioccarelli E, De Luca F, Iervolino I (2012) Preliminary study of Emilia (May 20th 2012) earthquake ground motion records V2.11. Available at www.reluis.it

Convertito V, Emolo A. Zollo A (2006) Seismic-Hazard Assessment for a Characteristic Earthquake Scenario: An Integrated Probabilistic–Deterministic Method. Bull Seismol Soc Am 96:377–391

Cordova PP, Deierlein GG, Mehanny SS, Cornell CA (2000) Development of a two-parameter seismic intensity measure and probabilistic assessment procedure. In: Proc of The second US-Japan workshop on performance-based earthquake engineering methodology for reinforced concrete building structures, pp 187–206

Cornell CA (1968) Engineering seismic risk analysis. Bull Seismol Soc Am 58:1583-1606

Cornell CA, Krawinkler H (2000) Progress and challenges in seismic performance assessment. PEER Center News 3(2):1–3

Crowley H, Stucchi M, Meletti C, Calvi GM, Pacor F (2009) Revisiting Italian design code spectra following the L'Aquila earthquake. Progettazione Sismica, N. 3/2009 Special Issue, IUSS PRESS (ISSN 1973-7432)

Danciu L, Monelli D, Pagani M, Wiemer S (2010) GEM1 hazard: review of PSHA software. GEM Tech Rep 2010-2, GEM Foundation, Pavia

Eberhart-Phillips D (1998) Aftershocks sequence parameters in New Zeland. Bull Seismol Soc Am 88(4):1095-1097

Eguchi RT (1991) Seismic hazard input for lifeline systems. Struct Safety 10:193–198

El-Hussain I, Deif A, Al-Jabri K, Toksoz N, El-Hady S, Al-Hashmi S, Al-Toubi K, Al-Shijbi Y, Al-saifi M, Kuleli S (2012) Probabilistic seismic hazard maps for Sultanate of Oman. Nat Haz 64:173–210

Esposito S, Iervolino I (2011) PGA and PGV spatial correlation models based on European multi-event datasets. Bull Seismol Soc Am 101:2532-2541

Esposito S, Iervolino I (2012) Spatial correlation of spectral acceleration in European data. Bull Seismol Soc Am 102(6):2781-2788

Eurocode 8 (2004). Design of structures for earthquake resistance. part 1: General rules, seismic actions and rules for buildings, EN 1998-1, European Committee for Standardization (CEN), http://www.cen.eu/cenorm/homepage.htm

Field EH, Jordan TH, Cornell CA (2003) OpenSHA: A Developing Community-modeling Environment for Seismic Hazard Analysis. Seismol Res Lett 74(4):406-419

Forte G, De Falco M, Chioccarelli E, Cito P, Santo A, Iervolino I (2018) Seismic soil classification of Italy based on surface geology and shear wave velocity measurements (under preparation)

Fox MJ, Stafford PJ, Sullivan TJ (2016) Seismic hazard disaggregation in performance-based earthquake engineering: occurrence or exceedance? Earthq Eng Struct Dyn 45:835-842

Gardner JK, Knopoff L (1974) Is the sequence of earthquakes in Southern California, with aftershocks removed, Poissonian? Bull Seismol Soc Am 64(5):1363-1367

Giardini D, Danciu L, Erdik M, Sesetyan K, Tumsa MBD, Akkar S, Gulen L, Zare M (2018) Seismic hazard map of Middle East. Bull Earth Eng doi: 10.1007/s10518-018-0347-3

Giardini D, Woessner J, Danciu L, Crowley H, Cotton F, Grünthal G, Pinho R, Valensise G, Akkar S, Arvidsson R, Basili R, Cameelbeeck T, Campos-Costa A, Douglas J,

Demircioglu MB, Erdik M, Fonseca J, Glavatovic B, Lindholm C, Makropoulos K, Meletti C, Musson R, Pitilakis K, Sesetyan K, Stromeyer D, Stucchi M, Rovida A (2013) Seismic Hazard Harmonization in Europe (SHARE): Online Data Resource

Giorgio M, Iervolino I (2016) On multisite probabilistic seismic hazard analysis. Bull Seismol Soc Am 106(3):1223–1234

Gutenberg B, Richter CF (1944) Frequency of earthquakes in California. Bull Seismol Soc Am 34(4): 1985–1988

Iervolino I (2013) Probabilities and fallacies: why hazard maps cannot be validated by individual earthquakes. Earthq. Spectra 29:1125–1136

Iervolino I (2016) Soil-invariant seismic hazard and disaggregation. Bull Seismol Soc Am 106(4): 1900–1907

Iervolino I, Baltzopoulos G, Chioccarelli E (2016b) Case study: definition of design seismic actions in near- source conditions for an Italian site. Deliverable D9, DPC-Reluis 2015 - RS2 Project – Numerical simulations of earthquakes and near source effects, ReLUIS, Naples, Italy

Iervolino I, Chioccarelli E, Cito P (2016a) REASSESS V1.0: A computationally-efficient software for probabilistic seismic hazard analysis. In: Proc of the 7th European congress on computational methods in applied sciences and engineering (ECCOMAS), pp. 5999-6012, Crete, Greece

Iervolino I, Chioccarelli E, Convertito V (2011) Engineering design earthquakes from multimodal hazard disaggregation. Soil Dyn and Earthq Eng 31:1212–1231

Iervolino I, Chioccarelli E, Giorgio M (2018) Aftershocks' effect on structural design actions in Italy. Bull Seismol Soc Am 108(4):2209-2220

Iervolino I, De Luca F, Chioccarelli E, Dolce M (2010) L'azione sismica registrata durante il mainshock del 6 aprile 2009 a L'Aquila e le prescrizioni del DM14/01/2008 V.1 (in Italian). Web report available at http://www.reluis.it

Iervolino I, Giorgio M (2015) The effect of stochastic dependence on hazard validation studies. In Proc. CSNI Workshop on Testing PSHA Results and Benefit of Bayesian Techniques for Seismic Hazard Assessment, EUCENTRE Foundation, Pavia, Italy

Iervolino I, Giorgio M (2018) E' possibile evitare il superamento delle azioni di progetto nell'area epicentrale di terremoti forti? Progettazione Sismica 8: 25-32 (In Italian)

Iervolino I, Giorgio M, Galasso C, Manfredi G (2010) Conditional hazard maps for secondary intensity measures. Bull Seismol Soc Am 100:3312–3319

Iervolino I, Giorgio M, Polidoro B (2014) Sequence-based probabilistic seismic hazard analysis. Bull Seismol Soc Am 104(2):1006-1012

Inoue T, Cornell CA (1990) Seismic hazard analysis of multi-degree-of-freedom structures. Reliability of marine structures, RMS-8. Stanford, CA

Joyner WB, Boore DM (1981) Peak horizontal acceleration and velocity from strong motion records including records frm the 1979 Imperial Valley, California, Earthquake. Bull Seismol Soc Am 71:2011-2038

Katsanos EI, Sextos AG, Manolis GD (2010). Selection of earthquake ground motion records: A state-of-the-art review from a structural engineering perspective. Soil Dynam Earthq Eng. 30(4):157–169

Kramer SL (1996) Geotechnical earthquake engineering. Prentice Hall, Upper Saddle River, NJ

Lin T, Harmsen SC, Baker JW, Luco N (2013) Conditional spectrum computation incorporating multiple causal earthquakes and ground-motion prediction models. Bull Seismol Soc Am 103:1103–1116

Lolli B, Gasperini P (2003) Aftershocks hazard in Italy Part I: Estimation of time-magnitude distribution model parameters and computation of probabilities of occurrence. Journ of Seismol 7(2):235–257

Loth C, Baker JW (2013) A spatial cross-correlation model of spectral accelerations at multiple periods. Earthq Eng Struct Dyn 42(3):397-417

Luzi L, Hailemikael S, Bindi D, Pacor F, Mele F, Sabetta F (2008) ITACA (ITalian ACcelerometric Archive): a web portal for the dissemination of Italian strong-motion data. Seismol Res Lett 79:716-722

Luzi L, Pacor F, Puglia R, Lanzano G, Felicetta C, D'amico M, Michelini A, Faenza L, Lauciani V, Iervolino I, Baltzopoulos G, Chioccarelli E (2016) The Central Italy seismic sequence between August and December 2016: analysis of strong-motion observations. Seismol Res Lett 88:1219-1231

Mai PM, Spudich P, Boatwright J (2005) Hypocenter locations in finite-source rupture models. Bull Seismol Soc Am 95(3):965-980

Malhotra PK (2008) Seismic design loads from site-specific and aggregate hazard analyses. Bull Seismol Soc Am 98:1849–1862

Markhvida M, Ceferino L, Baker JW (2018) Modeling spatially correlated spectral accelerations at multiple periods using principal component analysis and geostatistics. Earthq Eng Struct Dyn 47(5): 1107-1123

Marzocchi W, Taroni M (2014) Some thoughts on declustering in probabilistic seismic-hazard analysis. Bull Seismol Soc Am 104(4):1838-1845

Masi A, Chiauzzi L (2009) Preliminary analyses on the mainshock of the Aquilano earthquake occurred on April 06, 2009. Web report available at http://www.reluis.it

Masi A, Chiauzzi L, Braga F, Mucciarelli M, Vona M, Ditommaso R (2011) Peak and integral seismic parameters of L'Aquila 2009 ground motions: observed versus code provision values. Bull Earthq Eng 9:139-156

McGuire RK (1976) FORTRAN computer program for seismic risk analysis. US Geol Surv Open-File Rept: 76-67

McGuire RK (1995) Probabilistic seismic hazard analysis and design earthquakes: closing the loop. Bull Seismol Soc Am 85(5):1275–1284

McGuire RK (2004) Seismic hazard and risk analysis. Oakland, CA, USA: Earthq Eng Research Institute

Meletti C, Galadini F, Valensise G, Stucchi M, Basili R, Barba S, Vannucci G, Boschi E (2008) A seismic source zone model for the seismic hazard assessment of the Italian territory. Tectonoph 450: 85-108

Montaldo V, Faccioli E, Zonno G, Akinci A, Malagnini L (2005) Treatment of ground motion predictive relationships for the reference seismic hazard map of Italy. Journ Seismol 9(3):295-316

Mood AM, Graybill FA, Boes DC (1974) Introduction to the Theory of Statistics. McGraw Hill, 480pp

Musson RMW, Toro GR, Coppersmith KJ, Bommer JJ, Deichmann N, Bungum H, Cotton F, Scherbaum F, Slejko D, Abrahamson NA (2005) Evaluating hazard results for Switzerland and how not to do it: a discussion of "Problems in the application of the SSHAC probability method for assessing earthquake hazards at Swiss nuclear power plants$ by JU Klugel. Eng Geol 82: 43-55

Nath SK, Thingbaijam KKS (2012) Probabilistic seismic hazard assessment of India. Seismol Res Lett 83 (1):135-149

Ordaz M, Martinelli F, D'Amico V, Meletti C (2013) CRISIS2008: A flexible tool to perform probabilistic seismic hazard assessment. Seismol Res Lett 84(3):495-504

Pagani M, Monelli D, Weatherill G, Danciu L, Crowley H, Silva V et al (2014) OpenQuake-engine: an open hazard (and risk) software for the Global Earthquake Model. Seismol Res Lett 85:692–702

Park J, Bazzurro P, Baker JW (2007) Modeling spatial correlation of ground motion intensity measures for regional seismic hazard and portfolio loss estimation. In Proc. 10th International Conference on Application of Statistic and Probability in Civil Engineering (ICASP10), Tokyo, Japan, 8 pp

Reasenberg PA, Jones LM (1989) Earthquake hazard after a mainshock in California. Science 243:1173-1175

Reasenberg PA, Jones LM (1994) Earthquake aftershocks: Update. Science 265:1251-1252

Reiter L (1990) Earthquake Hazard Analysis: Issues and Insights. Columbia University Press, New York

Reiter L (2004) When are ground motion estimates too high? Seismol Res Lett 74: 282

Scherbaum F, Schmedes J, Cotton F (2004) On the conversion of source-to-site distance measures for extended earthquake source models. Bull Seismol Soc Am 94(3):1053–1069

Schorlemmer D, Gerstenberger M, Wiemer S, Jackson DD, Rhoades DA (2007) Earthquake likelihood model testing. Seismol Res Lett 78: 17-29

Stafford PJ, Rodriguez-Marek A, Edwards B, Kruiver PP, Bommer JJ (2017) Scenario dependence of linear site-efect factors for short-period response spectral ordinates. Bull Seismol Soc Am 107(6):2859–2872

Stein S, Tomasello J, Newman A (2003) Should Memphis build for California's earthquakes? Eos Trans Am Geophys Union 84: 177-185

Stewart JP, Douglas J, Javanbarg M, Bozorgnia Y, Abrahamson NA, Boore DM, Campbell KW, Delavaud E, Erdik M, Stafford PJ (2015) Selection of Ground Motion Prediction Equations for the Global Earthquake Model. Earthq Spectra 31(1):19-45

Stucchi M, Meletti C, Montaldo V, Crowley H, Calvi GM, Boschi E (2011) Seismic hazard assessment (2003–2009) for the Italian building code. Bull Seismol Soc Am 101:1885-1911

Ullah S, Bindi D, Pilz M, Danciu L, Weatherill G, Zuccolo E, Ischuk A, Mikhailova NN, Abdrakhma-tov K, Parolai S (2015) Probabilistic seismic hazard assessment for Central Asia. Annals of Geoph 58(1):S0103

Utsu T (1970) Aftershocks and earthquake statistics (1): Some parameters which characterize an aftershock sequence and their interrelations. J Facul Sci Hokkaido Univ. Series 7, Geoph 3:129–195

Wang Z (2012) Comment on "PSHA Validated by Quasi Observational Means" by Musson RMW. Seismol Res Lett 83: 714-716

Wells DL, Coppersmith KJ (1994) New empirical relationship among magnitude, rupture length, rupture width, rupture area, and surface displacement. Bull Seismol Soc Am 84(4):974-1002

Yeo GL, Cornell CA (2009) A probabilistic framework for quantification of aftershock ground-motion hazard in California: Methodology and parametric study. Earthq Eng Struct Dyn 38:45–60